Winter 2015

Modeling, optimization, and sensitivity analysis of a continuous multi-segment crystallizer for production of active pharmaceutical ingredients

Bradley James Ridder
Purdue University

Graduate School Form 30
Updated 1/15/2015

PURDUE UNIVERSITY
GRADUATE SCHOOL
Thesis/Dissertation Acceptance

This is to certify that the thesis/dissertation prepared

By Bradley J. Ridder

Entitled

MODELING, OPTIMIZATION, AND SENSITIVITY ANALYSIS OF A CONTINUOUS MULTI-SEGMENT CRYSTALLIZER FOR PRODUCTION OF ACTIVE PHARMACEUTICAL INGREDIENTS

For the degree of Doctor of Philosophy

Is approved by the final examining committee:

Zoltan K. Nagy
Chair

James Litster

Keith Chadwick

Gintaras Reklaitis

To the best of my knowledge and as understood by the student in the Thesis/Dissertation Agreement, Publication Delay, and Certification Disclaimer (Graduate School Form 32), this thesis/dissertation adheres to the provisions of Purdue University's "Policy of Integrity in Research" and the use of copyright material.

Approved by Major Professor(s): Zoltan K. Nagy

Approved by: John Morgan 2/18/2015
Head of the Departmental Graduate Program Date

MODELING, OPTIMIZATION, AND SENSITIVITY ANALYSIS OF A CONTINUOUS MULTI-SEGMENT CRYSTALLIZER FOR PRODUCTION OF ACTIVE PHARMACEUTICAL INGREDIENTS

A Dissertation

Submitted to the Faculty

of

Purdue University

by

Bradley J. Ridder

In Partial Fulfillment of the

Requirements for the Degree

of

Doctor of Philosophy

May 2015

Purdue University

West Lafayette, Indiana

"We, the willing, led by the unknowing, are doing the impossible for the ungrateful. We have done so much, for so long, with so little, we are now qualified to do anything - with nothing." -Konstantin Jireček, Czech historian and diplomat

ACKNOWLEDGEMENTS

I first would like to thank my advisor, Dr. Zoltan Nagy, for his Job-like patience during my time here at Purdue. I recall fondly many chats in his office where he would give good advice on how to proceed with the project, while allaying my (many…!) fears and worries about school. I also would like to thank my group members David Acevedo, Yang Yang, and (again!) Andy Koswara. They were always willing to kick around ideas or consult about their findings in their own research. Furthermore, I extend great thanks to the former post-doc in our group, Dr. Aniruddha "Ani" Majumder now of the University of Aberdeen, Scotland. Ani offered a great deal of assistance with the implementation of the finite volume method, as well as answering my many conceptual questions. I would also like to thank my mother, who offered an immense amount of help and support during graduate school.

TABLE OF CONTENTS

Page

Page

Page

LIST OF TABLES

Table Page

LIST OF FIGURES

Figure Page

Figure Page

Figure Page

Figure Page

Figure Page

NOMENCLATURE

List of Mathematical Symbols

Symbol	Definition	Units
j	Refers to j^{th} crystallizer segment	-
A_{fit}	Solubility curve fitting parameter	mg/m^3
B_{fit}	Solubility curve fitting parameter	-
A_{total}	Total antisolvent allotment	ml/min
B_0	Nucleation rate law	#/m^3·s or #/kg·s
C_0	Initial concentration	mg/m^3 or kg/kg
C_{sat}	Saturation (solubility) concentration	mg/m^3 or kg/kg
L_1, L_2, L_3	Characteristic lengths	μm
L_{43}	Mass-mean crystal size	μm
N_{total}	Total number of crystals per unit volume	#/m^3
R^3	Three-space; 3D Cartesian coordinates	-
S_j	Flowrate of pure solvent into segment j	ml/min
S_{rel}	Relative solubility	-
S_{total}	Total pure solvent allotment	ml/min
T_{decomp}	Decomposition point of API	K

T_{freeze}	Freezing point of solution	K
$X_A^{\%}$	Antisolvent volume fraction percentage	%
X_w	Water mass fraction	-
a_j	Antisolvent apportionment into segment *j*	-
d_{inner}	Inner diameter of crystallizer	mm
$f_i(\boldsymbol{x})$	Objective function	-
$f_i^*(\boldsymbol{x})$	Optimal value of objective function	-
$f_{v,target}$	Target volume fraction distribution	1/m
f_v	Volume fraction distribution	1/m
k_b	Nucleation law rate constant	#/m^3·s
k_d	Dissolution law rate constant	m/s
k_g	Growth law rate constant	m/s
k_v	Shape factor	-
n_0	Initial (seed) crystal size distribution	#/m^4
n_{v}	Volume-based crystal size distribution	m^3/m^4
n_j	Crystal size distribution in segment *j*	#/m^4
s_j	Pure solvent apportionment into segment *j*	-
u_x, u_y, u_z	Velocities in the Cartesian directions	m/s
x_{AS}	Antisolvent mass fraction	-
x_{total}	Total length of crystallizer	m
$\boldsymbol{x}_{LB}$	Lower bound on $\boldsymbol{x}$	-

$\boldsymbol{x}_{UB}$	Upper bound on $\boldsymbol{x}$	-
∇_{ext}	Gradient over the external coordinates	-
∇_{int}	Gradient over the internal coordinates	-
γ_b, γ_g	Multipliers of base-case nucleation and growth constants in section 4.5.2	-
γ_j	Dissolution correction in segment j	-
δ_{seed}	Mean size of seed distribution	μm
$\mu_{1,0}$	Mean size of number distribution in figure Figure 2.8	μm
$\mu_{3,0}$	Third moment of seed distribution	-
μ_k	k^{th} moment	depends on k
ρ_c	Density of solid crystalline API	kg/m^3
ω_{seed}	Standard deviation of seed distribution	μm
ΔC	Absolute supersaturation	mg/m^3
Ψ	Energy, mass, momentum, or population	-
B	Birth rate of new particles	#/m^4·s
C	Concentration of API	mg/m^3 or kg/kg
CV	Coefficient of variation	-
D	Death rate of particles	#/m^4·s
D	Dissolution rate	m/s
G	Growth rate	m/s
K	Number of crystal size bins	-

L	Internal characteristic length coordinate	μm
N	Total number MSMA-PFC segments	-
S	Supersaturation ratio	-
T	Temperature	K
Y	Yield	-
b	Nucleation order	-
d	Dissolution order	-
f	Number fraction distribution	1/m
g	Growth order	-
n	Number density (crystal size distribution)	#/m^4
q	Parameter in equation	-
s	Standard deviation of CSD in figure Figure 2.8	μm
t	Time	s
u_j	Antisolvent apportionment decision variable in section 4.4.3	-
x, y, z	Cartesian directions	m
$\boldsymbol{A}$	Vector of antisolvent flowrates	ml/min
$\boldsymbol{F}$	Multiobjective criteria vector	-
$\boldsymbol{G}$	Vector of growth rates	m/s
$\boldsymbol{d}$	Vector of decision variables	-
$\boldsymbol{g}(\boldsymbol{x})$	Vector of inequality constraints	-
$\boldsymbol{h}(\boldsymbol{x})$	Vector of equality constraints	-

$\boldsymbol{x}$	State vector	-
γ, p	Parameters in equation (2.7)	
ξ	Seed mass loading percentage	%
τ	Residence time	s
φ	Dissolution multiplier	-

List of Acronyms

Acronym	Definition
%RH	Percent relative humidity
API	Active pharmaceutical ingredient
ATR FT-IR	Attenuated total reflectance Fourier transform infrared spectroscopy
CFD	Computational fluid dynamics
COBC	Continuous oscillatory baffled crystallizer
CPM	Continuous pharmaceutical manufacturing
CPP	Critical process parameter
CQA	Critical quality attribute
CSD	Crystal size distribution
CSTR	Continuous stirred tank reactor
CT	Couette-Taylor
DEM	Discrete element method
DOE	Design-of-experiments
DSC	Differential scanning calorimetry
FBRM	Focused beam reflectance measurement
FDA	Food and Drug Administration
FDF	Final dosage form
FEM	Finite element method
FV	Finite volume

GA	Genetic algorithm
IR	Infra-red
MILP	Mixed-integer linear program
MINLP	Mixed-integer nonlinear program
MIS	Management information systems
MOCH	Method of characteristics
MOM	Method of moments
MOO	Multiobjective optimization
MSMA-PFC	Multi-segment, multi-addition, plug flow crystallizer
MSMPR	Mixed suspension, mixed product removal crystallizer
NSGA-II	Nondominated sorting genetic algorithm
PAT	Process analytical technology
PBE	Population balance equation
PBM	Population balance modeling
PCA	Principal component analysis
PFC	Plug flow crystallizer
PLS	Partial least squares
PVM	Particle vision monitoring
PWC	Plant-wide control
QbD	Quality-by-Design

QbT	Quality-by-Testing
RTR	Real time release
SDC	Simultaneous design and control
SQP	Sequential quadratic programming
SSE	Sum of the squared errors
WENO	Weighted essentially non-oscillatory method
XRD	X-ray diffraction

ABSTRACT

Ridder, Bradley J. Ph.D., Purdue University, May 2015. Modeling, Optimization, and Sensitivity Analysis of a Continuous, Multi-Segmented, Multi-Addition Plug-Flow Crystallizer for the Production of Active Pharmaceutical Ingredients. Major Professor: Zoltan Nagy.

We have investigated the simulation-based, steady-state optimization of a new type of crystallizer for the production of pharmaceuticals. The multi-segment, multi-addition plug-flow crystallizer (MSMA-PFC) offers better control over supersaturation in one dimension compared to a batch or stirred-tank crystallizer. Through use of a population balance framework, we have written the governing model equations of population balance and mass balance on the crystallizer segments. The solution of these equations was accomplished through either the method of moments or the finite volume method. The goal was to optimize the performance of the crystallizer with respect to certain quantities, such as maximizing the mean crystal size, minimizing the coefficient of variation, or minimizing the sum of the squared errors when attempting to hit a target distribution. Such optimizations are all highly nonconvex, necessitating the use of the genetic algorithm. Our results for the optimization of a process for crystallizing flufenamic acid showed improvement in crystal size over prior literature results. Through the use of a novel simultaneous design and control (SDC) methodology, we have further optimized the flowrates and crystallizer geometry in tandem.

We have further investigated the robustness of this process and observe significant sensitivity to error in antisolvent flowrate, as well as the kinetic parameters of crystallization. We have lastly performed a parametric study on the use of the MSMA-PFC for in-situ dissolution of fine crystals back into solution. Fine crystals are a known processing difficulty in drug manufacture, thus motivating the development of a process that can eliminate them efficiently. Prior results for cooling crystallization indicated this to be possible. However, our results show little to no dissolution is used after optimizing the crystallizer, indicating the negative impact of adding pure solvent to the process (reduced concentration via dilution, and decreased residence time) outweighs the positive benefits of dissolving fines. The prior results for cooling crystallization did not possess this coupling between flowrate, residence time, and concentration, thus making fines dissolution significantly more beneficial for that process. We conclude that the success observed in hitting the target distribution has more to do with using multiple segments and having finer control over supersaturation than with the ability to go below solubility. Our results showed that excessive nucleation still overwhelms the MSMA-PFC for in-situ fines dissolution when nucleation is too high.

CHAPTER 1. INTRODUCTION

1.1 Motivation

In recent years, the continuous production of pharmaceuticals has grown considerably in research attention. Currently, most pharmaceuticals are produced via batch processes, at considerable expense and difficulty. A variety of financial [1]–[11] and regulatory [12] pressures on the pharmaceutical industry has motivated the research into cost-saving, streamlined approaches to their operations. The "blockbuster drug" business model has proven financially unsustainable. Drugs can take from 10-15 years to develop, have only a 20% chance of FDA approval, and cost between $800 million and $1 billion to bring to market [13]–[15]. Many currently-available, on-patent drugs lack suitable profit-generating replacements once their predecessors go off-patent, and the drug industry faces stiff competition from generic manufacturers.

Crystallization is an area of considerable interest from the standpoints of continuous drug manufactures as well as process systems engineering. While useful for small quantities of drugs, drugs which require higher production volumes would benefit greatly from continuous crystallization. As a pure systems problem, crystallization processes are interesting due to their high nonlinearity.

These processes demand a different set of mathematical tools to model and optimize them properly, as well as different solution approaches.

Continuous crystallization systems, while already heavily used in many other industries, have attracted new interest for application to pharmaceuticals. Current methods of crystallization are focused overwhelmingly on batch systems. This is problematic, since batch systems have intrinsic drawbacks related to design, control, and scale-up. Continuous crystallization systems can be considered a sub-field of the more general research field of process intensification.

A variety of new crystallizer designs have been proposed that can, via novel flow chemistry, crystallize drugs with a greater level of precision and control. One particular type of continuous crystallization is the plug flow crystallizer (PFC), which has been the subject of several investigations in recent literature (see Table 4 beginning on page 84). Lakerveld et al. [16] pointed out the need for more investigation into the crystallizer design itself, and that detailed modeling would be needed for the optimization thereof. A new design based on the PFC is the multisegment, multi-addition plug flow crystallizer (MSMA-PFC). This crystallizer is a group of PFCs linked in series, with an independent supersaturation actuator for each segment. This design allows for greater control of supersaturation in one dimension versus a stirred tank.

Currently, there is a lack of design and optimization methodology in the literature for continuous crystallization systems. Multiobjective optimization is a useful tool for fully

investigating the tradeoffs between possible designs of a system, as well as identifying the envelope of attainability [17]. Much benefit could be achieved by use of an integrated framework for the design, optimization, and robustness analysis of new crystallizer designs, of which the MSMA-PFC is a contemporary example. Such a methodology would help trim the design space considerably when searching for an optimal design.

The robustness and sensitivity of continuous crystallization systems for pharmaceutical use has also gone unstudied. The topic of sensitivity in crystallizers has been examined for the case of batch crystallizers by Ma et al. [18] using a worst-case framework, which among other conclusions showed that inaccurate control can wipe out the entire benefit of optimal control. For effective design and operation of new crystallizer technologies, it is important to know the impact of parametric uncertainty, random disturbances, control error, and observer uncertainty on quantities of interest (e.g. shift in CSD shape, purity).

1.2 Research Aim and Objectives

The aim of this research is to develop a framework for modelling and optimizing a new type of antisolvent plug-flow crystallization systems, the MSMA-PFC. To analyze continuous crystallization system, we borrow the concepts of constrained optimization from the field of process systems engineering. By use of this modelling and optimization framework, we can investigate the capabilities of the system for achieving desirable properties of the generated crystals. Such a framework can gauge the feasibility of a plug-

flow crystallization system for producing high-quality crystals of a particular drug, given correct experimental parameters. It can also predict correct operating conditions and vessel designs that will produce crystals with desired properties. We summarize our aims as:

a. To gain a broad view of the impact of continuous crystallization's potential via a thorough literature review of the continuous drug manufacturing research field.
b. To develop a model-based simulation framework for modelling the plug-flow crystallization process.
c. Unite the simulation framework with a multiobjective optimization methodology in order to investigate possible control strategies. This combined simulation-optimization based framework is used throughout this work as a method of optimizing the properties of crystals at the exit of the crystallizer.
d. As an example of this framework in action, analyze the performance of a new type of plug-flow crystallizer, termed the multi-segment, multi-addition plug-flow crystallizer (MSMA-PFC). This apparatus consists of a group of PFC's linked in parallel, each with independent supersaturation control. To demonstrate this framework in action, our chosen crystal properties have been the size and spread of the crystal size distribution – though the framework is extendable to other important quality measures such as polymorph content or aspect ratio.
e. Examine the sensitivity of the crystallization process, and determine the how this sensitivity affects the design considerations for design and control.
f. To create a simultaneous design and control methodology which optimizes over not only flowrates but the actual crystallizer geometry as well.

g. To investigate the feasibility of plug-flow antisolvent crystallization for eliminating undesirable small crystals ("fines").

1.3 Research Contributions

The main contributions of this thesis are summarized as:

a. This thesis surveys not only the continuous crystallization literature, but the continuous pharmaceutical manufacturing field holistically. By overviewing the research field in this manner, it becomes more apparent how our contributions fit into the greater network of ideas and concepts.

b. Through use of a population balance model-based framework, we have developed a model for the MSMA-PFC, coupled with the mass balance equation, which can track the properties of drug crystals at the exit of the crystallizer. This model incorporates the effects of dilution and also dissolution.

c. Demonstrated that the optimization of a multi-segment plug-flow crystallizer is a nonconvex problem.

d. Used multi-objective optimization (aided by the genetic algorithm) to investigate the envelope of performance of the crystallizer, and compared obtained values with prior literature results. Our results compare favorably (e.g. larger crystals). This methodology was able to successfully surmount the observed nonconvexity of the MSMA-PFC optimization problem.

e. Investigated the sensitivity and robustness of the MSMA-PFC with respect to uncertainty in important values such as flowrate and kinetic rate parameters. Using a Monte-Carlo method, we determined that error in flowrate significantly affects the performance of the MSMA-PFC. Also, we found that significant

coupling exists between errors in crystallizer inputs, which significantly impacts the design and operation of the crystallizer.

f. Through use of a simultaneous design and control (SDC) methodology, we successfully optimized not only the individual flowrates in the MSMA-PFC, but the geometry of the crystallizer as well. Significant improvement is shown when using SDC versus optimizing flowrates alone on a static geometry.
g. Demonstrated that the dissolution of fine crystals in-situ is a sub-optimal strategy for the MSMA-PFC class of crystallization problems.

1.4 Thesis Structure

CHAPTER 1 of this thesis gives a broad overview of the remainder of the work. This is to supply the reader with a "bird's eye view" of the topics discussed herein.

CHAPTER 2 provides the reader with a literature review. We begin with a discussion of the current manufacturing process in pharmaceuticals, and discuss various problems and challenges related to it. New continuous technologies are discussed as well in areas outside of crystallization. We move then onto the importance of crystallization in the manufacture of drugs, and how continuous crystallization can solve many current problems encountered with batch crystallization. The remainder of the chapter is background information to help the reader understand the work in

CHAPTER 3 provides a more specific literature review on the topic of continuous crystallization. We give an overview of many contemporary devices for crystallization. A table at the end of the chapter neatly summarizes many studies of continuous crystallization for the reader.

CHAPTER 4 is the first contribution chapter of this work. It presents our results on the multiobjective optimization of the MSMA-PFC. We further investigate the robustness of the design with respect to uncertainty in kinetic parameters as well as flowrate.

CHAPTER 5 revisits the system from CHAPTER 4 on the simultaneous design and control (SDC) problem. In this problem, we optimize the crystallizer not only over the flow profile, but the vessel geometry as well. Significantly more control over mean size is shown possible by optimizing both design and control in tandem.

CHAPTER 6 is the final contribution of this work. In this chapter, we have investigated the use of the MSMA-PFC for in-situ dissolution of fine crystals. Unlike in Chapter 4, the new MSMA-PFC is capable of going below solubility, thus dissolving fine crystals while keeping large ones. The results show however, that dissolution is shown to be a sub-optimal strategy. Comparison with prior in-situ fines dissolution work is given as well.

CHAPTER 7 is our summary and future directions chapter. In this chapter, we summarize the results of the previous chapters. We furthermore expound upon new

technologies and extensions of this work that can be of significant impact in crystallization design and control.

CHAPTER 2. LITERATURE REVIEW

2.1 Introduction

We begin with a general overview of the present state of pharmaceutical manufacturing, which foreshadows the benefits of continuous pharmaceutical manufacturing (CPM) discussed in section 2.2. The flowchart in Figure 2.1 below gives an overview of a drug manufacturing process (based on the diagrams in [1], [19]). This flowchart will serve as a useful guide in the discussion of pharmaceutical manufacturing. Once the basic process overview behind pharmaceutical manufacturing is presented to the reader, it will be clear what problems affect the process, and how our work fits in as a solution to some of those problems.

2.1.1 Synthesis

In Figure 2.1 below, raw materials enter the process at two points. At the start of the process, raw material precursors are transported to the manufacturing site for use in synthesis to create that active pharmaceutical ingredient (API). The API is the molecule which actually provides the curative effect to the patient.

During this phase of the operation, precursors are reacted together, which usually takes several reactions and work-up steps to attain the desired molecular form. In certain instances (e.g. penicillin), a bioreactor or fermenter is used to directly synthesize the API, followed by a variety of cleaning and filtration steps. Multiple syntheses reduce overall yield significantly. During this phase, workers may be in contact with toxic amounts of precursor or final API compounds. The solution containing the API is contaminated with unreacted compounds and organic solvents, and requires a separation.

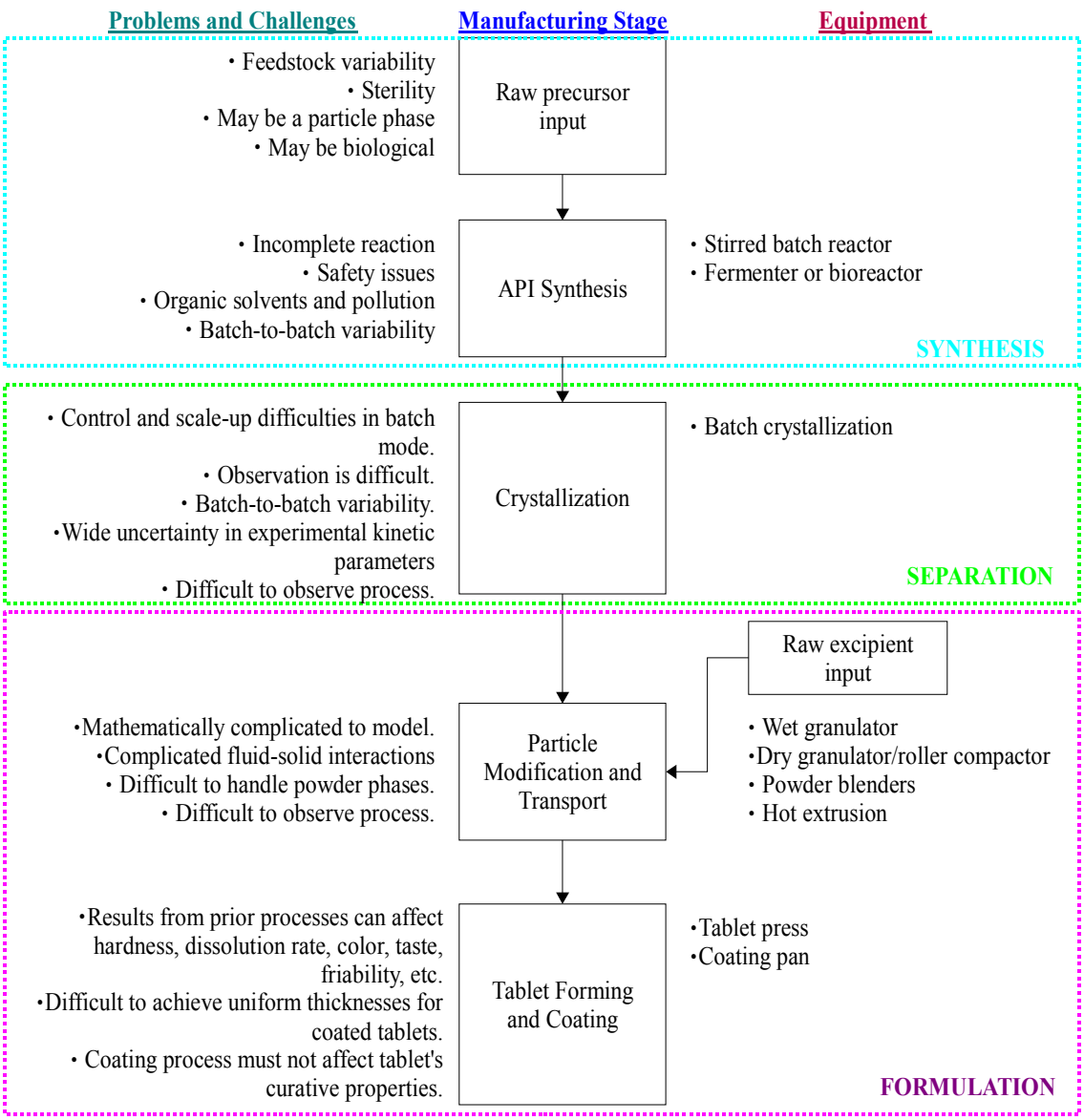

Figure 2.1 Basic flowchart of a pharmaceutical manufacturing process.

2.1.2 Separation

Observing the middle of Figure 2.1, crystallization is the secondary process in pharmaceutical manufacture [1], [19]. This section directly relates to this thesis, as we are

investigating a new type of crystallizer. This new MSMA-PFC design is an intensified process that alleviates many of the problems described in the crystallization section of Figure 2.1. Crystallization is a key pre-formulation operation in pharmaceuticals [1], [5], [20]–[23], and between 80% and 90% of drugs are purified in this way [21], [22], [24]. Crystallization is predominant because it can achieve very high purities (> 98%). Crystallization also does not require harsh conditions (e.g. distillation), which would likely destroy most API molecules. Multiple crystallizations may be necessary to achieve sufficient purity, much in the same way that multiple equilibrium stages are required for distillation, liquid-liquid extraction, and gas-liquid extraction. Following crystallization, crystals require filtration, washing, and drying. The performance of the filtration, washing, and drying processes are highly dependent on the properties of the product crystals. The performance of downstream formulation processes are also dependent on crystal properties.

2.1.3 Formulation

"Formulation" is meant the final steps required to convert refined pharmaceutical crystals and various excipients into a "final dosage form" (FDF). As the name implies, an FDF is meant to deliver a precisely metered quantity of API to the patient. Besides the quantity of drug, the dosage form must possess the desired physical and pharmacological properties that ensure proper bioavailability in the human body. The complexity of the human body places tight constraints on the properties of the FDF [25]. FDF's can take on

many forms, which can dramatically change the formulation process. Examples are too numerous to list exhaustively, but include oral tablets (hard tablets, lozenges, chewable tablets for children, sublingual tablets), injectable drugs, topical creams, and inhalants. Each of these FDF's has a variety of engineering challenges associated with continuous manufacturing. Since crystallization often cannot produce crystals with the desired properties, a variety of particle modification processes are used to remedy this during formulation. These include agglomeration operations such as wet granulation, roller-compaction, and hot-melt extrusion [26]–[29]. Subsequently, API crystals are blended with a variety of excipients to attain desired properties (e.g. dissolution rate, color, sweetness, etc.). Excipients may also be process control agents, such lubricants, which can enhance qualities such as flowability [29]. Excipients often compose the majority of the dosage form [30]. Blending of powders together is another challenging process, since it is difficult to mix powders with consistent homogeneity. Following blending is typically a granulation process, which turns fine powders into larger chunks. Granulation is done for a variety of reasons, such as making the powder phase easier to handle, make tablets easier to press [25], and reducing the respiratory and explosion hazards from dust clouds [19]. Increasing the level of control over the CSD would simplify much of the formulation stage. Once powders are sufficiently mixed and/or granulated, they are pressed under mechanical force to create tablets. The thesis by Cipich on gives a good overview of several processes involved in continuous tablet production, including continuous blending, dry granulation via roller compaction, and a continuous tablet press [29].

To summarize the pharmaceutical manufacturing process, the operations commonly found in the pharmaceutical industry are complicated from a scientific and engineering standpoint. Most operations after the synthesis stage possess at least two phases, such as crystallization slurries or wet granulation mixes. Analysis, design, scale-up, observation, and control of these processes is difficult to do. This is further complicated by the batch nature common to most of these processes, which are not only spatially complex, but time-dependent as well. Few major improvements to these processes have been attempted. Our objective in this work is, through the use of a rigorous modeling and optimization framework, investigate the potential use of the MSMA-PFC for producing pharmaceutical drugs.

2.1.4 Problems Related to Batch Processes in General

Most pharmaceutical manufacturing operations, such as crystallization, are performed using inefficient batch processes, and basic understanding of these important unit operations is limited. This is in contrast to the bulk chemicals, food, and semiconductor industries which are mostly run continuously in well-understood processes [9], [31]. Manufacturing costs accounts for about 30% of sales for brand-name drug manufacturers [11], with 30-40% as the general industry average [7], [11]. In addition to being labor-intensive and environmentally wasteful, current drug manufacture is error-prone [32], leading to costly recalls and contamination [7], [9], [15], [19]. The drug industry's batch operations are also widely distributed geographically, which requires costly, time-

consuming transport of material between manufacturing plants [33]. Clearly, complete manufacturing within a single manufacturing site would be preferable to playing "factory pinball" with various drug components.

Despite being worth over $250 billion [8], the pharmaceutical industry's manufacturing apparatus has become antiquated. Most industries shift to continuous production as quickly as affordable [13]. This is because, at large economies-of-scale, continuous mode is more efficient than batch processes. The reader might wonder, "Why the lag in technology?" The reason for this lag, is that the pharmaceutical industry has historically been tightly regulated, with even minor changes to processes requiring re-approval [13], [34]. However, recent reforms [12], [35], [36] to the regulatory framework have greatly lessened this impediment and given much more freedom to make process changes within an approved "design space" (see [34]). To address this lag in technology, the pharmaceutical industry has recently expressed great interest in upgrading and streamlining its research, development, manufacturing, and logistical operations.

2.1.5 Problems Related to Batch Crystallization

We are especially interested in this work on problems related to batch crystallization, and how continuous crystallization can solve many of these problems. The continuous crystallization of pharmaceuticals is a research endeavor with very high potential impact, as crystallization is a ubiquitous process operation in pharmaceuticals and a key stage at

which quality can be engineered into the final product. This folds in with the concept of "QbD", discussed in section 2.2.1. Most industrial pharmaceutical crystallization is done batch-wise, which has a variety of drawbacks related to scale-up, observation, and control. Efficient, controlled production of drug crystals with desired properties has been described as a "primary bottleneck" to large-scale production of certain drugs [37]. Improving crystallization operations can improve the manufacturing process as a whole, since the properties of the produced crystals affect the performance of subsequent processes [21], [38]. Table 1 below summarizes the problems associated with batch crystallization. Plumb [19] neatly summarizes the problems associated with batch manufacturing as follows: "Batch processes are poorly understood, time-dependent, and scale-dependent operations." This is in contrast to continuous processes, which are capable of attaining a physically and mathematically well-defined steady-state of dynamic equilibrium. Batch processes also fail to process all material in a uniform, consistent fashion, due to the existence of uncontrollable spatial gradients in fluid velocity, supersaturation, temperature, solids fraction, and chemical composition. This is in contrast to a steady-state, continuous flow process, over which significant control over these gradients is possible, as well as tight residence time distributions.

Table 1 Tradeoffs between batch and continuous crystallization.

	Pros	Cons
Batch	• Infrastructure already exists in industry. • Sophisticated modeling, control, process optimization, and informatics management methods exist. • Laboratory versions of equipment are simple (e.g. a beaker.)	• Difficult to scale-up. • Batch-to-batch variability. • Attrition and breakage become problems at larger sizes. • Safety issues with large volumes of fluid. • Impeller required to mix fluids; great difficulty in scaling this properly. • Entire batch must be discarded in event of disturbance; costly and environmentally unfriendly. • Labor-intensive operation. • If target crystal size distribution is not achieved, milling operations are required.
Continuous	• Easier scale-up (depending on exact setup) due to better mixing and/or heat transfer. • Easier to control. • Much less fluid hold-up; safer to operate. • More cost-effective at larger economies of scale. • Less environmental impact if disturbance causes problems. • Small equipment size.	• New technology; requires new capital investment. • Modeling and control methods not well developed. • Observation of system difficult; sensors disturb flow. • Plugging and fouling is a problem.

Scale-up is another serious problem encountered in batch crystallization. In chemical engineering, a common problem is taking a small, laboratory-scale system, and increasing its production capacity to meet mass-market demand. For drugs, API crystallization is almost entirely done batch-wise, and direct scale-up from the laboratory model is difficult to achieve [39]. The main reason the scale-up of agitated crystallization vessels is difficult is due to incongruous scaling rules for heat, mass, and momentum transfer. To scale-up a crystallizer, one calculates a set of dimensionless numbers based upon the geometry of the crystallizer, the impeller design, fluid properties, and the power input to the impeller. Dimensional analysis of the governing equations shows that it is impossible to preserve all dimensionless groups with increasing tank size, regardless of agitation speed [39], [40]. The phenomena described by these dimensionless numbers – such as heat transfer rate, hydrodynamic flow patterns, shear rate, and suspension velocity - scale in opposing ways [40], [41]. Plumb [19] provides numerical results clearly indicating this problem, and Mersmann and Foster [42] gives a large table of dimensionless correlations for stirred vessels. Significant changes in the velocity field can result upon scale-up, resulting in supersaturation gradients and ultimately a CSD that does not meet desired characteristics [40], [43]. Scale-up also leads to changes in the internal hydrodynamics of the crystallizer that are difficult to model and predict [39], [44]. These issues are discussed at length by Genck [39], Wei [45], and in the text by Peker and Helvaci [46]. In continuous crystallization (and CPM in general), we replace large-volume process equipment with smaller apparatus that output lower, constant volumetric flow rates. Continuous operation requires somewhat more time to accomplish for the

same relative amount of material to be processed, but at the gain of superior control over the product properties.

A workaround for the scale-up problems is to avoid scaling-up the batch apparatus, and just use a larger number of batch crystallizers in parallel. This however, leads to much greater capital and operating costs, and the problem of batch-to-batch variability [19], [24], [47]. This variability results from the fact that even small discrepancies in operating conditions can drastically change the physical properties of the obtained crystals [21]. There are a variety of causes for this problem, such as differences in feedstocks [21], [30], [48] (upstream variation), mechanical wear and fouling, and reusing the same vessel for multiple processes [49]. These changes can alter the hydrodynamic and/or heat and mass transfer characteristics of the equipment slowly over time, thus altering the CSD obtained from a particular vessel.

Lastly, despite the simplicity of the equipment, batch crystallizers are highly complicated nonlinear systems [19], [38], [40], [50], [51], and complex dynamic behavior arises with increasing complexity of the crystallizer network. Tavare has compiled an expansive table of dynamic phenomena observed in conventional MSMPR systems, which are stirred tanks similar to a batch system [51]. Multiplicities of steady-states, oscillations, orbits, and limit cycles have all been observed [47], [50], [52], and appear generally to be caused by the recycle of re-dissolved fines. Time-dependence of the CSD is highly undesirable, since disturbances in the crystallizer can propagate downstream to other processes, and render the final product's quality inconsistent [20], [53], [54]. A

continuous approach solves many of these problems, as continuous processes are not as difficult to control and scale-up. The analysis of the MSMA-PFC is a step forward towards the "blue sky" vision of fully continuous, automated drug manufacture by streamlining a crucial separation step.

To summarize, particulate processes in the drug industry are poorly understood; this goes for not only crystallizers but also dry-powder-phase processes and liquid-powder processes. The drug industry is looking to remedy these problems by shifting to the more economical continuous mode of operation. This motivates our study into new crystallizer designs, that can produce high-quality crystals consistently with much less severity of scale-up and much easier mechanisms of control over batch processes.

2.2 Overview of Technologies for Continuous Pharmaceutical Manufacturing

The pharmaceutical industry is modernizing its research, manufacturing, and logistical operations. The technologies discussed in section 2.1.1 are almost entirely run in batch mode currently, which is inefficient at the pharmaceutical industry's economy of scale. Research effort is increasingly being done toward continuous pharmaceutical manufacturing (CPM). Several industry-academic partnerships have appeared to develop technologies along this line, such as the Novartis-MIT Center for Continuous Manufacturing [23], [55], and the Center for Structured Organic Particulate Systems [9], [56]. These technologies snap a panorama of the chemical engineering corpus, and are

highly inter-disciplinary, such as the continuous feeding of powders, continuous blending, freeze-drying and granulation [9], [28], [29], [31], [57]. The work by Mascia et al. [23] at the MIT group is a good summary of the benefits possible with continuous manufacturing. That work discusses a variety of improvements their continuous tablet plant has made over conventional batch, especially in the reduced number of unit operations and an 84% reduction in plant residence time. This research has great potential benefit in reducing manufacturing costs, increasing product quality, and improving consumer safety. Preliminary estimates of the impact of CPM show cost reductions between 25%-40% [5], [20], [23], or higher [19]. Equipment efficiencies of 30% are common today, but continuous processing can attain over 80% efficiency [19].

2.2.1 Quality-by-Design (QbD) Thinking

Variability is a ubiquitous problem in contemporary pharmaceutical processes [19], [48]. Raw material variations in composition can affect the yield of API produced during chemical reaction, as well as contamination. Variability in excipient properties is a serious problem as well, [48], [58]. Even though these components contain no API, excipients are added to alter the physical properties of the final dosage form; especially the dissolution rate. Variation in particle size distribution, composition, and other properties of an excipient can lead to off-specification FDFs [48]. The pharmaceutical industry's current approach to handling off-specification product is to simply throw the batch out, which increases costs and environmental impact.

The variety of possible FDF's, tight constraints on product quality, high manufacturing costs, and wide variability in final products has motivated the introduction of Quality-by-Design (QbD) thinking into pharmaceutical process design. Strongly encouraged by the FDA [35], Quality-by-Design (QbD) is a methodology for reducing product variability during manufacturing. Through a complete process understanding of inputs, outputs, and disturbances, and a list of target specifications for the final product, it becomes possible to "build quality into" the final product [59]. When successfully implemented, product specifications are very likely to be on-target at the end of the process [34], [60]. Our own work directly relates to the concept of variability as shown in CHAPTER 4 and CHAPTER 5, where the mathematical framework we developed was used to directly attempt to minimize unwanted variability in the crystal product.

2.2.2 Critical Quality Attributes and Critical Process Parameters

Wu et al. [9] discuss the concept of QbD at length in their comparison of chemical engineering successes and opportunities in the pharmaceutical and semiconductor industries. QbD involves defining the product fully in terms of critical quality attributes, or CQA's. CQA's are primarily linked to product requirements and safety, but can also be tied to other important "marketing" type characteristics, such as having the proper color or shape. Then, the proposed manufacturing process is studied in detail using models, experiments (especially design-of-experiments, or DOE, approaches [1], [34], [61]), and other prior knowledge [62], to identify the critical process parameters (CPP)

that impart the most variability into the final product. A CPP may also be an important process disturbance. The collection of process inputs and CPP's defines the "control space," within which we capable of hitting any of the accept CQA's in the "design space." In our work , an example of the CQA would be the size of the produced crystals, while a CPP would be any of the flowrates. Further discussion of CQAs and CPPs is given by Bondi and Drennen [34]. The QbD archetype stands in contrast to the traditional method of Quality-by-Testing (QbT) for pharmaceuticals, where large samples of drug products are destructively tested at the end of the process, while still failing to test the quality of all the drug product intended for public release.

2.2.3 The Problem of Quality-by-Testing

Figure 3.1 below demonstrates the inadequacy of Quality-by-Testing. In Figure 2.2, each colored square represents an allotment of drug that has been randomly selected for quality-assurance testing. When performing lot testing, the samples taken for analysis are obviously checked, but their sibling products are not, and are merely assumed to be safe or dangerous based on the results of sampled ones. In Figure 2.2(a), the random selection has worked as intended – some of the contaminated samples are discovered, deeming the lot unsafe. However, in Figure 2.2(b), the random selection has chosen solely on-specification samples, but several contaminated ones evade detection. Bear in mind, that all of the samples in Figure 2.2(a) would be rejected – not just the two off-specification samples identified. This problem neatly demonstrates the goal of QbD – to eliminate the

need for off-line testing by tightly controlling all variability in the process, with continuous monitoring and logging of all product properties from entrance-to-exit. In this manner, the entirety of the released drug product is tested and guaranteed to be safe, at far lower cost than using repeated off-line testing. Currently, testing is done a priori using analytical techniques such as near-infrared spectroscopy [48] and nuclear magnetic-resonance spectroscopy [30]. However, since feedstocks are usually natural products [30], there are many potential sources of variability [58], and it is impossible to eliminate them all. Given measurements of feedstock properties, it can be difficult to know what process adjustments should be made to achieve a consistent final dosage form. The correction of this variability by advanced process control strategies and novel process designs are some of the major thrusts of research in continuous pharmaceutical manufacturing.

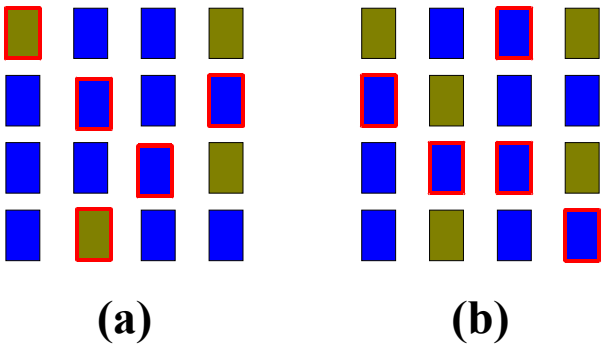

Figure 2.2 (a) Depiction of pharmaceutical lot testing. Blue samples are safe, but brown ones are off-specification.

2.2.4 QbD and Crystallization

Crystallization is a key operation in drug manufacture. In crystallization, one typically desires large crystals with little size variance – or more generally, desires a certain CSD. As we have mentioned previously, crystallization is typically near the beginning to the middle of the flowsheet. There is significant interaction between the CSD obtained during crystallization, and the efficiency of other downstream process operations. Proper development of crystallization processes can provide much greater control over these important properties earlier in the process, making downstream processing much easier – or eliminating certain unit operations altogether. At the same time, it can also greatly improve the drug's final quality. Batch crystallizers, as discussed in section 2.1.4 have serious shortcomings in the way of scale-up, monitoring, control, and product consistency, making it difficult to apply QbD to the full drug manufacturing process. This motivates the development of more novel crystallization technologies, with better control over crystal quality and more economical scale-up [21]. To summarize, proper control of crystallization processes is necessary for quality to be designed into the drug product.

2.2.5 Process Analytical Technology

Process analytical technology (PAT) encompasses a variety of advanced mathematical tools, data management methodologies, and chemical analysis equipment that aid in the production of safe, cost-effective drugs via improved process observation [36]. One might consider PAT to be the evidence-based analog of drug manufacturing, compared to

"evidence-based medicine" in the practice of medicine [34], [63]. Bondi and Drennen [34] bring up the simple but astute point that, unlike virtually every other product a consumer might use in his daily life, he has no idea whether the medicine he is using is working or not. It is critical that drugs released to the public not only be safe, but actually work as intended using proven scientific methods. This is hardly the case with the drug industry today, which relies heavily on end-product testing and strict adherence to master recipes as a means of quality assurance [32]. We discuss several definitions which will be of benefit to the reader. From Yu et al. [64]:

- In-line: Real-time measurement of the process material as it is being processed. This is the ideal method of observing a CPM process.
- On-line: Process material must be diverted to analysis equipment, but is still monitored during the process.
- At-line/Offline: Process material must be taken elsewhere for analysis. This is the standard manner in which pharmaceuticals are tested. At-line refers to analysis at the manufacturing site, offline is elsewhere. Both are undesirable, as they are slow, expensive, and a risk factor for process contamination.
- Invasive: An observation probe must be in contact with the process for a reading to occur. This situation is unfavorable for obvious safety and health reasons. There are also problems associated with fouling of the sensor, chemical attack, and laborious cleaning and sterilization processes.
- Non-Invasive: No probe is necessary. A reading can be obtained without any contact with the process material.

The Venn diagram in Figure 2.3 illustrates which of these qualities belongs to various types of analytical chemistry tools. Monitoring of pharmaceutical and crystallization processes is generally difficult, and significant technical challenges exist in practical implementation of these apparatus for adoption by industry. Non-invasive process analytical technology (PAT) sensors are highly favored by regulators and industry, since there is less direct contact with the process material. The Venn diagram in Figure 2.3 below shows the relationship between the previous categories and the current technologies in use [13], [64]–[71]. Clearly, there is a dearth of noninvasive sensors. The extensive table in Scott and Wilcock mentions virtually every process involved in drug manufacture except crystallization [32]. Process analyzers for pharmaceutical manufacturing are an active field of research, and crystallization is not the only subfield of CPM where new sensors are being developed. Gradinarsky et al. investigated the user of a coaxial microwave probe sensor for the measurement of moisture content in a wet granulator [72]. The use of new PAT sensors for the monitoring of chemical reactions, granulation, and freeze-drying have been reviewed extensively by Scott and Wilcock [32]. Concentration (more generally, supersaturation) is a critical variable in for monitoring in crystallization processes, since nucleation and growth are direct, strong functions of the supersaturation [37]. Sensors such as FTIR [37] and Raman spectroscopy can feasibly measure concentration. FTIR is also suitable for simultaneous measurement of multiple concentrations in a multi-component mixture. Raman spectroscopy is particularly attractive, due to the non-invasive nature of the instrument. Particle vision measurement is probably the most intuitive to understand of all the analytical techniques discussed here – essentially, the technique is simply taking pictures of the crystals, and visually

computing sizes and shapes. However, the image analysis algorithms used to accomplish this physically are complicated. Furthermore, very high solids concentrations will make image analysis impossible, since it will become impossible to differentiate individual crystals.

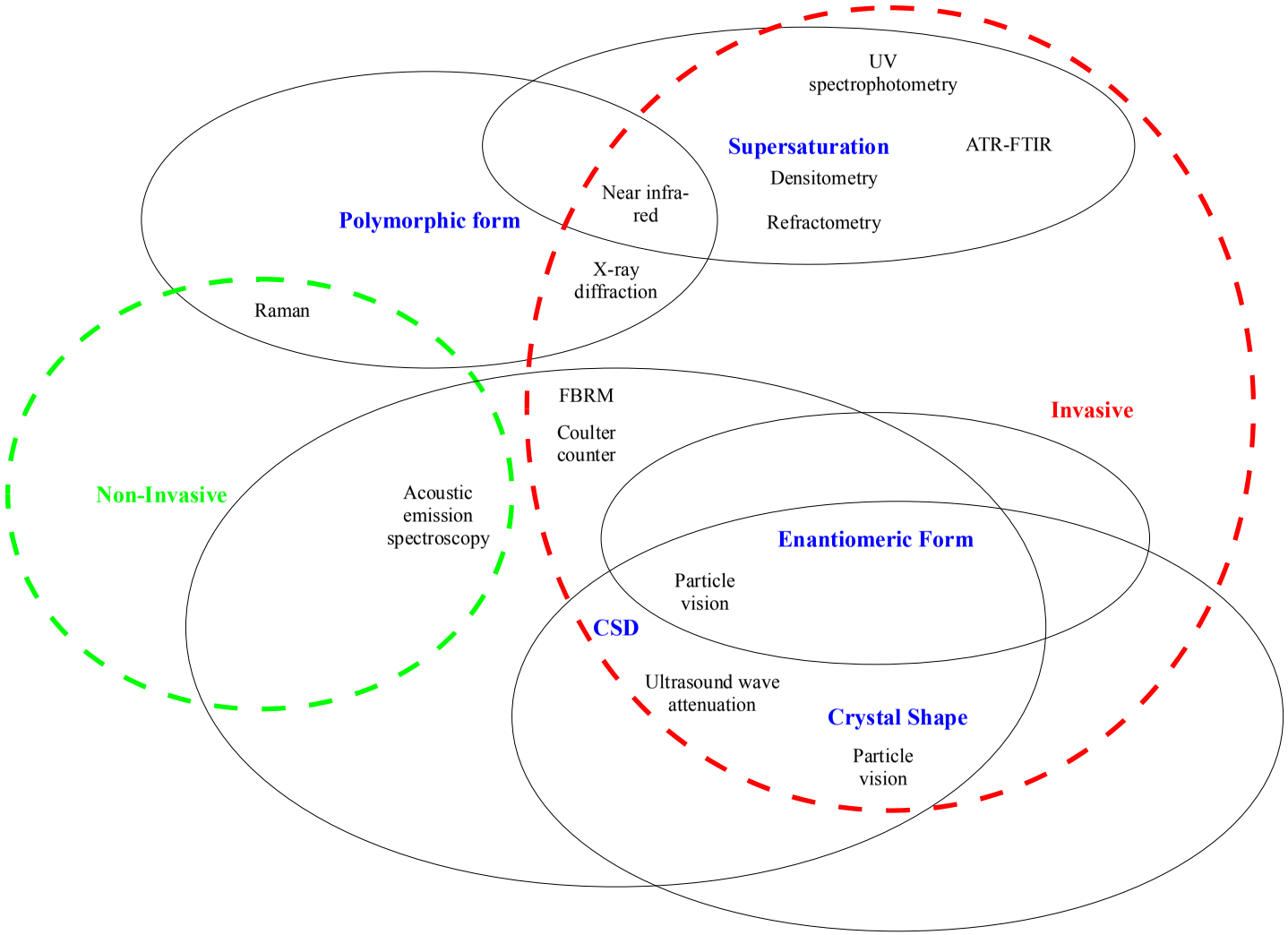

Figure 2.3 Venn diagram of critical process parameters of interest for measurement. As can be readily seen, the overwhelming majority of sensors are invasive.

2.2.6 Real-Time Monitoring and Real-Time Release

Real-time PAT monitoring and control abrogates the need for costly post-hoc rejection testing, and makes feasible the concept of real-time release (RTR), e.g. where the drug is ready to be packaged and distributed as quickly as it is manufactured, with its quality assured [73]. Implementation of PAT for real-time monitoring, feedback control of CPPs (e.g. concentration, purity, temperature, etc.) would permit adjustments within the design space as necessary to keep the product on-spec [13]. This would be a boon to the drug industry, which currently requires about 95 days to turn input raw materials into a final dosage form [32]. RTR also has the significant advantage over batch testing, since the entire drug product being sold has actually been inspected. As reported in Scott and Wilcock, to obtain similar levels of quality assurance with rejection testing would increase the cost of drugs by about 20% [32].

Besides inspecting the entire drug production run, online monitoring also has the potential to do a better job. This is because end-product testing can only detect serious deviations from normal quality and high contamination. Furthermore, end-product testing can only detect bacteriological contaminants that will grow in available biological media reasonably quickly. Online sensor monitoring using PAT tools (e.g. spectroscopy) would be significantly more sensitive to contamination or disturbances than end-product testing. A challenge in crystallization, is the development of sensors that can function without causing contamination, and can operate correctly despite the presence of a liquid and dispersed solid phase.

2.2.7 Multivariate Statistical Methodologies

The complex nature of pharmaceutical manufacturing and crystallization in particular, sometimes make first-principles modeling very difficult, or outright infeasible. In such situation, multivariable statistical "black box" modeling methods can be helpful. Such methods do not seek to match inputs to outputs from a contrived model, but only to find a model that does match by use of experimental data. Techniques such as partial least squares (PLS) and principal component analysis (PCA) can use ostensibly unrelated measurement data to infer and predict system properties [59], [71]. PCA and PLS are useful tools as well for "data-reduction", which is very helpful when dealing with the "data avalanche" typical of CPM processes [13], [74]. Such tools have been used for some time the field of chemometrics [13]. As shown in Bondi and Drennen, methods such as principal component analysis (PCA) can be useful quality assurance parameters, capturing the effect of many variables into a single number, whose deviation from a certain value is a red-flag that something is amiss [34]. The solution of overdetermined systems of equations and redundant measurements can be used to create "soft sensors", which are not actual hardware sensors, but instead are a mathematically-sophisticated state observer [71], [75]. Soft sensors can reconcile large amounts of measurement data with the governing equations to infer an optimal estimate of the true value of the data (e.g. the Kalman filter [75]). By utilizing multiple measurements of completely different natural phenomenon, a more accurate state estimate can be obtained. We cover only small portion of the "CPM-metrics" field here, as the body of literature is extensive. Other methods, such as design-of-experiments (DOE), response surfaces, and Bayesian statistics are discussed elsewhere in the literature [59]. A major challenge in modeling of

crystallization processes is in accurate estimation of their kinetic parameters. Wong et al. [76] have used an artificial neural network to model the crystallization kinetics of lactose, including the agglomeration effect. Using first principles to develop a model including the effect of stirrer speed would have been very difficult. Wu et al. [77] used a full factorial design (3^3) and a combination of linear regression models and a neural network to investigate and model the co-precipitation of naproxen (Aleve™) and Eudragit™. Other works have focused on dimensional reduction, which is a very powerful method for simplifying the data analysis, control, and fault diagnosis [59], [78], [79] of experiments involving CPM processes. Tomba et al. applied a multivariate statistical framework for organizing and analyzing data from a granulation and tabletting process [59]. PCA was used extensively in that work to identify dominant variables amongst a large possible set, in order to properly identify critical process parameters. Routinely a space of 10 or more variables could be described with only 2 or 3 principal components. Such an approach can be highly useful in CPM processes. The thesis by Cipich discusses the use of several multivariate tools for the detection of systematic ("gross") errors in a continuous tablet pressing process [29]. In that work, several statistical tests are used for fault detection, and a quadratic programming problem is solved to reconcile the process measurements.

2.2.8 Technologies for Powders, Particles, and Tablets

While this work is focused mainly on crystallization, it is important for the reader to have an understanding of the CPM field as a whole. Over 80% of drug FDFs are oral tablets,

which are manufactured by blending API with powder-phase excipients and pressing them [29], [80]. Proper control over crystal properties is necessary to achieve a good press. Oral tablet FDF's have a variety of manufacturing difficulties caused by the complicated interactions within multicomponent powder mixtures. Powders possess properties significantly different from the bulk phase. Particle modification processes are often necessary to ease handling, such as wet or dry granulation. Such powder systems are difficult to mathematically model, and cannot be realistically modeled as fluids. Kleinbudde [28], Vervaet and Ramon [31], and Pernenkil and Cooney [57] have reviewed the processing of pharmaceutical powders in depth. A vast amount of research has been done on process design, modeling, and simulation of pharmaceutical powder processes. We present a brief summary of the research on solid pharmaceutical processing in Table 2 below. Boukouvala et al. [81] modeled and simulated continuous blending processes for the homogenization of two-powder mixtures. Four-dimensional population balance models have been used to track the distributions of size, composition, liquid content, and porosity of particles within a wet granulator [25]. The discrete element method has been used to examine the variability in film properties of liquid-coated tablets in rotary coating equipment [82]–[84]. Sinha et al. used finite element methods borrowed from the field of soil mechanics to investigate the compaction of powders during tablet pressing [85].

Table 2 Summary of pharmaceutical solids processing technologies.

Technology(ies)	**Applied Towards**	**Reference**
Population balance model, discrete element method simulation	Continuous blending of dry powders	Boukouvala et al. [81]
Four-dimensional population balance model	Wet granulation	Barrasso and Ramachandran [25]
Discrete element method	Coating of tablets	Kalbag and Wassgren, Freireich and Wassgren, Freireich et al. [82]–[84]
Finite element method	Modeling the tablet compaction process in a die	Sinha et al. [85]
Fault detection and exceptional events	Tablet pressing and dry granulation	Cipich [29], Hamdan [80]

2.2.9 Pharmaceutical Informatics

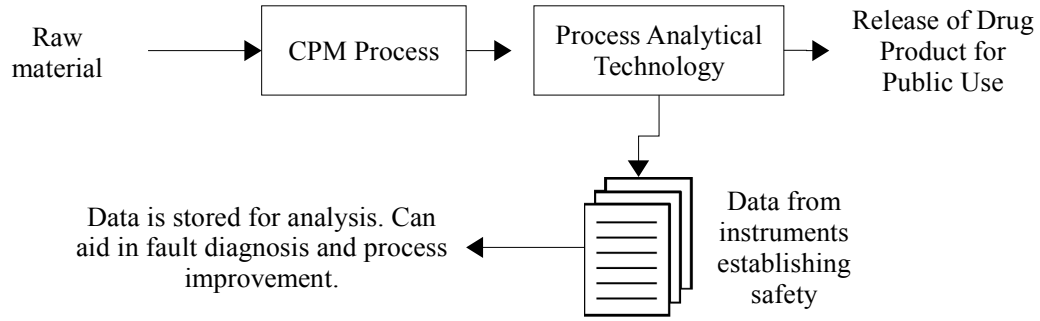

Figure 2.4 Conceptual diagram of CPM implementing PAT for real-time release of final drug products. Information collected from analytical chemistry equipment (among other things) provides evidence of safety and quality.

Pharmaceutical informatics is the application of management information systems (MIS) tools to the observation and improvement of pharmaceutical manufacturing processes and quality control [13], [32]. Figure 2.4 above illustrates how the large amounts of data that can be collected from monitoring tools are another route for implementing QbD and continuous improvement. Informatics and data mining methods are useful for finding unforeseen process defects and rapid fault correction [86]. The enormous amounts of data produced and demanded by the pharmaceutical supply chain forms a complicated data management problem. Venkatasubramanian [74], [87] and Zhao [88] discuss pharmaceutical informatics in greater detail. Further discussion of information management/big-data analytics applied to pharmaceutical manufacturing is beyond the scope of this work.

2.2.10 Process Control

The last major topic for review is a discussion of the optimization and process control of CPM processes, in which continuous crystallization is utilized. In the manufacture of chemical products, a proper control system is vital for ensuring process stability and safety. This is especially true in the drug industry, since not only plant personnel but the customer depend on the proper operation of controllers. For smaller-scale processes, separate control loops for each unit operation provide a simple method for controlling the entire process. However, for much larger plants and production levels, the number of control loops can reach into the thousands, and there can be a significant amount of detrimental interaction between different unit ops. The optimal control strategy for the process as a whole will be much different (and significantly more efficient) than a strategy that is optimal unit-op-by-unit-op. Model-based control of batch and continuous crystallizers is reviewed in [86], [89]–[91]. This problem of plant-wide control (PWC), refers to the choices of controlled variables, manipulated variables, what measurements will be made, and what types of controllers will be used [92]. It is a problem of immense difficulty and practical importance, and its difficulty is compounded by the presence of disturbances and uncertainty in process parameters, as well as the fact that the optimal control structure can shift with time due to market conditions [92], an issue of great importance to the pharmaceutical industry. Plant-wide optimization and plant-wide control has been applied extensively in other areas of the chemicals industry. Challenges arise in the full optimization of CPM flowsheets, due to the complexity of the models used to describe underlying physical phenomena. Among other methods, an optimization approach can be applied to PWC, by sifting through possible control structures in some

fashion, simulating the plant with the generated structure and assumed disturbances, and then calculating a scoring function based upon the observed dynamic and steady-state performance (typically profit maximization.) In general, this is a difficult constrained combinatorial optimization problem (generally, a mixed-integer nonlinear programming problem, or MINLP), requiring a great deal of computing power to iteratively simulate the plant. CPM processes are especially difficult to rigorously optimize due to model complexity. There are a variety of computational difficulties related to fast and accurate solution of the model equations involved. In addition to solving the mass and energy balance equations for the plant, the population balance equations must also be solved for relevant unit operation. Powder processing operations, such as granulation, blending, and tablet coating, require costly discrete element method (DEM) simulations to model correctly, as mentioned in section 2.2.8. This problem stymies the use of rigorous optimization for solving the plantwide-control problem for CPM processes [91]–[93].

2.2.11 Specific Examples of Plantwide Simulation, Control, and Optimization

A review of various plant-wide control methodologies is given by Vasudevan and Rangaiah [93]. In that work, one can observe a variety of industrial chemical processes for which PWC has been applied; none of these are pharmaceutical processes. Clearly, there is a limited amount of literature available on the subject. However, an important result from the literature studies discussed here is that parameters upstream from the process can have a significant impact on the quality of the final drug product. Mascia et

al. utilized a two-layer approach to control system design for their continuous tablet manufacturing pilot plant [23]. One layer was used for stabilization, whilst the other was for controlling quality. The stabilization loop kept each unit operation within its specified bounds, while the quality controller focused on guiding the process to ensure the produced tablets met quality standards. They present data that demonstrate process resilience against disturbances. Lakerveld et al. examined the use of optimal average level control to control disturbances in a buffer tank downstream from a crystallizer and upstream from a chemical reactor. The exit concentration and outlet flowrate of the buffer tank was used to stop the propagation of disturbances from affecting the downstream reactor. The overall work shows robustness is an important requirement for effective control of a pharmaceutical process. Sen et al. [53] reported results for modeling and simulation of a continuous pharmaceutical process. The process consisted of a continuous cooling crystallizer, filter, fluid-bed dryer, and screw blender process for production a final drug product. Using a dynamic PBM-DEM (population balance model-discrete element method) model, they investigated the effect of various parameters on the homogeneity of the API-excipient mixture produced by the blender. As expected, altering the cooling profile of the crystallizer changes the output crystal CSD. However, the different CSDs obtained showed a different dynamic response in the API content of the blended drug formulation, with some profiles being more sluggish than others to reach the desired final value. Suggested in their study, optimization of the cooling profile could produce a faster result in the blending process, decreasing the amount of wasted product. Benyahia et al. [20] performed a much larger dynamic flowsheet simulation. A CPM pilot plant was simulated using a sophisticated dynamic model, totaling 10^4 differential

equations and 2×10^3 algebraic equations. The simulated plant produced drugs directly from scratch; taking in raw reactant material at the entrance, and producing coated tablets at the exit. The effect of changing raw material, excipient, and equipment parameters upon the final product purity was experimented with via simulation. Impurities emanating from the first reactor in their flowsheet were found to have a significant impact on the performance of the entire process. Ward et al. [91] have developed a plant-wide control approach for a combined process consisting of reaction in a CSTR, MSMPR crystallization, and then filtration with liquid recycle back to the CSTR. While not explicitly applied to pharmaceutical processes, the scenario is general enough to warrant discussion here. Despite being able to find well-performing control structures for the process, some would require real-time monitoring of CSD (or average size) as well as supersaturation, with no measurement error or time delay. While various monitoring setups have been demonstrated in the literature for measuring supersaturation and CSD, this is generally not the case in industry. Finally, a different problem was solved altogether by Levis and Papageorgeiou [33]. In that work, the investigators formulated a large mixed-integer linear programming (MILP) problem for large-scale optimization of an entire pharmaceutical enterprise. The problem was to optimize over a choice of possible products, how the geographically-distributed manufacturing network would be set up, what sales goals would need to be met, and how much inventory to hold on hand, subject to a large number of constraints, for a time span of 13 years (3 years of clinical trials, 10 years of profitability). This work demonstrates the combinatorial nature of decision-making pharmaceutical manufacturing management. It is interesting to note that the time required to scale-up a process is explicitly incorporated into the problem

formulation. The work also demonstrates how much the geographical distribution of operations complicates decision-making in the drug industry, and suggests how much easier it would be if drugs could be processed entirely in a single location.

2.2.12 Uses of Simulation

As mentioned previously, an important issue in the design of CPM processes is understanding how different unit operations interact with each other, either regarding the change in location of the steady-state with various parameters, or transient interactions in their dynamics. Simulation is of great usage in the study of chemical processing plants. Related to pharmaceutical manufacture, even slight variations in an upstream process (or more likely, a feedstock), could propagate in a highly counter-intuitive fashion downstream, rendering the final drug product ineffective or unsafe. Dynamic models permit analysis of transient responses, allowing one to see how long the process requires to reach steady state [1]. This is especially important in drug manufacture, as API is often expensive to waste, and precise quality is required [5]. Programs such as gPROMS and PARSIVAL have been used in the literature for such simulation work, along with custom-written programs [53], [94]. In this work, we have opted to write our own software in MATLAB for simulating and optimizing the crystallization process.

To summarize our thoughts on continuous pharmaceutical manufacturing (CPM), a variety of technologies are being researched in this field. By using process systems

engineering concepts for planning the process combined with real-time monitoring and control, variability in the final product can be greatly reduced or eliminated altogether. Quality-by-Design (QbD) is a manner of designing the process as such that all variability is minimized, eliminated, monitored, and controlled. Batch crystallization is a barrier to implementation of QbD, since batch processes impart uncontrollable variability into the final product. A variety of new analytical sensors are being designed in order to enabled noninvasive, continuous on-line and in-line process monitoring. Multivariate statistical methodologies are also being applied as "soft sensors", where knowledge of model equations and a known set of observations can be used to refine the current state estimate. Population balances, finite element methods, and discrete element methods have been applied to the difficult matter of modeling solids processing operations, such as wet/dry granulation, tablet pressing, tablet coating, and of course, crystallization. Plant-wide control and multi-unit modeling and optimization have been applied to pharmaceutical processes.

2.3 The Basic Science of Crystallization

Crystallization can affect important physical properties of drug products, such as enantiomeric excess, polymorphic composition, and CSD (see Shekunov and York [21]). These variables are directly related to either the dissolution rate, or in the case of enantiomeric excess, whether the drug is therapeutic or outright toxic. Table 3 below discusses the type of impact that crystallization can have on the final drug properties, as

well as the current degree of control capability. The table also shows how certain properties may impact the process heavily, but not the curative properties of the drug, and vice versa. This is especially true of enantiomeric form, which has virtually no impact on the process, but can mean the difference between producing an effective drug or a deadly toxin.

A short tutorial on crystallization can be found in [38], and the review article by Chen [24] discusses matters specific to pharmaceuticals. Work by Jones [40] and Tavare [51] focus more on engineering aspects. The science of crystallization is discussed at length in the review article by Dirksen and Ring [95], as well as books by Desiraju et al. [96] and Davey and Garside [97]. The basic principle behind crystallization is to alter the ambient conditions of the liquid solution (such as by cooling, evaporation, or drowning out) so as to create a solution which is holding more solute than the solubility limit would prescribe. Such a liquid is known as a supersaturated solution, and supersaturation is the driving force for the nucleation and growth of crystals. Figure 2.5 below depicts the solubility curves for antisolvent and cooling crystallization. Before discussion antisolvent and cooling crystallization in detail, we make general remarks true about *any* solubility phase diagram.

Table 3 The impact of crystallization on important drug properties, and the current capability of control.

Property	Biological Impact	Process Impact	Controllability
CSD shape	• Dissolution kinetics. • For multivariate CSD, becomes conflated with crystal shape.	• Shape affects tableting strength. • Fines more difficult to separate. • Affects washing and drying processes. • Affects flowability.	Moderately good
Polymorphic form	• Dissolution kinetics. • Solubility. • Bioavailability. • Shelf-life stability of drug.	• Effect is conflated with crystal shape. • Affects hygroscopicity.	Poor
Crystal shape	• Not much impact - unless conflated with a different polymorphic form.	• Needles cause filtering problems. • Affects suspension rheology. • Affects flowability and bulk density.	Poor
Enantiomeric form	• Wrong enantiomeric form can either be non-curative, or harmful to the patient.	• Virtually none. Enantiomeric crystals are, by definition, mirror images of each other.	Varies
Amorphous character	• Dissolution rate increases with increasing amorphous character. • Affects shelf-life stability.	• Amorphous form is unstable; may be difficult to manufacture.	Poor
Purity	• Safety and curative properties of drug.	• Generally, small purity deviations will cause little impact.	Difficult for very low impurity levels

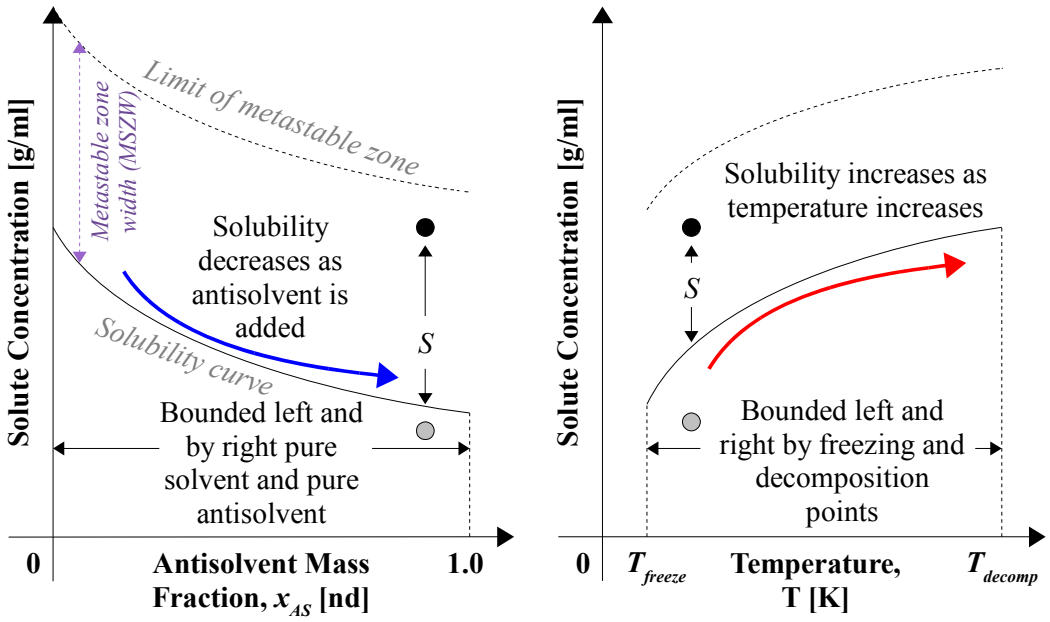

Figure 2.5 Antisolvent addition and cooling crystallization methods, and illustration of the solubility curve. The metastable zone is the supersaturation limit at which primary nucleation occurs. The black points are supersaturated solutions, and the gray points are undersaturated.

- Below the solubility curve, dissolution occurs. The solution is *undersaturated*.
- On the curve, the crystals are in equilibrium with the liquid phase. The liquid phase is said to be *saturated*.
- Above the solubility curve lies the metastable zone, where crystal nucleation and growth occur. Here the liquid phase is said to be *supersaturated*, and the distance above the solubility curve is known as the *supersaturation*. Nucleation occurs here after a period of time known as the *induction time*.

- Above the metastable region lies the *limit of the metastable zone* (also known as the *labile region*). In this region, nucleation is triggered immediately.

Supersaturations above the metastable boundary can result in amorphous solids and oils [43]. While gas-phase crystallization is possible, industrial practice is typically confined to a liquid phase, especially concerning pharmaceuticals [98]. Crystals are produced by creating a supersaturation (S) within the API solution. A variety of phenomena can be employed to create a supersaturation. Here we introduce the two most-common methods of crystallization: antisolvent and cooling.

2.3.1 Antisolvent Crystallization

Antisolvent crystallization (left in Figure 2.5) is performed by adding a second liquid to a saturated solution in which the solute is much less soluble. Addition of this this second liquid, termed the antisolvent (also termed the co-solvent or diluent), gradually reduces the solubility of the mixture, generating a supersaturation. Manipulation of pH can also work in this fashion [99]. The ordinate of this solubility curve is the solute concentration, and the abscissa is usually either the mass fraction or volume fraction of antisolvent in the mixture. The upper and lower bounds on possible antisolvent mass fractions, of course, are $x_{AS} = 0$ to $x_{AS} = 1$.

2.3.2 Cooling Crystallization

Cooling crystallization (right in Figure 2.5) exploits the temperature-dependence of solubility. In this method, a saturated hot solution is rapidly cooled, which decreases solubility, and hence generates a supersaturation. The lower and upper bounds on temperature are the freezing point of the solution (T_{freeze}), and the decomposition temperature of the API molecules (T_{decomp}). If T_{decomp} is very low, then cooling crystallization becomes impractical, which motivates the use of the antisolvent method. While the discussion of additives and impurities is beyond the scope of this work, it is worth mentioning that solubility curves can be sensitive to impurities even down to the ppm level [40]. We also note that cooling and antisolvent crystallization can be done simultaneously.

2.3.3 Other Methods

Antisolvent, cooling, and vacuum crystallization represent the overwhelming majority of industrial crystallization methods in practice, but there are some more rare methods used or encountered in nature. An arcane example is high pressure crystallization. This method has been used specifically for the separation of mixtures of cresols by using high pressures to manipulate the melting points of the individual cresol species in the mixture [51], [100]. Evaporation is another crystallization method. Under moderate heating, the liquid phase can be driven off by evaporation, which causes a rise in solute concentration due to loss of liquid volume. An evaporative salt pond is an example of such a

"crystallizer." A combination of evaporation and cooling can be done in tandem with vacuum crystallization, which applies suction to the system to more rapidly remove vaporized solvent. A much rarer example is reverse osmosis. Reverse osmosis can also be used to generate a supersaturation by the expulsion of the solvent across a semipermeable membrane. While almost never used for practical crystallizations, reverse osmosis crystallization is known to precipitate kidney stones and gallstones in the human body [51]. More recently discovered methods of generating supersaturation utilize bubbles from dissolved gases, electric fields, and lasers. Rungsimanon reports the use of focused lasers to crystallize γ-glycine, with subsequent dissolution upon deactivation of the laser [101], [102]. Similar results are reported by Yuyama for L-phenylalanine [103]. The references in Llinas and Goodman [99] discuss laser nucleation in greater depth. Aber et al. report the use of strong electric fields to trigger nucleation of γ-glycine in aqueous solution [104]. Knott et al. report a variety of results related to their work on triggering crystal nucleation of aqueous glycine by shaking dissolved argon gas bubbles out of the solution [105]. Ultrasound-induced crystallization [99]. While the mechanism is still unknown, it is conjectured that the collapse of cavitation bubbles causes a large local increase in temperature. This creates a great increase solubility, followed by subsequent cooling from contact with the bulk solution, generating a large supersaturation. Narducci et al. [106] have experimented the use of ultrasonic waves for shape control of adipic acid particles. In both continuous and batch mode, smaller, rougher, spherical crystals were produced than other methods – such as wet milling. The authors suggest improved mixing from the ultrasound as the mechanism for the shape changes.

2.4 Kinetic Processes in Crystallization

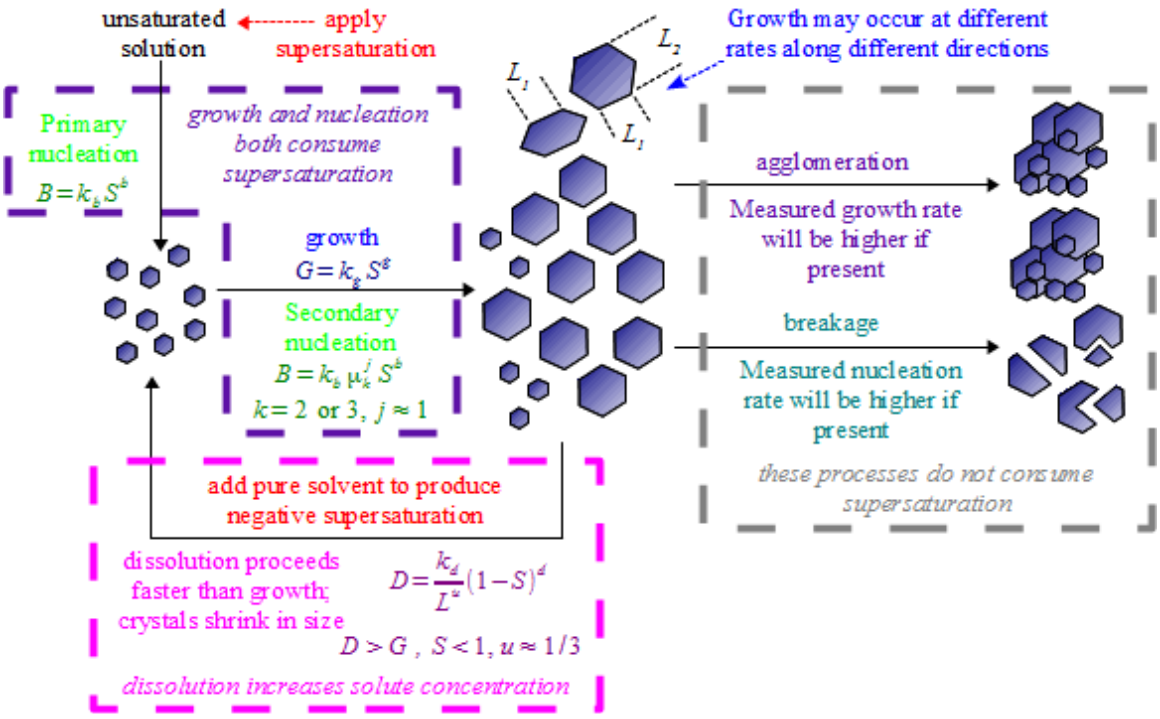

Figure 2.6 Basic kinetic phenomena in crystallization processes.

An understanding of the basic kinetic processes is essential to understanding crystallization. The diagram in Figure 2.6 above summarizes the important kinetic phenomena in crystallization processes. More detailed discussion of crystallization kinetics can be found in [97], [107]–[109]. Supersaturation provides the driving force for nucleation and growth; the greater the supersaturation, the higher the rates of nucleation and growth. Supersaturation is some measure of the quantity S in Figure 2.5. However, supersaturation goes by a variety of monikers. The most commonly encountered measures of supersaturation encountered in the literature are:

Supersaturation difference, or commonly "the supersaturation" is given by:

$$\Delta C = C - C_{sat} \tag{2.1}$$

Where C is the solute concentration (kg/m^3 or kg/kg solution), and C_{sat} is the solubility concentration (the dark curve in Figure 2.5).

The dimensionless "supersaturation ratio":

$$S = C/C_{sat} \tag{2.2}$$

Or lastly the "relative supersaturation"

$$S_{rel} = (C - C_{sat})/C_{sat} \tag{2.3}$$

As we shall see in the further sections, greater supersaturation leads to faster rates of nucleation and growth.

2.4.1 Nucleation

Nucleation is a fundamental process in crystallization. In nucleation, new crystals are formed due to a supersaturation. Nucleation can occur in a variety of ways, such as primary, homogeneous, hetereogeneous, and secondary modes. The exact mechanisms for growth and nucleation are currently not well understood [24], [47]. The most common theory is that of nuclei or classical nucleation theory. Upon reaching a certain critical radius, incipient crystals (termed "embryos") no longer dissolve back into solution, but continue to grow and form a crystal lattice. Nucleation rate increases not only with the supersaturation, but the absolute solubility as well. This is due to the fact that the rate of

cluster formation depends on the probability of solute molecule collisions, which increase monotonically with increasing solubility. Hence, a lower supersaturation is required to achieve a given nucleation rate at a higher solubility [110]. Furthermore, nucleation rate is dependent on liquid viscosity, since greater viscosities impart greater diffusional resistance from solute particles interacting with a cluster [110].

Primary nucleation is any nucleation process in which *no crystals are initially present*. In any supersaturated solution is a large collection of liquid-phase molecular arrangements with the potential to become crystals, termed *embryos*. The transition from embryo to crystal requires passage over a free energy barrier. The energy barrier to crystal formation is formed by two opposing thermodynamic processes. First is the *unfavorable* process of increasing the surface area of a new phase (e.g. the crystal). Secondly is the *favorable* process of a solute molecule transitioning from the liquid phase and integrating into a new solid phase. Once an embryo reaches a *critical radius*, r_c, the free energy barrier rolls downhill. Once this occurs, crystal formation becomes spontaneous, and a new crystal pops into existence. The theory of primary nucleation is explained in more detail elsewhere ([40], [97], [109], [111]).

Homogeneous nucleation occurs when crystals nucleate directly within the bulk phase of the solution, away from interfaces such as vessel walls and suspended impurities. Homogeneous nucleation is only achievable under highly contrived experimental conditions, and is almost never observed in nature. It also requires very high supersaturation levels to observe, showing that the barrier to homogeneous nucleation is

large. Small droplets dispersed within a two-phase immiscible flow are one such way to experimentally observe homogeneous nucleation [110]. Large volumes (> 100 μl [110]) are typically incapable of homogeneous nucleation, since impurity contamination is too difficult to control.

More commonly encountered is heterogeneous nucleation, where nuclei form on external surfaces in contact with the liquid phase. Foreign particles and vessel walls are typical nucleation sites. When no seeds are present in the solution, no extra surfaces are available for nucleation. This leads to a nucleation law of the form:

$$B = k_b S^b \tag{2.4}$$

Where B is the nucleation rate (#/m^3·s), k_b is the nucleation rate constant (#/m^3·s), S is the supersaturation ratio (dimensionless), and b is the nucleation order (dimensionless). Any of the other definitions of supersaturation described in section 2.4 are also valid with (2.4).

When crystals are already present in the system (a "seeded" solution), the extant crystals provide extra sources of nucleation. During secondary nucleation, the extra surface area provided by the extant crystals possesses more nucleation sites than the solution by itself. Furthermore, processes such as shear-induced crystallization and crystal-crystal contact can trigger additional nucleation as well. The number of nucleation sites scales upward with the content of crystals in the slurry, and thus expressions for secondary nucleation include an intensive quantity term for total crystal content. This leads to secondary nucleation, with a rate law of the form:

$$B = k_b \mu_k^j S^b \tag{2.5}$$

Where μ_k is the k^{th} moment of the crystal size distribution. Often, $j \approx 1$, and $k = 2$ or 3. The moments are directly related to the quantity of crystals in the solution, so this expression intuitively makes sense (see [111] for a discussion of crystal moments). The more crystals there are in the solution, the more secondary nucleation we would expect. The units of k_b depend on the values of k and j, but the units of B are still #/m^3·s. Typical bounds on B are given on page 60 of Tavare [51] as $10^6 - 10^{16}$ #/kg·s for primary nucleation, and $10^2 - 10^{10}$ #/kg·s for secondary nucleation. Nucleation order tends to be $0 < b < 5$.

2.4.2 Growth

While some nucleation is required in an unseeded solution to "get the ball rolling", nucleation is generally undesirable in crystallization processes. Crystal growth is the main phenomenon we wish to encourage in our crystallization. More growth means larger crystals, and larger crystals are generally better. During crystal growth, solute molecules integrate, layer by layer, into the crystal lattice. Typically, growth is generally bottlenecked by the surface integration step, where incoming solute molecules must possess a particular intramolecular configuration to be able to bind properly to the crystal lattice. Growth may be diffusion limited as well. While other expressions do exist, as given by [112], the most common form of the growth rate encountered in the literature is:

$$G = k_g S^g \tag{2.6}$$

Where G is the growth rate (μm/s), S is the supersaturation ratio, k_g is the growth rate constant, and g is the growth order. Typical bounds on G are given by Tavare [51] as $0.001 < G < 1$ μm/s, and typical bounds on the kinetic constants are $0.001 < k_g < 1$ μm/s, and $0 < g < 3$. For size dependent growth, a common expression is [113]:

$$G = k_g S^g (1 + \gamma L)^p \tag{2.7}$$

A common feature (and manufacturing difficulty) of pharmaceutical drugs is their very slow growth rates and poor water solubility (~10^0-10^1 μg solute/g H_2O) [114]. Pharmaceutical API's are typically complicated organic molecules with many internal degrees of freedom [22], which creates a high entropic barrier to surface integration, even when enthalpy change is highly favorable. Growth rate dispersion is the phenomena observed where crystals of the same size, under the same ambient conditions, display two different growth rates. The root cause of this phenomena is the intrinsic stochasticity of crystal growth. The stochastic nature of crystallization is apparent at low liquid volumes, where it is possible to observe nucleation in one small volume of liquid, but not in another. Likewise, growth rate dispersion is also a stochastic process (or can be modeled as such) as solute molecules have a chance associated with themselves at any instant of time to choose to integrate into the crystal lattice of a given crystals in the slurry.

Chemical additives can stunt growth along certain directions, leading to a preferred crystal habit [47]. The addition of chemical additives (or, "process control agents") to the

crystallizing solution can have a variety of helpful benefits. Typically, one uses additives with a similar structure to the subject molecule. The presence of even small amounts of additive can change the relative growth rates between various crystal faces, altering the crystal's shape. Additives can also improve the tableting process [21]. The use of additives is unexplored territory concerning our work. In this thesis, we have only exploited supersaturation as a control, while a more sophisticated scheme for controlling crystal shape could use additive concentration as a control as well.

2.4.3 Dissolution

The dissolution rate of pharmaceuticals strongly impacts their bioavailability. When an oral dosage form is ingested, the excipient binder is digested away in the stomach, and eventually discharged to the small intestine. In the small intestine, drug uptake is achieved and the drug finally enters the blood stream. However, the degree of uptake is dependent on the drug's concentration at the tissue surface. This of course, depends on how well the drug dissolves in aqueous solution. Most pharmaceutical drugs are poorly soluble in water, on the order of a few micrograms per gram. The poor solubility and dissolution rates have led to many engineering approaches to increase dissolution rate, including mechanical micronization, and the production of small crystals and nanocrystals, and amorphous forms. Amorphous solid forms are of interest, since they are less stable than crystalline forms, and as such exhibit faster dissolution.

The gray points in Figure 2.5 on page 44 indicate a solution that is *below* solubility. When concentration is below the solubility concentration, the solution is said to be *undersaturated*, which leads to the dissolution of crystals. During dissolution, crystallized solute molecules break of and dissolve back into the solution. This causes the solute concentration to rise to the solubility curve and attain equilibrium. Dissolution is typically much faster than growth, since there is no surface integration step. Some expressions for dissolution from the literature include [113], [115]:

$$D = \frac{k_d(1-S)^d}{L^q} \tag{2.8}$$

The exponent of the dissolution law is usually 1, which makes for much faster "reverse growth." Typically also $k_d \gg k_g$. Furthermore, small crystals typically dissolve much faster due to the Gibbs-Thomson effect [116]. CHAPTER 6 incorporates dissolution into the framework, in an effort to exploit the phenomena to eliminate fine crystals.

2.4.4 Agglomeration and Breakage

Agglomeration and breakage do not consume supersaturation, but affect the CSD in other ways. Breakage is typically cause by a moving surface, such as the impeller. Agglomeration is caused by high surface energy. Both agglomeration and breakage greatly complicate the solution of population balance equations, since these phenomena are mathematically expressed as an integral. Further discussion of agglomeration and

breakage are beyond the scope of this work. A detailed discussion of agglomeration and breakage are beyond the scope of this work.

2.5 Polymorphic Form and Chiral Form

While this thesis is concerned with the control of crystal size, polymorphism is a critical quality attribute for pharmaceutical manufacture. We give a brief overview of polymorphism in this section, as well as recent developments in observation and control of solid forms. Polymorphism has substantial impact on drug discovery, manufacture, and efficacy [22], [96], [43], [117]. Some polymorphic forms of an API are more preferable for pharmaceutical use, due to faster dissolution rates and higher bioavailability. The proclivity of a substance to take on different polymorphic forms during crystallization complicates the development, patenting, and manufacture of pharmaceuticals. Desiraju et al. [96] discusses several industry case studies that led to lawsuits, recalls, and product failure – namely the anti-ulcer drug Ranitidine (Zantac), and the AIDS drug Ritonavir. Generally, the thermodynamically most-stable form is preferred to remove the possibility of a phase change on-the-shelf, but a more bio-active, kinetically-trapped form may be preferable.

2.5.1 General Background and Properties of Polymorphs

Solid-phase forms fall into four types: polymorphs, solvates, desolvated solvates, and amorphous compounds [21]. While these each have their own nuances that are important to product and process development, for brevity we focus only on true polymorphs. Two or more different polymorphic forms of a substance possess the same chemical formula, but have different molecular packing arrangements that generate the lattice [22], [96]. Complicated organic molecules, such as pharmaceuticals, are typically bedeviled by several polymorphic forms due to many internal and external degrees of freedom for arrangement [99]. While aspirin only has one known form, carbamazepine has four, and olanzapine has six [99]. Polymorphism affects a variety of macroscopic properties, such as color, density, crystal habit, melting point [22], [96], [43], [99]. Internal transport properties, such as thermal and electrical conductivity, can also substantially differ. Furthermore, the surface exposure of certain chemical moieties and crystal faces can impart increased chemical reactivity, dissolution rate, and solubility in one form compared to another [22], [99], [118]. This is especially true of amorphous solid forms. Dissolution rate and solubility directly impact the potency of oral tablets, the most popular dosage form [22]. Many common pharmaceutical unit operations (e.g. crystallization, freeze-drying, milling) can alter the solid form in difficult-to-predict ways [21]. Milling and other size-reduction operations are known to induce polymorphic changes in fed crystals [21]. Maintaining target solid-form and while maintaining other process variables is also difficult. Reutzel-Edens mentions a study in which the filtration and drying produced the desired solid-form of the API, but that solvent removal dramatically altered the crystal size distribution [22].

2.5.2 Polymorph observation and control

While critical to product safety and quality, monitoring and control of polymorphic crystallizations is still poorly understood. Both observation and control of polymorphic form are major challenges in crystallization [119]. More work is listed therein pertaining to other process variables, such as concentration and crystal shape. Raman spectroscopy, near-IR, and mid-IR have been used for observation of solid form previously. Indirect approaches to polymorph observation and control have been applied [22]. One study mentioned in [22] successfully prepared one form of an enantiotropic compound by seeding the process with the desired polymorph, and keeping the temperature below the intersection temperature on the two solubility curves. Another study inferred polymorphic form by the investigators noticing that, for their particular API, the formation of an undesired solvate also formed a quasi-emulsion. Studies using particle vision measurements (PVM) allowed the research team to identify correct operating conditions to avoid the emulsion formation, as well as generating the desired non-solvate form. Solid-form can be ascertained by X-ray powder diffraction (XRD), differential scanning calorimetry (DSC), relative humidity measurement (%RH), and Laue diffraction [21]. Such methods however, are not readily amenable to continuous monitoring. Continuous, quantitative control and monitoring of solid-phase form is a major research challenge. Some methods for altering the solid-phase form is manipulation of the solvent used for crystallization. The solvent used can strongly impact the crystallized polymorph [118]. Supersaturation is theoretically useful as a control, however, this is only for the production of amorphous forms, and can only be done at very high supersaturation [21]. Rungisimanon et al. have demonstrated an interesting

new method for direct and selective crystallization of certain polymorphs using laser radiation [101], [102].

2.5.3 Chiral Form

The enantiomeric form of the molecules composing a given crystal, while practically irrelevant to the manufacturing process, can be critical to the final product quality and safety [120].

About 50% of sold drugs are chiral [21]. Chiral crystallization is often difficult and expensive to do, rendering many drugs infeasible to produce. A variety of methods are possible for controlling enantiomeric form, depending upon what level of separation resolution is required. Direct crystallization into two chiral forms (also referred to as "preferential crystallization") can be done by cycling between optically-pure seed crystals of each stereoisomer, while avoiding nucleation. Often this method is not possible, since crystallization into a solid racemate is often thermodynamically favorable [21]. Other methods are also possible for more difficult cases, such as performing the crystallization in a chiral compound, or reacting the racemate of the API to create a new substance for which preferential crystallization is possible [21]. Selectivity in chiral form can be achieved by seeding with the desired chiral form [121], as well as polymorphic form [118].

2.6 The Quantitative Framework of Crystal Size Distributions

During crystallization within solution, imperfect mixing causes spatial gradients in supersaturation. These localized gradients, along with the stochastic nature of growth and nucleation processes, produces crystals of non-uniform size and shape. To mathematically describe these variations in crystal size, one uses the concept of a crystal size distribution (CSD). The framework is discussed in exhaustive detail in the books by Jones, Garside and Davey, and Randolph and Larson [40], [97], [111]. We present here the most crucial aspects for understanding this work.

A characteristic length is a chord piercing through a crystal along an arbitrary direction in R^3. A chord is any line joining two faces of the crystal polytope. For an irregularly shaped, nonspherical crystal, (Figure 2.7a) there is no unique chord with which we can measure the length of a given crystal. A perfectly spherical crystal (Figure 2.7b) is the only crystal which can be uniquely defined with the single characteristic chord length. Crystal shape can be described in this way by using multiple length measurements for each crystal, yielding a multidimensional CSD [111]. Additional lengths provide more information about the crystal size population, at the cost of increasing complexity. The distribution of characteristic lengths in a collection of crystals defines the crystal size distribution, a critical quantity in assessing the performance of crystallization processes and drug manufacture.

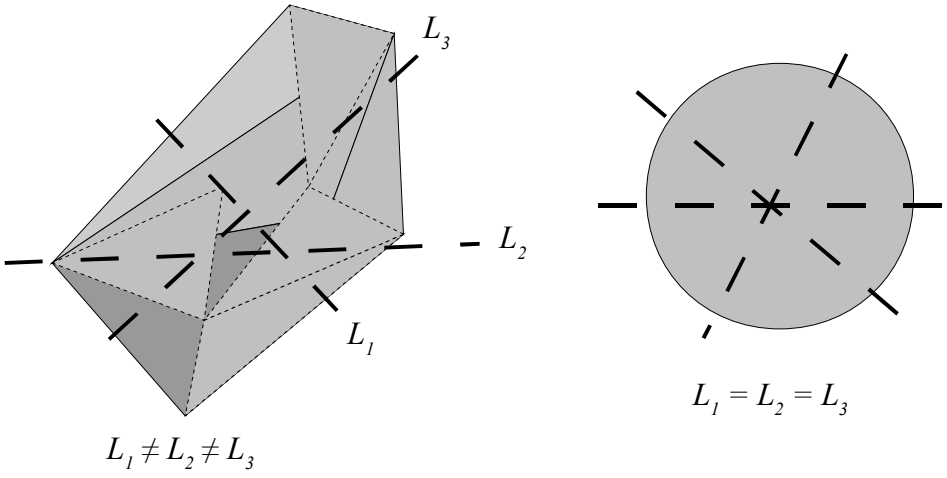

Figure 2.7 (a) An irregularly shaped crystal has an infinite number of possible characteristic lengths one can arbitrarily choose for measuring its size. (b) The only shape possessing a unique direction is a perfectly spherical crystal, for which all of the possible characteristic lengths (passing through the sphere's center) are exactly the same.

2.6.1 Crystal Size Distributions and General Mathematical Properties.

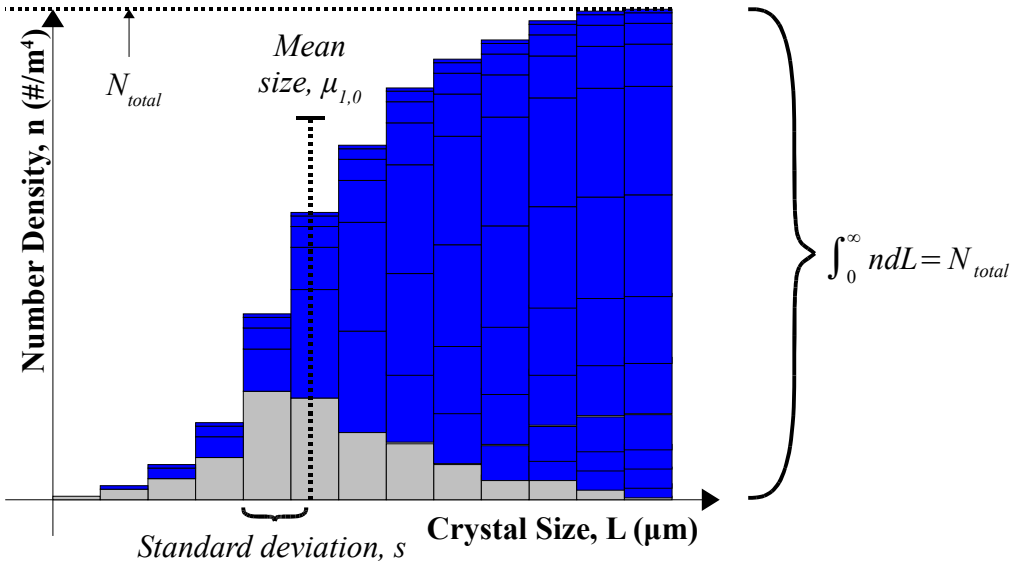

Figure 2.8 Crystal size distribution and the attendant cumulative summation.

The CSD is synonymous with the number density, $n(L)$, (#/μm^4), where L is the characteristic length. This quantity gives the number of crystals between size L and $L + dL$, per unit control volume. CSD is a critical variable in measuring the performance of a crystallization process and the final drug product. Figure 2.8 above illustrates a typical CSD, its cumulative summation/integral, and several other quantities. Several possible representations of a crystal size distribution are possible. All crystal size distributions possess a mean ($\mu_{1,0}$ in the diagram) and a standard deviation (s). On physical grounds, the number density must be greater than zero everywhere, since we cannot have negative quantities of crystals. Furthermore, we cannot have negative crystal sizes, and so we only consider distributions defined for $L > 0$. Since we would very much like to share this universe with the crystals, we note that $\lim_{L\to\infty} n(L) = 0$.

Integration over the entire domain will always give the total number of crystals, per unit control volume, in the control volume. A very similar quantity is termed the *number fraction distribution*, f ($m^{-1}_{crystals}$):

$$f(L) = \frac{n(L)}{\int_0^\infty n(L)dL} \tag{2.9}$$

Where f is the *fraction* of the total crystal population with a size between L and $L + dL$. It is easy to show that $\int_0^\infty f dL = 1$. We note that the integrals of *any* fractional distribution *must* have dimensionless units, as f is analogous to a probability density function.

2.6.2 Volume Size Distributions

Many analytical instruments do not measure number density, but instead measure *volume density*, n_{v} ($m^3_{crystals}/m^3_{external} \cdot m_{crystals}$), given by:

$$n_{\mathrm{v}}(L) = k_v L^3 n(L) \tag{2.10}$$

Where k_v is a dimensionless shape factor ($\pi/6$ for spheres), and n_{v} is the volume of the crystals of size L to $L + dL$. The total volume of all the crystals, per unit of control volume, is given by $V_{total} = \int_0^\infty n_{\mathrm{v}} dL$. Analogous to the number fraction distribution is the *volume fraction distribution*, f_{v}:

$$f_{\mathrm{v}}(L) = \frac{n(L)L^3}{\int_0^\infty n(L)L^3 dL} \tag{2.11}$$

Just like the number fraction distribution, $\int_0^\infty f_{\mathrm{v}} dL = 1$. A variety of other distributions can be defined, such as mass and area fraction. Area fraction is especially important when studying chemical reactions on the surfaces of particles, as the exposed area is where the chemical reaction occurs (either for a direct reaction with the particle surface or a heterogeneous catalytic reaction).

2.6.3 The Impact of Crystal Size Distribution and Crystal Properties

The CSD is known to impact the efficiency of further downstream processing steps (e.g. filtering and washing), as well the mechanical strength of pressed tablets for oral dosage

forms [24], [37]. It also strongly affects the dissolution kinetics within the human body, which impact final product quality and safety [21], [37], [122]. There are a variety of benefits from producing a proper CSD in the produced crystals, such as high bioavailability and improved tablet stability [21], [37], [49]. Furthermore, good control of CSD can abrogate the need for various size-reduction processes, such as milling, that are commonly used in drug manufacture [24], [37], [49]. Generally in crystallization, one desires the largest crystals possible. Large crystals make downstream processing operations, such as washing and filtering [97], much easier. For some applications, extremely small crystals are preferred. The use of nano-sized crystals in drug products is a possible work-around to the poor solubility of many of today's drug APIs [123], as well as for the production of inhalable powders and injectable suspensions [21]. In both cases however, a narrow CSD is often preferred. More generally than the CSD, a variety of other crystal properties affect drug performance as well. Table 3 on page 43 summarizes these properties, the motivation for wanting to control them, and how much controllability exists in the current state-of-the-art [21], [24], [38], [40], [86], [89], [96], [97], [43], [124], [125].

2.7 Population Balances

Most chemical engineers are familiar with the four main balance equations in chemical engineering: mass, energy, momentum, and entropy balance. We shall not state these

individually, and instead direct the reader to any of the textbooks ([126]–[128]) for an exhaustive treatment. However, we will state the general form of each equation in words:

$$\begin{aligned}\frac{d}{dt}\begin{pmatrix}\text{quantity of } \Psi \\ \text{in the control volume}\end{pmatrix} &= \begin{pmatrix}\text{rate of } \Psi \text{ entering} \\ \text{the control volume}\end{pmatrix} - \begin{pmatrix}\text{rate of } \Psi \text{ leaving} \\ \text{the control volume}\end{pmatrix} \\ &+ \begin{pmatrix}\text{rate of } \Psi \text{ generated} \\ \text{inside the control volume}\end{pmatrix} \\ &- \begin{pmatrix}\text{rate of } \Psi \text{ consumed} \\ \text{inside the control volume}\end{pmatrix}\end{aligned} \tag{2.12}$$

Where Ψ is any of the four quantities previously discussed. However, the two main equations of mass and energy balance are not sufficient to model particulate processes. The main reason for this is due to an infinite number of populations that can close the same mass balance. Figure 2.9 illustrates the problem geometrically. In the diagram, a given mass of raw material is operated upon by a process, producing a product. In (a), both the raw material and product are monolithic. However, in (b) the raw material and product are discrete particles of different sizes, which have the same *total* mass as the original blocks in (a). If individual sizes are important variables, mass and energy balances alone are not capable of modeling this phenomena; any number of chopped-up versions of the original blocks in (a) would close those two equations.

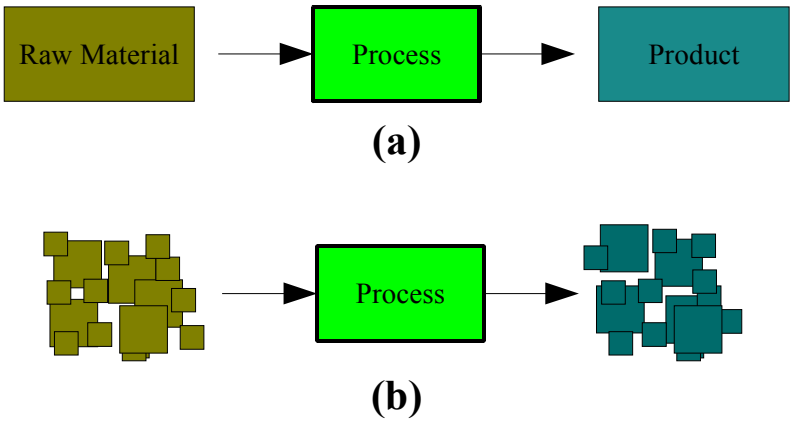

Figure 2.9 Depiction of equal mass closures for two different populations of particles.

This is not a problem that can be approximated away or swept under the rug. Particle phases are widely encountered in engineering processes, and the properties of the collective population of particles is often critical to ease of processing, and final product quality [47]. Ignoring the momentum and entropy balances, a third balance equation is required in addition to the mass and energy balance. This third balance is important to pharmaceutical manufacture, since particulate phases are so common in pharmaceutical production. The operations of crystallization, granulation, tableting, etc., produce crystals, granules, and tablets – all involve discrete particles. The population balance gives a third conservation law for describing the internal property distribution of populations of entities. A population balance model (PBM) neatly summarizes all of the operations occurring in a system that affects the number of particles with a particular set of characteristics residing within the control volume, such as birth, death, agglomeration, compression, expansion, and a host of different breakage processes [129], [130]. This

framework has been used to model all sorts of interesting phenomena involving discrete particles, such as biological cells, sterilization processes [47], [131], aerosols, solid rocket engines [111], and polymerizations [47], [131], [132], pharmaceutical granules, purity of pharmaceutical crystals, and enantiomeric excess of pharmaceutical crystals. The equation is given by:

$$\frac{\partial n}{\partial t} + \nabla_{ext} \cdot (\boldsymbol{v} n) + \nabla_{int} \cdot (\boldsymbol{G} n) + B + D = 0 \tag{2.13}$$

Where n is the number density (#/m^4), t is the time, $\boldsymbol{v}$ is a vector of external velocities, $\boldsymbol{G}$ is a vector of internal velocities (crystal growth rates), B is the birth function (e.g. nucleation, breakage), and D is the death function (e.g. breakage, agglomeration). Both B and D have units of #/m^4·s. The two gradients are taken with respect to either the external coordinates ($x, y,$ and z), or the internal coordinates (L_1, L_1, …, L_m for and crystals with m characteristic lengths). The general population balance equation is a partial differential equation [111], and solution is generally difficult. Solving this equation coupled with the other balance equations yields the correct CSD. The equation was first proposed in Hulburt and Katz [133]. Good introductions to the formulation and solution of these models are found in the books by Randolph and Larson [111], Jones [40], Garside and Davey [97], and Ramkrishna [132], as well as the paper by Rawlings [47]. While the mass balance equation is typically an ordinary differential equation (ODE), PBMs are partial differential equations (PDE), which are significantly more burdensome to solve. Solution of crystallization systems is generally difficult for several reasons –the large number of variables, vast differences in time and length scales, and the inherent discontinuity of the system due to the phenomena of nucleation, breakage, and

agglomeration [37], [134]. To solve these equations, we discuss two important methods used in this work.

2.7.1 The Method of Moments (MOM) and Finite Volume Method

Due to the mathematical structure of PBMs, it is possible to reduce them to a system of ODEs by an integral transformation known as the "method of moments." This is a widely used method for solving PBM equations, and is popular due to the rapidity of solution. The k^{th} moment of the crystal size distribution is given by:

$$\mu_k = \int_0^\infty nL^k dL \tag{2.14}$$

The moment form of the population balance equation is formulated by taking the k^{th} moment of the equation, which expresses the original PBE solely in terms of μ_k [111]. Instead of a partial differential equation, $k + 1$ ordinary differential equations need to be solved (the extra equation is the mass balance). This problem is significantly easier to solve than the original. We discuss this method in greater detail in section 4.4.2.

While easier to solve, the MOM loses the CSD in its entirety, making prediction of the full CSD impossible. Such information is needed for applications such as matching a target CSD. Furthermore, depending on the phenomena being modeled, the method of moments may lead to the "closure problem", where the k^{th} moment equation is expressed in terms of moments greater than k, for any k [133], [134]. This motivates the

use of a variety of other integration methods for solving moment equations, such as the quadrature method of moments. Accurate solution is done by decomposition to a large system of ODEs, using the method of weighted residuals or the finite volume method. The finite volume method has been applied to the modeling of a multi-segment plug flow crystallizer previously by Alvarez and Myerson [135]. Number density may itself be a function of external position, motivating the use of combined CFD-PBM models. The approach has been used to model impinging jet and antisolvent crystallizers [136]–[138].

2.7.2 More Sophisticated Population Balance Modeling Approaches

There has been much work done with computational fluid dynamics (CFD) simulations using special software packages, to clearly examine what the flow patterns are within the crystallizers. These models involve not only the population balance equation, but the fluid transport equations as well. The k-ε model has been used to investigate turbulent effects [40]. While these simulations do provide useful data in the form of shear profiles, temperature profiles, and the location of solids in the crystallizer [44], they are time-consuming to run, and the countermeasures one can take on scale up are still limited. Furthermore, if prediction of changes to the CSD is desired, a combined CFD-PBM simulation is required, to account for spatial variation in particle number density. Such simulations are even more time-complicated than the original CFD simulations [45].

Essentially all phenomena in crystallization are random in some way. Nucleation, breakage, growth, and agglomeration are all based on some chance encounter between either two particles, or a particle and a molecule for growth, or an ensemble of molecules for nucleation [139]–[141]. Monte-Carlo methods are based on using computer-generated random numbers to simulate physical random (or presumptively random) phenomena. Braatz has discussed several papers which utilized stochastic PBM models and were solved with MC methods [37]. MC methods are able to model this type of phenomena in fine detail, but are computationally burdensome. We note that MC is a general tool, and has been applied to crystallization in other ways to crystallization other than solving the PBM equation. Jones has described the use of MC to explicitly account for a residence-time distribution in an MSMPR crystallizer [40].

2.7.3 Current Challenges in Continuous Crystallization and Population Balance Modeling

Challenges abound in the application of process systems engineering knowledge to pharmaceuticals. This thesis fills an important literature gap by addressing the need for an integrated modeling, optimization, and design framework for the identification of optimal crystallizer designs. This framework can be applied to many other crystallization systems which have not been rigorously modeled, such as some of the crystallizers described in CHAPTER 3.

Currently, general solution of the population balance equation is not known, and numerical methods tend to exhibit significant tradeoffs in speed and accuracy [134]. Speed is required for utilizing the model for model-predictive control, and accuracy is required to make the benefits of optimal control worthwhile.

Related to the issue of robustness is the issue of dynamic stability. Due to the high nonlinearity present in crystallization systems, the effect of time usually requires numerical solution to observe on the CSD. In MSMPRs, oscillations in the CSD are a known and undesirable phenomena. Dynamics in general have been studied for the conventional batch and MSMPR crystallizers, as well as networks of MSMPRs. However, newer crystallizer designs, such as the MSMA-PFC, have not had such analyses done for them. Furthermore, in newer crystallizer designs (such as the MSMA-PFC), it is unknown what type of dynamic behavior may be present, e.g. limit cycling or chaos. Bifurcation analysis of such systems is nearly impossible to do analytically. Rigorous computational studies are one method addressing this literature gap.

Another challenge, separate from the mathematical difficulties, is the issue of parameter estimation. The full description of the process requires a great deal of information [40], including solubility data, crystal density, liquid transport properties, crystal growth rate(s), and nucleation rate [40]. Accurate estimation of kinetic parameters for growth, nucleation, and dissolution is one of the most difficult hurdles to surmount in constructing an accurate crystallization PBM [37], [47]. As pointed out by Rawlings [47], the results produced by model-based optimizations rely upon estimated parameters, and as such, will

be sensitive to experimental error. Without very accurate parameter estimates, all of the effort expended upon optimizing the crystallization equipment and process operation may be for naught, with virtually no benefit realized. This goes not only for continuous crystallization, but the entire CPM flowsheet. Model complexity becomes even more acute when phenomena such as size-dependent growth, non-uniform residence-time distributions, agglomeration and breakage, and growth-rate dispersion are added to the model [47]. The complicated nature of such models has motivated the use of Monte-Carlo methods for their solution [40].

2.8 Multiobjective Optimization in Crystallization Design and Research

We have utilized multiobjective optimization extensively in our work in CHAPTER 4. In preparation for this chapter, we provide the reader with useful background information on multiobjective optimization. Multiobjective optimization is a generalization of scalar optimization which accounts for the common situation when the decision maker has multiple conflicting objectives he wishes to optimize over. In general, global optimization of each function at the same time is unattainable [142]–[144], thus motivating the concepts of Pareto optimality, trade-off, and non-dominated solutions. This framework has been applied to batch crystallization by several workers [120], [145]. Such a framework appears quite applicable to analysis of PFCs, since it provides detailed information on what CSDs are attainable. Bhat and Huang [120] applied the approach to enantioselective crystallization by incorporating enantiomeric excess into one the

objectives for maximization, in addition to maximizing size, while minimizing CV and batch time. Sarkar et al. [146] simultaneously extremized several quantities, and supplied Pareto frontiers.

Typically in crystallization control, one desires larger crystals with compact shape, since these have superior filtering and dry properties. However, sometimes smaller crystals, which dissolve faster, are preferable. The purpose of this section is to give the reader a brief background on the subject of multiobjective optimization (MOO) and discuss several important issues related to the practical solution of MOO problems. This section draws heavily from the books by Deb [147], Gen and Cheng [148], and Chambers [148], which give in-depth discussions of evolutionary algorithms applied to multi-objective problems in engineering.

2.8.1 Basic Problem Formulation

The standard formulation for an MOO problem is:

$$\min_{\boldsymbol{x}} [f_1(\boldsymbol{x}) \quad f_2(\boldsymbol{x}) \quad \cdots \quad f_m(\boldsymbol{x})]^T$$

Subject to:

$$\begin{gathered} \boldsymbol{g}(\boldsymbol{x}) \leq \mathbf{0} \\ \boldsymbol{h}(\boldsymbol{x}) = \mathbf{0} \\ \boldsymbol{x}_{LB} \leq \boldsymbol{x} \leq \boldsymbol{x}_{UB} \end{gathered} \tag{2.15}$$

Multiobjective optimization is a natural consequence of the fact that real problems, especially in engineering, often cannot be characterized in terms of a single objective. Frequently, we must optimize over a variety of objectives, such as capital cost, operating cost, volume, weight, energy consumption, and other objectives specific to a particular problem. No single design can simultaneously optimize all objectives in the vector.

2.8.2 Pareto Optimality and the Pareto Frontier

The Pareto-optimal (or also, "non-dominated") set of solutions to an MOO problem is the MOO analog of the global minimum for a single-objective problem. Due to multiple objectives though, the solution is expressed as a set of points instead of a single point. These points describe a curve, called the Pareto frontier, for which a tradeoff exists between any two points on the curve. When a point lies on the Pareto frontier, moving in any direction leads to a desirable reduction in one objective and a concomitant, undesirable increase in another objective. In mathematical terms, the globally-optimal Pareto frontier satisfies the property that:

$$f_i^*(\boldsymbol{x}) \leq f_i(\boldsymbol{x}) \tag{2.16}$$

for all feasible $\boldsymbol{x}$ and for all $1, 2, \ldots, m$ objectives. That is, there is no point that can improve any at least one of the objectives while leaving the others unchanged.

2.8.3 Use of the Genetic Algorithm

Many methods exist for solution of problem (2.15), which depend on the difficulty of the problem. We do not discuss gradient-based approaches in this work, as these approaches

are of little use in crystallization problems. The most direct method for solving an MOO problem is by stochastic optimization. Many such schemes exist, such as simulated annealing, bacterial foraging, ant-colony, and particle-swarm optimization. In this work, we have used the genetic algorithm (GA), which mimics the Darwinian process of natural selection to generate the Pareto frontier. In the GA, a pool of solutions are first generated, and the objective function is evaluated for each of them. The "fittest" solutions are allowed to pass on to the next generation. Then a variety of mutation, transposition, and selection operators create a new set of "child" solutions created from the "genes" of the parent solutions. This helps preserve the good qualities of the prior solutions, but offers a chance to improve the solution further by moving elsewhere in the search space. Unlike gradient-based approaches, the GA is robust against local minima.

CHAPTER 3. CURRENT LITERATURE ON CONTINUOUS CRYSTALLIZATION TECHNOLOGIES

We present in this chapter a more specific literature review focusing solely on continuous crystallization designs that have been proposed and tested in the literature. The purpose of this chapter is to expose the reader to the breadth of the continuous crystallization literature. It also helps place our work in the greater context, as we have investigated in this work solely the MSMA-PFC. A handy table at the end of this chapter summarizes the key findings and experimental attributes of many studies in the field of continuous crystallization.

3.1 The MSMPR, MSMPR Cascade, and CoFlore™ Crystallizers

The mixed-suspension, mixed-product removal (MSMPR) crystallizer is the workhorse of large-scale chemical manufacture, used for productions of ~1-50 tons/day [47]. It is the crystallization analog of a continuous stirred-tank reactor (CSTR). Large, scaled-up examples of such devices can be seen in Larsen et al. [38]. Aside from large-scale use, the MSMPR (as well as batch crystallizers) is used often in the laboratory for experimentally determining growth and nucleation rates, and also for detecting size-dependent growth [47], [51].

Mascia et al. utilized MSMPRs for their crystallizations in their study of a continuous tablet manufacturing pilot plant [23].Quon et al. [149], Zhang et al. [150], and Alvarez et al. [151] demonstrate the use of multiple MSMPR's in series for cooling and antisolvent crystallization of pharmaceuticals. Newer MSMPR technologies have explored novel new mixing methods to allow for better process control. A highly intensified version of the MSMPR cascade is the CoFlore™ reactor, which has been recently applied to the continuous reactive crystallization of *N*-iodomorphlonium salt by Browne et al. [152]. Originally developed for chemical reactions, the CoFlore™ reactor utilizes several agitated compartments, along with bulk agitation with a linear oscillator, to keep solids suspended while crystallization is taking place [152]. A major problem with continuous crystallizers of all kinds is the issue of plugging and fouling, and high shear mixing is one method of forestalling buildup. Unlike larger MSMPRs, the smaller Coflore™ crystallizer offers superior mixing characteristics, enabling swift mass transfer and avoiding the problems with solid suspension discussed in section 2.1.4. Narducci et al. [153] used power ultrasound as well the conventional stirrer.

3.2 Plug-Flow Crystallizers

The plug-flow crystallizer (PFC) is analogous to the plug-flow reactor (PFR). It can be shown analytically that the MSMPR cascade, in the limit of infinitely small CSTRs, asymptotically converges to the PFC [154]. Cascades generally converge to a PFC within about 5 units. For fast crystallizations, PFCs can be practical, while slow crystallizations

require too great of a residence time (and thus too slow of flow velocity) to be useful. A common feature of plug-flow crystallizers (and other types discussed in §3.3) in the recent literature on pharmaceutical crystallization is the exploration of various mixing methods. Among others, we observe vortex mixers ("Roughton" type [155]), impinging jets [136], [137], [156], and static mixers (e.g. the Kenics mixer [135]). Such mixers have been investigated for flow-dependent reaction syntheses previously, and more recently for use in crystallization research. The topic of static mixers is discussed at length in the review by Thakur et al. [157]. Generally, such mixers are found to be significantly more efficient than active mixers, and, with proper design, can rapidly achieve plug flow. Typically, good mixing can be achieved using vortex mixers, or static helical mixers. Simulations by Woo et al. [136] show that vortex mixers possess mixing times well below the induction time of crystallization, which ensures that there are no confounding effects from supersaturation gradients. Eder et al. [158], [159] have investigated a stage-wise cooling PFC for continuous aspirin crystallization. Their PFC consists of a flexible coiled tube, which permits a long residence time, but occupies little space. Control over the supersaturation trajectory is achieved by chilling separate coiled sections. This permits the creation of a clearly-defined temperature profile along the length of the PFC. For the case of antisolvent crystallization, The plug flow crystallizer is often not a practical tool for pharmaceutical crystallization, since residence times must be so long to achieve a larger crystal size. This leads to very low flow rates and low velocities, which leads to settling of the crystals and fouling of the inner surfaces with API. Very low flow velocities also lead to self-contradiction if the "plug-flow" crystallizer is operated in the laminar flow regime. Lawton et al. [160], used a PFC augmented with baffles and a

pulsating “thumper” to drive flow continually back and forth, while maintaining a net positive forward flow. The logic in using these baffles is to obtain better turbulent mixing along the length of the crystallizer, while avoiding high flow rates which would normally be necessary to produce it. High velocity is achieved without shortening residence time. FBRM was used for observation of crystal size via chord-length distribution. Their results showed vast reduction in production time.

3.2.1 Multi-Segmented Plug-Flow Crystallizers

A feature of this thesis is investigation into using multiple crystallizer segments in series. This allows for spatial control over supersaturation in on dimension, which is not possible in a stirred tank (batch or continuous) crystallizer. Variation of supersaturation with length allows for improved control over growth and nucleation, which leads to a better final crystal product. Prior work in this area has been done by Alvarez on antisolvent crystallization, Majumder and Nagy on the modeling of cooling crystallization, and Ridder et al. on modeling antisolvent crystallization. Alvarez and Myerson have investigated a multi-segment PFC, with separate antisolvent injections into each stage [135]. Their segmented PFC system was modeled with a set of PBM equations and a mass balance equation, and compared to experimental results. The kinetic and solubility parameters of ketoconazole, flufenamic acid, and L-glutamic acid were determined experimentally for use in the model. FBRM was used for measuring CSD, and comparing to model prediction, though no feedback control was used. In that work, a Kenics screw-

type static mixer was used to ensure good homogenization of the liquor and antisolvent streams, but other approaches have been used as well. Majumder and Nagy investigated the use of in-situ dissolution in plug-flow cooling crystallization in order to eliminate fine crystals [113]. Ridder et al. investigated the crystallization of flufenamic acid via a simulation and optimization-based study [161], [162]. The sensitivity to kinetic crystallization parameters was investigated as well.

3.3 Other Types of Continuous Crystallizers

Nguyen et al. [163] have investigated the use of this crystallizer. In a CT crystallizer, liquor flows into the hollow gap between a cylindrical shell and a concentrically-located spinning cylinder. When rotated at high speed, the fluid eventually exhibits Couette-Taylor flow, where the fluid segregates into an "accordion" of concentric toruses, with fluid rotating concentrically about the axes of the individual toruses rather than about the axis of the spinning cylinder. Unlike the COBC, which directly compartmentalizes various elements of fluid, each torus might be considered its own "compartment", and mixing occurs within toruses as well as between them. These toruses can be modeled as separate compartments in a compartment flow model. The CT crystallizer allows for high slurry velocity, which improves mixing and avoids the problems of settling and fouling at low velocity. However, residence time can be controlled purely by inlet flow. Thus a decoupling can be achieved between flow velocity and residence time for the continuous CT crystallizer.

A type of spray-drying crystallization using electrically-stimulated liquid jets has been investigated by Wang et al. [123] for the production of carbamazepine nanocrystals. Similar to spray-drying, an electrospray device generates fine jets of liquid by applying electric potential to a saturated liquid solution. The charged fine droplets naturally repel each other in flight, until they land on a grounded surface. Rapid evaporation leads to amorphous crystals. This approach is interesting, in that it provides a continuous production route to a particular (though, in this case, unstable) solid-form, in the nano-sized regime. Significantly more work could be done in terms of modeling of this system, such as population balance modeling of the generated droplet cloud.

Another design is the electrospray crystallizer. This type of device, originally developed for plastic injection molding, utilizes two opposing streams of high-velocity liquid sprayed at an intersecting point. The region where these two streams collide creates a zone of intense mixing, avoiding the aforementioned trouble with supersaturation gradients. Details about the design of this crystallizer can be found in the original patent [156]. The Braatz group at MIT has done extensive work on the modeling, simulation, and optimization of this type of crystallizer [136], [137] for the case of the drug lovastatin and L-histidine. Woo [136] performed combined CFD-PBM-micromixing simulations of the impinging jet crystallizer within the mixing chamber. Their results show that, given a sufficiently high Reynolds number, thorough mixing is achieved before fluid exits the mixing chamber. The results of that study were further used in [137], where the obtained crystal size distributions from the previous modeling were used as decision variables in an optimization problem. By utilizing a repertoire of known CSDs for given jet velocities,

a series of quadratic programming and nonlinear least squares optimizations were solved to identify the optimal control strategy for seed input into a CSTR. By adjusting jet velocity as a function of time, a variety of peculiar CSDs were obtained. Their numerical results show that, theoretically, significant control over the target CSD exists.

3.3.1 Continuous Microcrystallizers

Borrowing from the field of chemical reaction engineering, is the concept of the microcrystallizer [164]–[166]. Due to the aforementioned problems with crystallizer scale-up, an alternative approach is to use multiple, smaller continuous flow devices in parallel. Once a single microreactor has been design and tested thoroughly, the process of scale-up to a larger mass flow rate is greatly simplified, as multiple units can be used in parallel instead of enlarged. This is termed "number up", as opposed to "scale-up." However, the technical problems of fluid distribution and lack of flexibility in inputs leaves "number up" can still be challenging for proper scale-up [167]. Microcrystallizers have pharmaceutical use as high-throughput screening platforms for drug discovery and development, and lab-scale process optimization [167]. Currently, they are not usable for drug production, due to plugging and fouling of the vessel interior [167]. Microfluidic crystallization is mainly used for high-throughput screening of optimal experimental procedures for protein crystallization. However, use has been demonstrated for high-throughput screening of pharmaceutical salt forms and polymorphs. Llinas and Goodman

cite a case where over 2000 screening experiments were performed for polymorph identification using only 2 grams of API [99].

3.4 Table of Continuous Crystallization Technologies

Table 3 below summarizes a wide variety of studies encompassing these crystallizer designs.

Table 4 Table of continuous crystallization literature related to pharmaceuticals.

Paper	Crystallizer Type	Mode	Solvent/Antisolvent	Solute	Investigated What?	Key Findings
Eder et al. 2011 [168]	PFC	Cooling	Ethanol	Aspirin	• Effect of input seed mass on average crystal size.	• Moderate supersaturation encourages growth; avoids nucleation. • More seeding reduced final size. • Fast convergence to steady-state.
Alvarez and Myerson 2010 [135]	Multi-segment PFC	Antisolvent	• Methanol/water • Ethanol/water • Water/acetone	• Ketoconazole • Flufenamic acid • L-Glutamic acid	• Effect of antisolvent sidestream injection configuration on CSD. • Compared population balance model prediction to experimental result.	• Improvement in average crystal properties for some sidestream configurations. • Model doesn't fit well, unless growth-rate dispersion is accounted for.
Ferguson et al. 2012 [155]	PFC	Antisolvent	Ethanol/water	Benzoic acid	• Investigated ability to monitor process using in-situ PAT (FBRM, ATR FT-IR, PVM)	• Can achieve much lower crystal sizes than batch. • PVM can't see smaller crystals.

Table 4 continued.

Quon et al. 2012 [149]	Two MSMPR cascade	Reactive	N/A	N/A	• Crystallized aliskiren hemifumarate, and determined kinetic parameters. •	• Significant tradeoff between crystal purity and crystal yield.
Alvarez et al. 2011 [151]	Three MSMPR cascade	Cooling	Acetone	Cyclosporine	• Estimated kinetic parameters for cyclosporine crystallization, • Effect of recycle ratio on yield and purity	• Significant tradeoffs between purity, yield, and and mean size. •
Narducci et al. 2011 [153]	MSMPR	Cooling	Water	Adipic acid	• Effect of ultrasound probe power on crystal properties and process dynamics.	• Crystal size greatly reduced by sonication. • Fouling interferes with heat transfer and sonication. • Agglomeration reduced by sonication.

Table 4 continued.

Lawton et al. 2009 [160]	Continuous oscillatory baffled crystallizer (COBC)	Cooling	Unwritten	Proprietary	• Effect of oscillation parameters and cooling rate on CSD and habit.	• Larger sizes with slower cooling rate. • 20%-50% decrease in capital cost vs. batch.
Nguyen et al. 2012 [163]	Couette-Taylor (CT)	Antisolvent	Water/Methanol	Guanosine 5-monophosphate	• Effect of feeding configuration and residence time on crystallinity and mean crystal size. • Effect of rotational speed on crystallinity, yield, and mean crystal size.	• Requires shorter residence time required vs. MSMPR. • Increasing crystallinity and yield with increasing rotational speed; decreased mean size.
Wang et al. 2012 [123]	Electrospray	Parallel disk	Methanol	Carbamazepine	• • Investigated electrical current, concentration, and flow rate on obtained crystals.	• Rapid crystallization produced product. • Obtained crystals of sizes ~300-1700 nm

Table 4 continued.

Besenhard et al.	Segmented plug flow	Cooling	Ethanol	Acetylsalicylic acid	• Injected air into line to create segmented “slug flow.” • Cooling crystallization with many variables explored using a small DOE approach.	• Breakage is negligible. • Agglomeration observed • Sensitive to initial seed mass loading.

CHAPTER 4. MULTIOBJECTIVE OPTIMIZATION AND ROBUSTNESS ANALYSIS OF THE MULTI-SEGMENT, MULTI-ADDITION PLUG-FLOW ANTISOLVENT CRYSTALLIZER (MSMA-PFC)

4.1 Abstract

In this chapter, we present optimization and simulation results related to a new type of crystallizer for the production of pharmaceutical APIs. We develop the population balance and mass balance model framework, as well as the multiobjective optimization framework for investigating the design of the crystallizer. The governing model equations are derived and presented. Landscape plots of mass-mean size (L_{43}) and coefficient of variation (CV) indicate great sensitivity to flowrate and nonconvexity, necessitating the use of stochastic optimization via the genetic algorithm. Using multi-objective optimization, we calculated optimal designs for this crystallizer in terms of maximizing L_{43} and minimizing CV. A tradeoff exists between these two quantities. Mean size was improved over prior literature results while maintaining similar spread. The optimal solution was sensitive to uncertainty in the kinetic parameters of nucleation (k_b) and growth (k_g). Lastly, we have investigated the sensitivity to flowrate for the MSMA-PFC using a simple Monte-Carlo technique. The greatest sensitivity is observed in the first and third segments, while the second and fourth have little process impact. This work is substantially composed of work from the paper [161]. Adapted with permission from B. J. Ridder, A. Majumder, and Z. K. Nagy, "Population Balance Model-Based Multiobjective

Optimization of a Multisegment Multiaddition (MSMA) Continuous Plug-Flow Antisolvent Crystallizer," Ind. Eng. Chem. Res., vol. 53, no. 11, pp. 4387–4397, Feb. 2014. Copyright 2014 American Chemical Society. It also contains work substantially composed of from the conference paper [162]. Adapted with permission from B. J. Ridder, A. Majumder, and Z. K. Nagy, "Population balance model based multi-objective optimization and robustness analysis of a continuous plug flow antisolvent crystallizer," American Control Conference (ACC), 2014, pp. 3530–3535, Jun. 2014. Copyright 2014 IEEE.

4.2 Introduction

As discussed in CHAPTER 1, financial pressures have caused the pharmaceutical industry to express interest in the development of new manufacturing technologies [3], [7], [15]. These problems translate into high manufacturing costs, though little attention has been historically paid to the problem. One such technology branch that is being researched is advanced crystallization processes. Crystallization is a major separation unit operation in fine chemical and pharmaceutical manufacture. The overwhelming majority of drugs are organic molecules crystallized from solution [24], [113], [169]. Predominantly, pharmaceutical crystallization is done batch-wise, despite clear evidence of the economic advantages of continuous manufacturing – such as steady-state operation, lower material hold-up, and superior control over the state of the final drug product [5], [24], [160].

An optimization problem has been indirectly suggested in the literature by Alvarez and Myerson [169]. Alvarez had attempted to improve the crystal output properties by manipulation of injection configuration and/or antisolvent flowrates in an MSMA-PFC. In previous work on batch crystallization, the goal was to manipulate supersaturation as a function of time to achieve an optimal set of crystal properties at the conclusion of the batch [145], [146], [170], [171]. Analogously in this work, we have manipulated the supersaturation profile in order to optimize the crystal properties at the outlet. The difference is that the supersaturation profile in the batch case is with respect to *time*, while here it is with respect to length into the crystallizer.

We have optimized an MSMA-PFC for the production of flufenamic acid, an anti-inflammatory drug [169], [172]. By altering the antisolvent flowrates in the various sections, the supersaturation can be controlled along the length of the crystallizer. The supersaturation within a segment strongly affects the nucleation and growth kinetics therein and thus gives us a method for manipulating the product CSD at the outlet. The process is modeled using a steady-state population balance model (PBM), and is solved using the method of moments as well as a high-resolution finite volume scheme [113], [173], [174]. A similar work has been performed by Vetter et al. [17] In that work, the authors investigated the attainable product regions of crystal size for a given residence time in continuous crystallizers. Such studies are helpful in estimating the performance and flexibility of such systems for practical use, with the impact on the final product in mind.

4.3 Methodology

To investigate this continuous flow system, we utilize a multi-objective optimization (MOO, also known as "vector optimization") framework. Such a framework is useful for fully investigating the capabilities of particular design. The solution of MOO problems is cast in terms of finding the non-dominated set of possible solutions, e.g., the solutions for which it is impossible to improve one objective without degrading another. This non-dominated set is referred to as the "Pareto frontier." Such a framework is highly amenable to crystallization problems, which often have a multitude of conflicting objectives in the problem definition. MOO has been applied previously to batch crystallization processes [145], [146]. We explore the multi-objective optimization (MOO) of the MSMA-PFC, with the objectives of maximizing the mass-mean size (L_{43}) and minimizing the coefficient of variation (CV). We show in this work that nonconvexities are encountered in the search landscape, making a stochastic optimization algorithm more appropriate. A widely-used solver for finding the Pareto front is the non-dominated sorting genetic algorithm (NSGA-II), which can efficiently identify the non-dominated set, and handle constraints[175], [176]. We also investigated the sensitivity of the Pareto front to uncertainty in the kinetic parameters. The simultaneous design and control framework for the MSMA-PFC is evaluated and it is shown that with appropriated crystallizer design, that takes the possibility of improved control into account, can improve product quality significantly.

4.4 Model Diagram, and Governing Equations

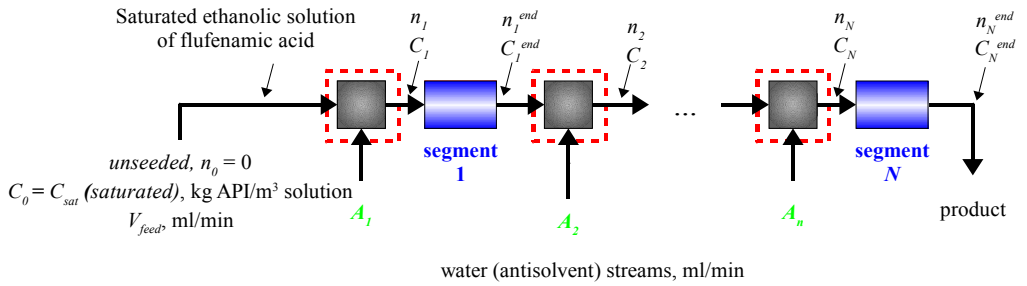

Figure 4.1 Model of segmented plug flow crystallizer system.

The idea behind the MSMA-PFC is to distribute antisolvent along the length of the crystallizer, which allows for the control of supersaturation in one dimension. The MSMA-PFC is based on the setup in Alvarez and Myerson [169]. It is modeled as a series of ideal plug flow elements, and antisolvent is added at the beginning of each segment (see). Each of the N segments is a separate PFC. A_i is the antisolvent flow rate added to the i^{th} segment. The inlet at the far left is the feed flow rate (V_{feed}), with an initial concentration of solute (C_0) and a seed crystal size distribution (CSD), n_0. The population and mass balance equations are solved for each segment, and the output of one segment becomes the input to the next segment. The CSD (n) and concentration (C) are adjusted for the dilution induced by the addition of antisolvent. The final CSD, n_N, is used for formulating the multi-objective optimization problem. The optimization problem is solved by manipulating the antisolvent flow rates in each segment (A_i). It is assumed that each of the N segments is a separate PFC, running in steady-state, isothermal

operation. The solvent and antisolvent streams are assumed to mix together perfectly, and attain plug flow. In this work, we consider only the unseeded case ($n_0 = 0$); however the same framework can be applied for seeded operation. The population and mass balance equations are solved for each segment, and the output of one segment becomes the input to the next segment. Isothermal operation abrogates the need for solution of the equation of energy.

4.4.1 Model Equations

The model equations for the crystallizer design explained above consist of a set of population balance equations (PBEs) describing the evolution of the CSD along the array of plug flow crystallizers, coupled with mass balance equations that take into account the depletion of solute concentration in the solution due to crystal growth and nucleation. Population balances are a key tool in the model-based control of crystallizers [40], [51], [70], [97], [124], [177]. In this work, our seed distribution at the inlet is zero; the process is unseeded. Number density changes along the tube length since birth and growth processes depend on the supersaturation (S). The model equations for the steady-state system are discussed below. The PBE for a PFC is derived by crossing off the irrelevant terms in the general equation given in (2.13):

$$\cancel{\frac{\partial n}{\partial t}} + \frac{\partial}{\partial x}(u_x n) + \cancel{\frac{\partial}{\partial y}(u_y n)} + \cancel{\frac{\partial}{\partial z}(u_z n)} + \frac{\partial}{\partial L}(Gn) - B + \cancel{D} = 0 \tag{4.1}$$

Since we are using the average velocity, $\partial u_x/\partial x = 0$. If one-dimension flow is assumed, then the other two velocity components are zero. We assume size independent growth, e.g. $\partial G/\partial L = 0$. Regarding the birth function, only nucleation occurs, which means only crystals of size L_0 enter the system. This is modeled using a Dirac delta function as $B = B_0\delta(L - L_0)$, where $\delta(L - L_0)$ has units of m^{-1}. There is no death function here, e.g. no agglomeration and breakage. Post-cancellation, the steady-state PBE for the MSMA-PFC is:

$$u_x^{(j)}\frac{\partial n^{(j)}}{\partial x} + G^{(j)}\frac{\partial n^{(j)}}{\partial L} = B_0^{(j)}\delta(L - L_0) \tag{4.2}$$

where the superscript j denotes the j^{th} segment of the MSMA-PFC, $u_x^{(j)}$ is the average velocity of the fluid, $n^{(j)}$ is the number density, and x is the length along the crystallizer. The average velocity is computed by adding up the total volumetric flow rates of solvent and antisolvent in the particular PFC segment, and dividing by the cross-sectional area of the PFC. In the PBM literature, L is referred to as the "internal coordinate", while x is referred to as the "external coordinate." Our boundary conditions are [111]:

$$n^{(j)}(0, x) = B_0^{(j)}/G^{(j)} \tag{4.3}$$

$$n^{(j)}\left(L, x_{j,in}\right) = \gamma_j n^{(j-1)}\left(L, x_{j-1,out}\right) \tag{4.4}$$

and $n^{(1)}(L, 0) = 0$ (e.g. the process is unseeded). Furthermore, $B_0^{(j)}$ is the nucleation rate, $G^{(j)}$ is the crystal growth rate and γ_j is the dilution factor. At the entrance of each PFC segment, the CSD and solute concentration were adjusted by multiplying with a factor which corrects for the dilution:

$$\gamma_j = \frac{V_{feed} + \sum_{i=0}^{j-1} A_i}{V_{feed} + \sum_{i=0}^{j} A_i}. \tag{4.5}$$

This factor is derived by performing a mass balance around all PFC segments and mixing points up to and including the j^{th} PFC segment ($A_0 = 0$, and $j = 1$ for the first PFC segment). Equation (4.2) tracks the CSD as solution passes through the PFC array. In addition to eq. (4.2) the solute mass must be tracked. We do this by simultaneously solving the mass balance equation:

$$u_x^{(j)} \frac{dC^{(j)}}{dx} = -3\rho_c k_v G^{(j)} \int_0^\infty L^2 n^{(j)}\, dL, \tag{4.6}$$

where $C^{(j)}$ is the concentration of dissolved solute in the liquid phase, ρ_c is the solid crystal density, and k_v is the crystal shape factor. C decreases along the length of the array via not only the processes of growth and nucleation, but also by addition of fresh antisolvent. Thus, the mass balance boundary condition is $C(x = 0) = C_0$ and

$$C^{(j)}\left(x_{j,in}\right) = \gamma_j C^{(j-1)}\left(x_{j-1,out}\right) \tag{4.7}$$

Equation (4.6) accounts for the depletion of dissolved solute from the supersaturated liquid phase by the layer-by-layer areal deposition of solute matter upon the exterior surfaces of nucleated crystals. Other ancillary equations are, the growth and nucleation rate equations:

$$G^{(j)}(S) = k_g (S^{(j)})^g, \quad B_0(S) = k_b (S^{(j)})^b, \tag{4.8}$$

and the percent antisolvent ratio, supersaturation, and solubility curve:

$$X_A^{\%(j)} = 100\frac{\sum_{i=0}^{j-1} A_i}{\sum_{i=0}^{j-1} A_i + V_0}\ , \quad S^{(j)} = C^{(j)} - C_{sat}^{(j)}\ , \quad C_{sat}^{(j)} = A_{fit}exp(-B_{fit}X_A^{\%(j)}), \tag{4.9}$$

Where S is the supersaturation, k_g, g, k_b, and b are growth and nucleation rate law parameters, $X_A^{\%}$ is the antisolvent volume percentage, C_{sat} is the solubility concentration, and A_{fit} and B_{fit} are fitted parameters for the solubility curve. The solubility and kinetic parameters used in this work are those regressed by Alvarez and Myerson for flufenamic acid [169]. Numerical values for the parameters discussed here are given in Table 5 below. Prior to the first injection, no antisolvent is in the feed stream.

Table 5 Parameters for crystallization optimization from Alvarez and Myerson [169].

Parameter	**Value**
Inner diameter, m	1.27×10^{-4}
Initial concentration, C_0, mg/m^3	1.24×10^{7}
Solubility parameter, A_{fit}, mg/m^3	3.36×10^{8}
Solubility parameter, B_{fit}, dimensionless	0.108
Shape factor, k_v, dimensionless	$\pi/6$ ($\approx$ 0.524)
Crystal density, ρ_c, mg/m^3	1.47×10^{9}
Mother liquor flowrate, V_0, ml/min	100
Segment length, m	0.6
Growth rate constant k_g, m/s	9.9×10^{-7}
Growth law exponent, g, dimensionless	1.1
Nucleation rate constant k_b, #/(m^3·s)	1.5×10^{8}
Nucleation law exponent, b, dimensionless	2.1
Antisolvent concentration in initial solution (mg/m^3)	0

4.4.2 Solution of Model Equations

Depending on the application or desired information, some solution methods are more appropriate than others. Typically various method of moments (MOM) are used to solve the population balance equations (PBEs), when only moments of the CSD are required, e.g., standard method of moments (MOM) [133] and quadrature method of moments

(QMOM) [134], [178]–[180]. The importance of moments lies in the convenient simplifications they impart to the solution of crystallizer modeling equations [40], [111], [181]. In the method of moments, progressively higher moments of (2.13) are taken, reducing the complicated, coupled, ODE-PDE system to a system of $m+1$ ODE's; the m moment equations, plus the mass balance in (4.6). The k^{th} moment of the CSD is given by:

$$\mu_k^{(j)} = \int_0^\infty L^k n^{(j)}(L,x)dL \tag{4.10}$$

The physical meaning of the moments is straightforward: μ_0 is the total number of crystals, μ_1 their total length, μ_2 their total surface area, and μ_3 their total volume – all per unit of control volume [111], [181].To obtain the moment form of the PBE, first take the k^{th} moment of the entire equation:

$$\int_0^\infty \left(u_x^{(j)}\frac{\partial n^{(j)}}{\partial x} + G^{(j)}\frac{\partial n^{(j)}}{\partial L}\right)L^k dL = \int_0^\infty B_0^{(j)}\delta(L-L_0)L^k dL \tag{4.11}$$

We can take the derivative out of the integral on the leftmost term on the lefthand side:

$$u_x^{(j)}\frac{d\mu_k^{(j)}}{dx} + G^{(j)}\int_0^\infty \frac{\partial n^{(j)}}{\partial L}L^k dL = B_0^{(j)}L_0^k \tag{4.12}$$

The term $\int_0^\infty \partial n^{(j)}/\partial L\, L^k dL$ can be integrated using integration by parts to finally obtain the k^{th}-moment equation:

$$\frac{d\mu_k^{(j)}}{dx} = \frac{kG^{(j)}\mu_{k-1}^{(j)} + B_0^{(j)}L_0^k}{u_x^{(j)}} \tag{4.13}$$

The full system of MOM equations is given by plugging in $k = 0,1,\ldots,5$ into (4.13):

$$d\mu_0^{(j)}/dx = B_0^{(j)}/u_x^{(j)} \tag{4.14}$$

$$d\mu_1^{(j)}/dx = \left(G^{(j)}\mu_0^{(j)} + B_0^{(j)}L_0\right)/u_x^{(j)}$$

$$d\mu_2^{(j)}/dx = \left(2G^{(j)}\mu_1^{(j)} + B_0^{(j)}L_0^2\right)/u_x^{(j)}$$

$$d\mu_3^{(j)}/dx = \left(3G^{(j)}\mu_2^{(j)} + B_0^{(j)}L_0^3\right)/u_x^{(j)}$$

$$d\mu_4^{(j)}/dx = \left(4G^{(j)}\mu_3^{(j)} + B_0^{(j)}L_0^4\right)/u_x^{(j)}$$

$$d\mu_5^{(j)}/dx = \left(5G^{(j)}\mu_4^{(j)} + B_0^{(j)}L_0^5\right)/u_x^{(j)}$$

$$dC^{(j)}/dx = -3\rho_c k_v G^{(j)}\mu_2^{(j)}/u_x^{(j)}$$

This set of equations provides the steady state moment model of the MSMA-PFC. This technique permits rapid solution in terms of moments, but loses the full CSD. The MOM requires computationally much cheaper function evaluations, making it more efficient in the optimization which requires multiple iterations within the genetic algorithm. These seven equations solve for two important average quantities at the exit of the MSMA-PFC. The exit ($j = N$) mass-mean crystal size is given by:

$$L_{43}{}^N = \mu_4^{(N)}/\mu_3^{(N)} \tag{4.15}$$

and the exit mass-mean coefficient of variation is given by:

$$CV^N = \sqrt{\mu_5^{(N)}\mu_3^{(N)}/(\mu_4^{(N)})^2 - 1} \tag{4.16}$$

The first six moments (0 through 5) were solved for, since these are required to fully calculate (4.15) and (4.16).

The main drawback to this approach is that knowledge of the full CSD is lost during the transformation. Theoretically, one can reconstruct a CSD by solution of a $K \times K$ linear

system, where K is the number of bins in the reconstructed CSD. There can be substantial numerical difficulty in calculating moments of very high order, since the calculation requires the number of moment equations to be equal to $(K-1)$. Figure 2 in McGraw [178] shows increasing deviation from the exact solution for increasing k, for the case of μ_1 through μ_5. Also, this $K \times K$ system is typically ill-conditioned, meaning that even slight changes in the matrix elements can dramatically change the uncovered CSD [111]. The method also cannot be used when the lower moments are functions of higher ones - solution becomes impossible since closure of the equations is never attained. This "closure problem" occurs when more complicated terms are used for the modeling of growth, breakage, and agglomeration [182]. For this reason, simplistic terms for growth, such as constant or linear size-dependence, are commonly used in the literature – and also why breakage and agglomeration are typically neglected.

However, other methods can circumvent this problem and allow us to solve for the full CSD. Various solution approaches are available to solve the PBEs for the full CSD, such as the high resolution finite volume (FV) technique [113], [173], [174], weighted essentially nonoscillatory (WENO) [183], [184], finite element method (FEM) [185], [186], method of characteristics (MOCH) [183], [187], Lattice-Boltzmann method (LBM) [188], [189], and Monte Carlo method[190], [191]. In this work the PBEs were solved using a high resolution FV technique, which is the combination of the semi-discrete FV technique with the van Leer flux limiter, for its efficiency and ease of implementation [113], [173], [174]. The method discretizes (2.13) into K ordinary differential equations, where K is the number of crystal size bins. The discretization started at 2 μm, and

progressed upward in 4 μm increments, for 249 additional increments, up to the maximum bin size of 998 μm, for a total of 250 bins. Just as in the MOM case, the mass balance equation (4.6) is also solved. This technique can capture the sharp front without numerical oscillations and provides at least second-order accuracy where the solution is smooth.

To summarize the two solution methods, the MOM method entails solving 7 simultaneous ODE's, while the FV method requires solving 251. The greater speed (about $1/16^{th}$ the wall-clock time of the FV method) of the MOM method makes it more appropriate for solving the optimization problems. The moment-transformed equations were solved using MATLAB's 'ode23' solver, while the FV equations were solved using Runge-Kutta numerical integration ('ode45' in MATLAB). In our approach we used the fast MOM method with the genetic algorithm to decrease the computation time for finding the optimal antisolvent profiles and crystallizer design, and then used the FV method to observe the full CSD for selected antisolvent profiles.

4.4.3 Multi-Objective Optimization Problem Formulation

The multiobjective problem formulation follows that given in section 2.8.1. With regards to our system, L_{43} and CV are strong functions of the antisolvent flowrate vector, $\boldsymbol{A}$, and manipulating $\boldsymbol{A}$ will change $\boldsymbol{F}$. While there are some instances in which small crystals are desired (e.g. inhalable powders and injectable drugs[21]), we generally desire a narrow

CSD (low CV) with a large mean size (high L_{43}). To solve the MOO problem, we used MATLAB's implementation of the non-dominated sorting genetic algorithm (NSGA-II), 'gamultiobj', to search over $\boldsymbol{A}$ for the non-dominated set, since it is found to work well for solving similar type of optimization problems[146], [192]. For each $\boldsymbol{A}$, the model equations discussed in the previous section were solved. The final result from the last crystallizer segment was used to calculate the objective function values. L_{43} and CV for $n(L, x_{end})$ were calculated using:

$$\boldsymbol{F} = \left[1/{L_{43}}^{N} \;\; {CV}^{N}\right]^{T}, \tag{4.17}$$

where $1/{L_{43}}^{N}$ is used because `gamultiobj' seeks to minimize functions. The actual decision variables used in the optimization were fractions of a required total antisolvent flowrate:

$$A_j = u_j A_{total}\,, \tag{4.18}$$

where u_i is the decision variable manipulated by the genetic algorithm for the j^{th} crystallizer segment, and A_{total} is the total required antisolvent flowrate. An equality constraint forced these percentages to sum to 1:

$$\sum_j u_j \; = 1 \tag{4.19}$$

Each individual decision variable was also bounded between 0 and 1:

$$0 \leq u_j \leq 1 \tag{4.20}$$

4.5 Results and Discussion

4.5.1 Nonconvexity of L_{43} and CV Landscapes

For the solution of the optimization problem both gradient-based and stochastic (GA) algorithms were investigated. Derivative-based algorithms generally offer much faster convergence when the objective function is smooth and convex or with relatively small number of local optima. When this is not the case however, stochastic methods are more appropriate, since such methods are more robust to poor initial guesses. A numerical analysis was performed to investigate the nature of the optimization problem to understand why the GA appeared to be more appropriate. To do this, we performed brute-force evaluation over the antisolvent profiles of L_{43} and CV for two injections, and plotted the responses. The crystallizer modeled using this approach used all the same parameters as in Alvarez and Myerson[169]. Missing sections of these plots denote an infeasible crystallization due to a negative supersaturation.

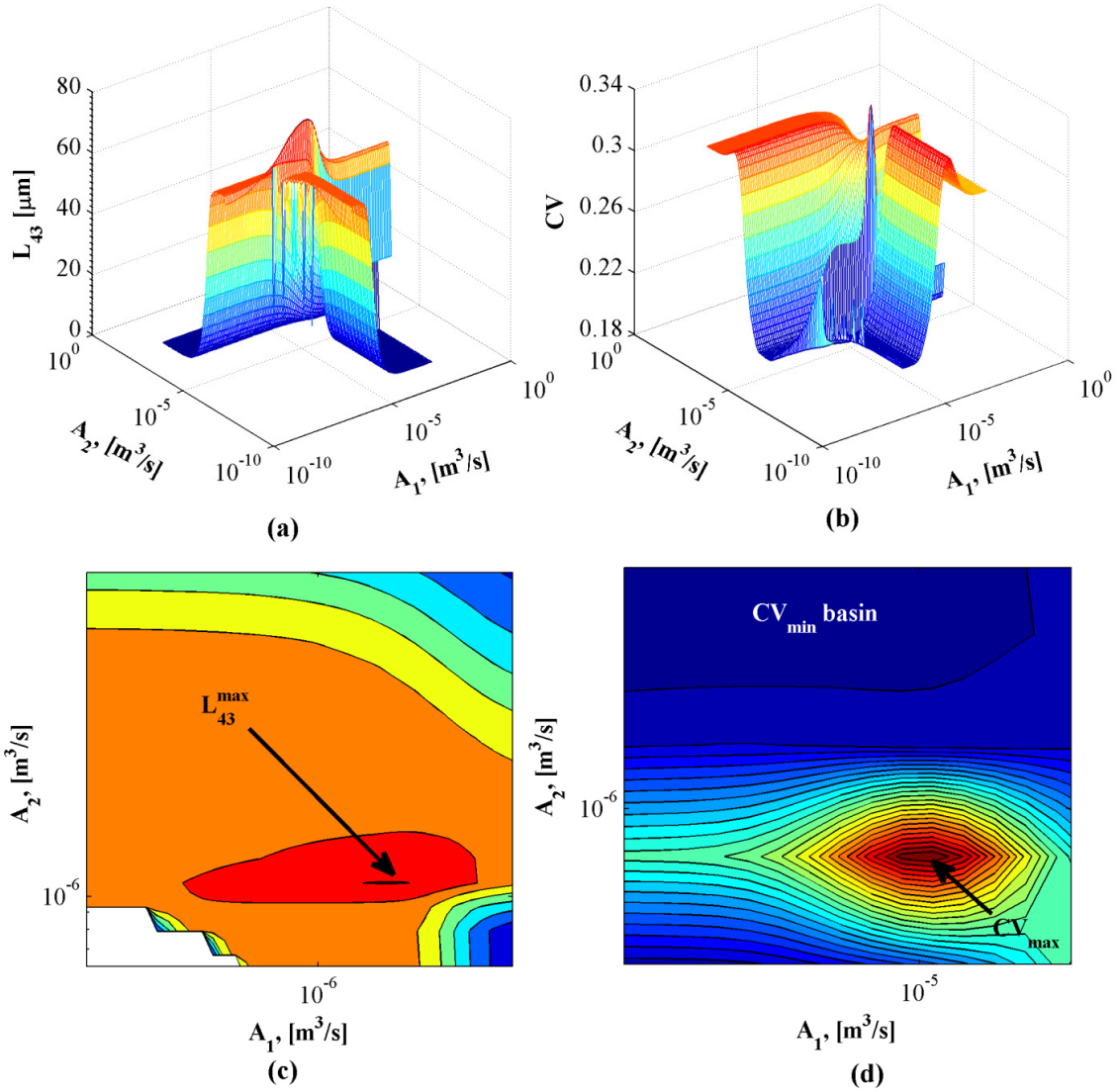

Figure 4.2 L_{43} and CV response surfaces for two injections. The landscapes (a) and (b) present nonconvexity that makes gradient optimization difficult. Great sensitivity to antisolvent flowrate is observed. The contour plots (c) and (d) are zoomed closer to the extrema for clarity.

Figure 4.2 shows the response surface for two injections. The nonconvexity we believe is due to the system, taken as a whole, alternating between nucleation-dominant and

growth-dominant regimes along the length of the array. We further remark that the objective landscape appears highly sensitive around some of the extreme points. The maximum L_{43} (80.2 μm, black arrow, Figure 4.2c), rests at the crest of a tall, knife-like ridge. This indicates that the optimal L_{43} is highly sensitive to model or implementation uncertainties. Small deviation in flow rate A_2 would greatly reduce the mean size of the actually obtained CSD. Furthermore, deviations in the crystallization kinetic parameters from the nominal values are also likely to lead to large deviations from the theoretically optimal performance. An analogous problem exists in the CV landscape, where we can see that global minimum and global maximum are in close proximity. The CV global minimum (0.195, white text, Figure 4.2d) lies in a narrow valley behind the sharp crest containing the CV global maximum (0.351, black arrow, Figure 4.2d). Any error in A_2 will fail to realize the global minimum CV.

4.5.2 Multi-Objective Optimization Results

In this section, different sets of kinetic parameters are used to generate the Pareto frontiers calculated by the NSGA-II algorithm. The motivation for analyzing this sensitivity lies in the fact that there can be appreciable uncertainty involved in the estimation of the kinetic parameters and as such it is a good idea to investigate the impact of these uncertainties on the crystallizer performance. These results are for a four-injection PFC array, with the same dimensions and flowrates as given by Alvarez and Myerson[169]. The total antisolvent flow rate was constrained to be 200 ml/min. The

obtained results are shown in Figure 4, where the default case is for $\gamma_b = \gamma_g = 1$. Altering the kinetic parameters (k_b and k_g) by ±50% affected the position of the Pareto front. The results indicate small sensitivity in the realized CV, though L_{43} shows higher sensitivity. The genetic algorithm used a population size of 100, and was permitted to run for a maximum of 500 generations, though on average finished after about 165 generations. In summary, for about 50% error in the kinetic parameters manipulated, little change can be observed in CV, and L_{43} varies by about ± 2.5 μm, which is also relatively small, indicating that the conclusions of the approach are relatively robust to variations in the model parameters. We wish to emphasize here that the parameters were manipulated prior to optimization, and thus these results indicate the sensitivity of the optimization to shifts in the kinetic parameters.

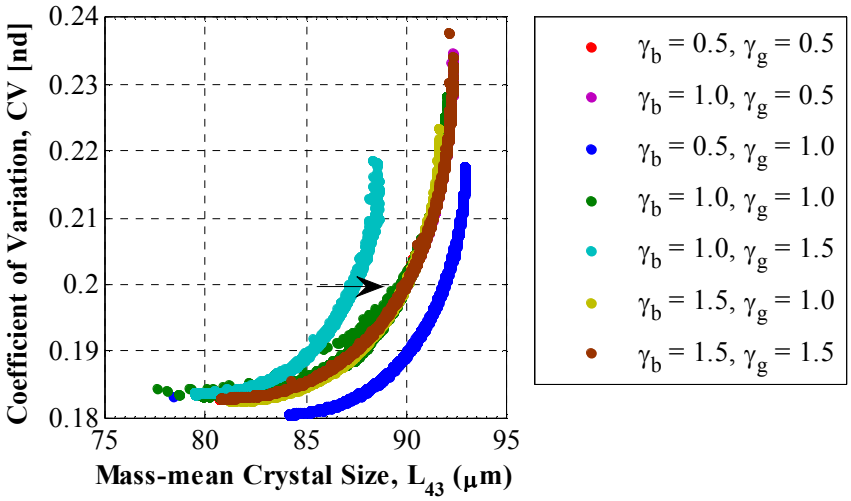

Figure 4.3 Pareto frontier plots for four injections (CV vs. L_{43}) and different sets of kinetic rate parameters, k_b and k_g. The γ's in the legend correspond to multipliers of the base case, e.g. $\gamma_b = k_b' / k_b$. The base case corresponds to $\gamma_b = 1$ and $\gamma_g = 1$, with $k_b = 1.3 \times 10^8$ #/(m^3·s), and $k_g = 9.9 \times 10^{-7}$ m/s. We observe that there is some sensitivity with respect to these parameters on the Pareto frontier, but mainly the effect appears in L_{43}. Little shift is seen in the realized coefficients of variation. For clarity, only the final 25 generations of each parameter set are plotted. The black arrow (L_{43} = 89.98 μm, CV = 0.20) is a representative point that is referred to in Figure 4.4, Figure 4.5, and Figure 4.6.

4.5.3 Investigation Into the Sensitivity to Kinetic Parameters

In the reverse case, we have chosen a representative point from Figure 4.3 (the black arrow), and varied the kinetic parameters by $\pm 50\%$ after the optimization has been performed (Figure 4.4). This gives us an idea of how sensitive the solutions themselves are to error in the kinetic parameters. As expected, L_{43} increases with the increase of k_g and decreases with the increase of k_b. Counter-intuitively, we see that CV decreases as k_b increases. We expected higher nucleation produce more fine crystals, thus increasing CV. To determine why this is, the finite-volume solver was used to plot the volume

fraction distributions of crystals at the three numerical labels in Figure 4.4b. These distributions are shown in Figure 4.5. It is observed that the mean size does indeed decrease with increasing k_b. However, CV slightly decreases due to the elimination of the second mode (the smaller hump in the blue curve in Figure 4.5). It appears that a higher k_b reduces the ability of growth processes to spread out the distribution. This is because a total antisolvent of 200 ml/min was used, thus "locking in" the total available supersaturation. Higher nucleation consumes more of this available supersaturation, leaving less available for growth. Thus we see a narrowing of the distribution due to having a tighter group of fines created during the crystallization.

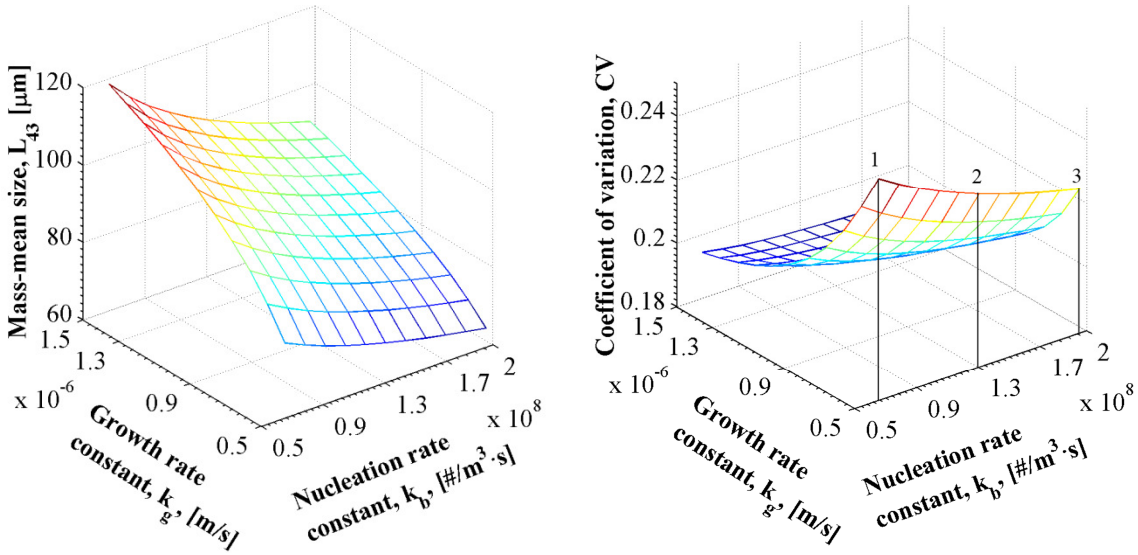

Figure 4.4: Variation in L_{43} and CV for the representative chosen point. Significant sensitivity is observed with respect to k_g. Copyright 2014 IEEE.

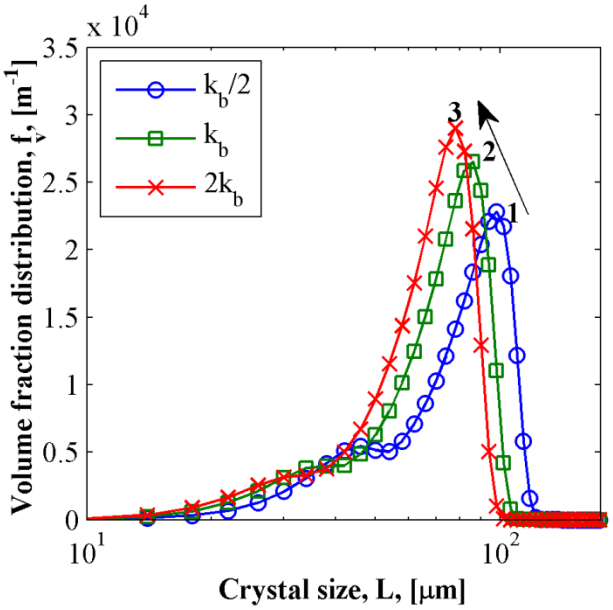

Figure 4.5: Volume size distributions of crystals as a function of nucleation rate constant, k_b. It is observed that increasing k_b decreases the mean size (approximately the mode), but shape-wise the peaks are isomorphic. The second mode in the blue curve is eliminated with increasing nucleation rate.

4.5.4 Comparison between Heuristic Antisolvent Profiles and Rigorous Optimization

Alvarez and Myerson [169] experimented with splitting 200 ml/min antisolvent equally over 1, 2, 3, and 4 injection points in the PFC array, and observed the effect on the volume size distribution. We show that rigorous optimization of antisolvent profile predicts a better result. Referring to the black arrow in Figure 4.3, we have selected a representative point from the Pareto front of the nominal case (L_{43} = 89.98 μm, CV = 0.20), which uses the original set of kinetic parameters ($k_b = 1.3 \times 10^8$ #/(m^3·s), and $k_g = 9.9 \times 10^{-7}$ m/s). Numerical values of the antisolvent flowrates for each of these

cases are given in Table 6. Plugging these profiles into the finite-volume solver generates the volume size distributions shown in Figure 4.6.

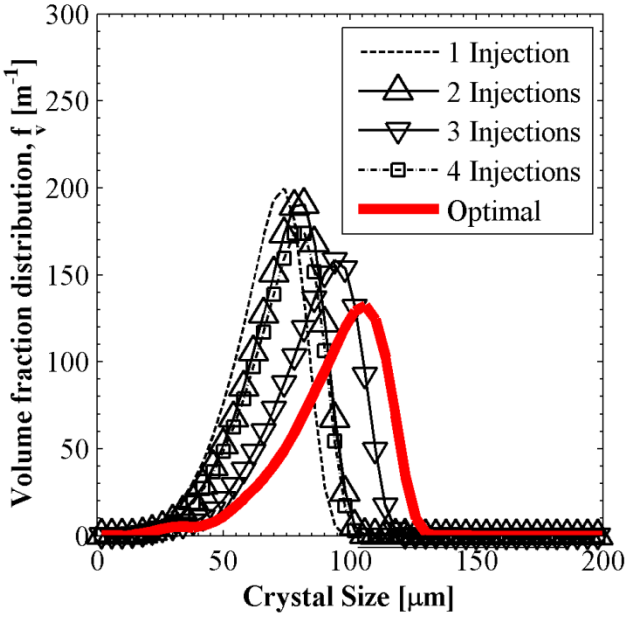

Figure 4.6: Volume fraction distributions of crystals for 1, 2, 3, and 4 equal-flow injections, and the optimal 4-injection profile of the antisolvent. In the 1, 2, 3, and 4 injection plots, 200 ml/min of antisolvent is split equally a corresponding number of ways among the injections. The optimal result uses the flows taken from the representative point (Figure 4.2, black arrow).

The corresponding antisolvent profiles are listed in Table 2. The optimization has left CV essentially the same, but has substantially increased L_{43}. The optimal profile is different from equal apportionment of antisolvent. The optimal antisolvent addition profile is such

that at the first segment about 30% of the total antisolvent is added which generates enough supersaturation so that nucleation occurs. At the second segment almost no antisolvent is added so that the crystals from the first segment can grow in moderate supersaturation without further nucleation. In the subsequent two segments the remaining 30% and 40% of the total antisolvent is added to facilitate the further growth of the crystals.

Table 6 Antisolvent flow profiles used to generate the crystal volume size distributions shown in Figure 4.6 and the corresponding performance index.

Cases	**Flow in injection port (ml/min)**				**Performance index**	
	1	**2**	**3**	**4**	L_{43} **(μm)**	**CV**
1	200	×	×	×	64.47	0.21
2	100	100	×	×	70.8	0.21
3	66.7	66.7	66.7	×	83.25	0.21
4	50	50	50	50	70.35	0.21
Optimal	59.9	1.22	57.72	81.02	92.05	0.21

It is interesting to note that the 4 equal injections case in Figure 4.6 is inferior to the 3 equal injections case, which disrupts the trend demonstrated from the L_{43} sizes produced from the preceding three cases. To understand the cause of this, observe the plot of concentration versus external length in Figure 4.7. It can be seen that in the 4-injection case, the operating point after the first injection is in the first segment is below the solubility curve, and thus the antisolvent addition generates no supersaturation, hence the first segment having no contribution to the crystallization process. In the second segment the crystallization is operated in the metastable zone, but without the first segment the total residence time available for the crystal growth after crystals can form is shorter than in the other cases, therefore crystals cannot grow to larger sizes. Since during antisolvent addition, the concentration in the system decreases due to the dilution effect simultaneously with the decrease in solubility, this dilution effect has to be taken into account to make sure that enough antisolvent is added in the system to reach supersaturation. In the case of the 3 equal injections, the first PFC segment already operates in the metastable zone, yielding nucleation and then growth in the rest of the length of the PFC. In the optimal case, it appears the best procedure is to generate a moderate supersaturation initially, and then quickly reduce it to a lower level. The likely interpretation of this result is that initially supersaturation is desired to be relatively high, encouraging nucleation as soon as possible so that there will be enough residence time for growth. Once sufficient crystals have been generated, lower supersaturation would then foster growth. The single addition generates very high supersaturation immediately promoting excessive nucleation in the system, whereas the two equal injection generates higher supersaturation than what is achieved in the second segment of the four additions

case, following a relatively similar operating curve in the phase diagram. This is in correlation with the results in Figure 4.6, which show that the final CSDs are similar for the 2 and 4 equal injection cases, with more pronounced nucleation in the latter case.

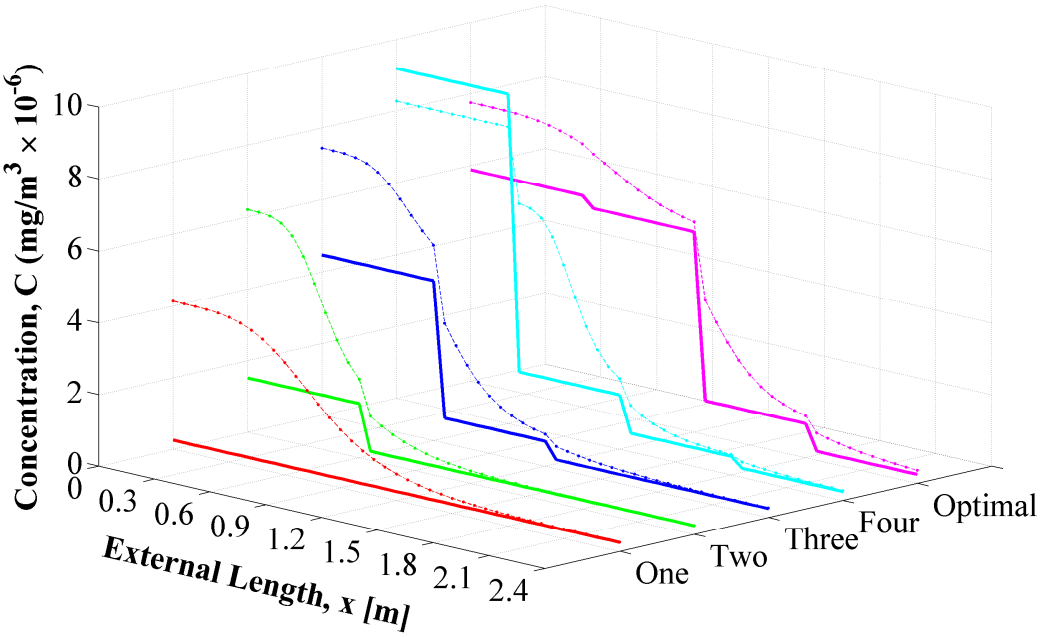

Figure 4.7 Concentration vs. external length plot for equal splits of total antisolvent across one, two, three, or four sections. The optimal result from the representative point is the "Optimal" line. Dotted lines are the concentration in the crystallizer. Solid lines are solubility concentrations.

4.5.5 Investigation of Design Robustness with Regards to Antisolvent Flowrate Error

In optimization and control practice optimal solutions are often sensitive to parametric and/or control variable uncertainty. It is important to know the robustness limits especially for equipment with the production of pharmaceuticals in mind, as designs with high variability are counterproductive to implementing QbD. In this section, we have investigated the sensitivity of the previous optimal profile to uncertainty in the antisolvent flow profile. We are especially interested in flow profile robustness, since the results in Figure 4.2 suggest there is great sensitivity to error in antisolvent flowrates. Error was simulated in the process by a simple Monte-Carlo simulation. Using the same optimal flow profile from Table II, random samples were taken from the nominal values over a range of $\pm$50%. These ranges are listed in Table 7 below.

Table 7 Flowrate Uncertainty Bounds For Robustness Analysis

Segment	**Nominal (ml/min)**	**Low (-50%)**	**High (+50%)**
1	59.90	29.95	89.85
2	1.22	0.61	1.83
3	57.72	28.86	86.58
4	81.02	40.51	121.53

The first robustness simulation only permitted error in a *single segment* in the entire apparatus. 10^4 trials each were done for each of the four flowrates. After a random flow vector was chosen, the MOM solver was used to solve for L_{43} and CV, and the results presented as scatterplots. The results for varying a single flowrate are shown in Figure 4.8 below. The red dot corresponds to the nominal (zero-error) case. Figure 4.8 clearly shows that uncertainty of flow in the first stage has the most impact on the process. The scatterplot has traced out a wide envelope of points that resemble a continuous curve. The uncertainty in subsequent flows is ineffectual, as the scatter plot of points have all hardly budged from the nominal point.

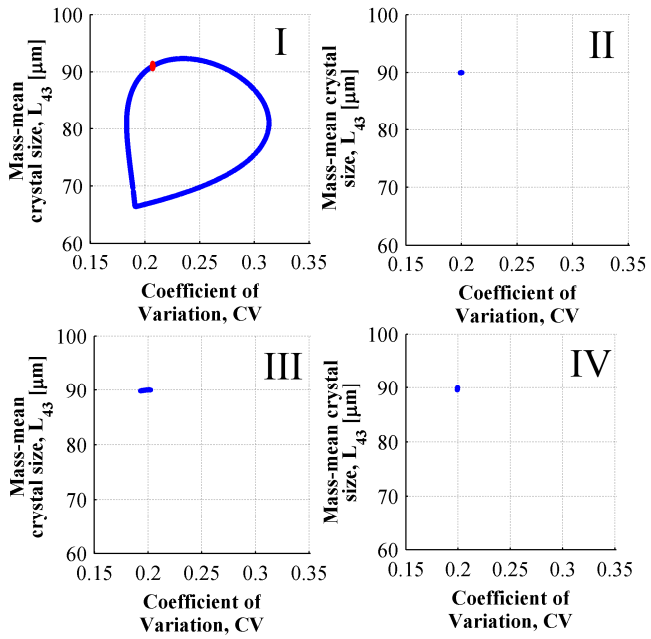

Figure 4.8 Robustness analyses with respect to flowrate by varying a single flowrate. The Roman numerals correspond to the particular MSMA-PFC segment for which random antisolvent flows are being sampled by the simulation. The red dot is the result for the nominal (zero-error) case. Copyright 2014 IEEE.

We further examined the effect of error in multiple simultaneous stages, by permitting the same level of variation, but also varying the stages cumulatively. Figure 4.9 below shows these results for 10^4 trials in each case.

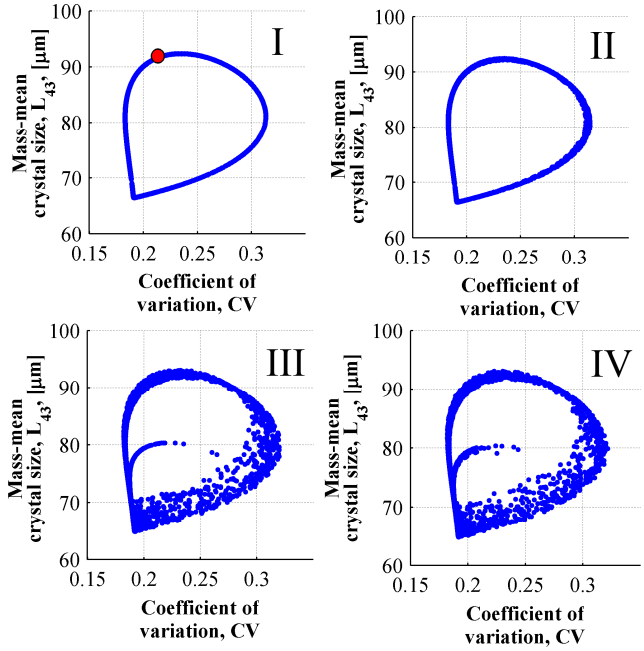

Figure 4.9 Robustness analyses for multiple varying flowrates. The Roman numerals refer to which stage, and all others preceding it, are being sampled by the simulation. The red dot is the result for the nominal (zero-error) case. Copyright 2014 IEEE.

Stage II imparts only mild change in the response, which is likely due to the small flowrate. However, significant variation is observed when stage III is reached, and many new points are reachable that are not present in Figure 4.8. Figure 4.9 suggests that the first stage, where primary nucleation occurs, is by far the most sensitive segment. Furthermore, the increase in nucleation in stage III also makes the process sensitive to the flowrate into that segment.

4.6 Summary and Conclusions Regarding Flufenamic Acid Optimization Work

The chapter describes a multi-segment multi-addition continuous plug flow antisolvent crystallization (MSMA-PFC) setup. We utilized an integrated simulation and optimization framework to analyze the performance and robustness of the MSMA-PFC. The population balance model of the MSMA-PFC was introduced, which was solved, depending on circumstance, with either the method of moments, or the finite-volume method. The model was used in a model-based multi-objective optimization framework to design optimal antisolvent addition policies that maximize mean size and minimize coefficient of variation, using a genetic algorithm for global optimization and to compute the Pareto frontiers, which were also analyzed in the case of uncertainties in the model parameters. Concerning the robustness analysis of the antisolvent flowrates, it appears the proper control of nucleation will have significant process impact, and that uncertainty in antisolvent flowrate will drastically affect performance wherever nucleation predominates over crystal growth. We also conclude that error is best treated by considering the flow profile as a whole, since there appears to be significant interaction between how the upstream stage impacts the downstream performance – a known issue in the subject of continuous pharmaceutical manufacture and process design in general.

CHAPTER 5. SIMULTANEOUS DESIGN AND CONTROL OF THE MSMA-PFC

5.1 Abstract

We have investigated the simultaneous design and control (SDC) of the MSMA-PFC. The SDC framework allows us to optimize not only over flowrates, but over the crystallizer geometry as well. By use of rigorous modeling and optimization, we solve a combined design and control problem to find superior crystallizer designs with corresponding optimal operating conditions for the MSMA-PFC. The procedure works by optimizing the MSMA-PFC crystallizer for various 2-tuples of total length and number of injections. In the first part of this study, we revisit the flufenamic acid optimization discussed in CHAPTER 4. The results indicate greater mean crystal sizes are attainable using the SDC approach. We then repeat this same analysis, but now also have feed flowrate and total antisolvent flowrate as decision variables. For both cases we examine the results derived by either maximizing the mass-mean crystal size, or minimizing the coefficient of variation. The results are plotted as landscapes with the number of injections and the total length as the independent variables. When feed and total antisolvent flowrate are used as decision variables, generally higher feed flowrates are observed when minimizing CV. There is little difference between the landscapes of total antisolvent addition. The residence time landscapes show that the optimal residence time is (roughly) a linear function of total length, and is independent of the number of

injections. Plots of the crystal size distributions show that minimization of CV leads to a much smoother crystal size distribution, albeit with much lower mean size. We investigated in greater depth the maximum case of 25 injections. Here, maximization of L_{43} leads to more complicated multimodal distributions. This is likely due to the calculation of L_{43} being heavily biased towards larger crystal sizes. When total flowrates are used as decision variables, the antisolvent addition profiles for the two cases do not exhibit any distinct patterns or cycling action as was seen previously when they were not used as decision variables. Antisolvent addition is always widely distributed across the length of the crystallizer, indicating that better results are obtained by lengthwise-distribution versus using a single addition at the beginning of a single tube. Adjustment of total length does not reveal any patterns in the antisolvent addition profiles. The growth and nucleation rate profiles show that most of the growth and nucleation take place in the first half of the crystallizer, and that nucleation and growth rates decline toward the end. There is significant differences between the growth and nucleation rate profiles obtained for different tube lengths.

5.2 Simultaneous Design and Control (SDC) Framework for the MSMA-PFC with Static Feed Flowrate and Static Total Antisolvent Flowrate

We examined a new type of optimization problem for the MSMA-PFC, in terms of not only the antisolvent profile, but the number of injections and the total crystallizer length as well. This problem is a simultaneous design and optimal control (SDC) formulation

that aims to provide the best MSMA-PFC design which can provide the overall best performance under optimal operating conditions. This problem leads to a more complicated mixed-integer nonlinear programming problem (MINLP) [193], [194], since the decision variables consist of a set of discrete variables (total length and number of injections), as well as a set of continuous variables (the individual antisolvent flowrates). The complexity of the SDC problem necessitates a single-objective approach. Figure 5.1 presents a flowchart that explains the method used, with the following steps:

1. To optimize the PFC array, an initial total length was assumed, x_{total}.
2. As shown in (4.4), this length is cut into progressively smaller fractional sub-segments of equal length. Antisolvent is injected at the beginning of each segment, just like in (4.4).
3. For each of these injection sub-cases, the single-objective genetic algorithm manipulates the antisolvent flowrates into each segment in order to either maximize the L_{43} crystal size at the exit, or minimize CV at exit.
4. After a maximum number of injections are iterated over (15 in this case), x_{total} is increased, and the process begins anew.
5. The loop continues until the last injection the final x_{total} is reached. The outputs of these optimizations generate landscapes of L_{43}, CV, and yield.

Yield was calculated according to the equation:

$$Y = \frac{C_{in}V_{feed} - (V_{feed} + \sum_{i=0}^{N} A_i)C_{final}}{C_{in}V_0}. \tag{5.1}$$

The MOM was used to speed up the solution of the model equations called by the genetic algorithm. Total antisolvent flow was constrained to be equal to 200 ml/min (the original value from CHAPTER 4), and the decision variables used by the GA were percentages of this amount (constrained to sum to 100%). The feed flowrate was kept static at 100 ml/min (again, the same value used in CHAPTER 4). An initial population of percentages was used for each start of the genetic algorithm, drawn randomly and made to satisfy this constraint. The population size scaled up with the problem size according to $100 + 25j$, where j is the number of injections for the current problem being solved by the GA. A maximum of 200 generations was used. All other solubility and kinetic parameters were kept the same as in Alvarez and Myerson[169]. At the conclusion of the optimization, the L_{43} crystal size, CV, and yield were calculated and stored for later plotting. The total length began at 10 meters, and was increased in 10 meter increments to 50 meters. The number of injections began at 2, and was increased in the inner loop to 15 maximum injections.

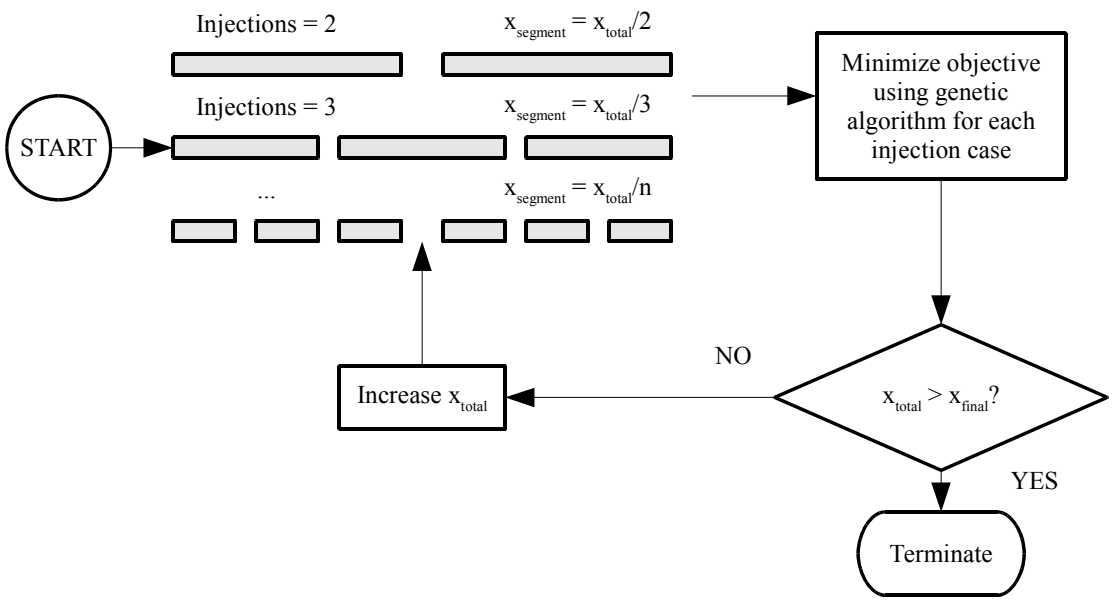

Figure 5.1 Flowchart for the simultaneous design and control (SDC) optimization of the MSMA-PFC array. The algorithm proceeds by cutting a PFC array of a given total length into progressively smaller subunits. Genetic algorithm optimization is performed on each case.

5.3 Results for Simultaneous Design and Control (SDC) Optimization with Feed Flowrate and Antisolvent Flowrate Kept Static

5.3.1 Landscape Plots of Total Length vs. Number of Injections

Figure 5.2 shows the results for the simultaneous design and control (SDC) optimization of the entire MSMA-PFC array. Generally, as expected we observe larger crystal sizes with increasing total crystallizer length, due to longer residence time. The number of injections does not appear to make much difference in L_{43} past about 5 injections. However, in Figure 5.2b, increasing the number of injections tends to reduce CV further. Figure 5.2c confirms that the yield is virtually identical in all cases, always achieving a

value of about 93%. This result stems from the fact that the total flow of antisolvent is fixed for all cases, inferentially controlling the overall yield of the MSMA-PFC.

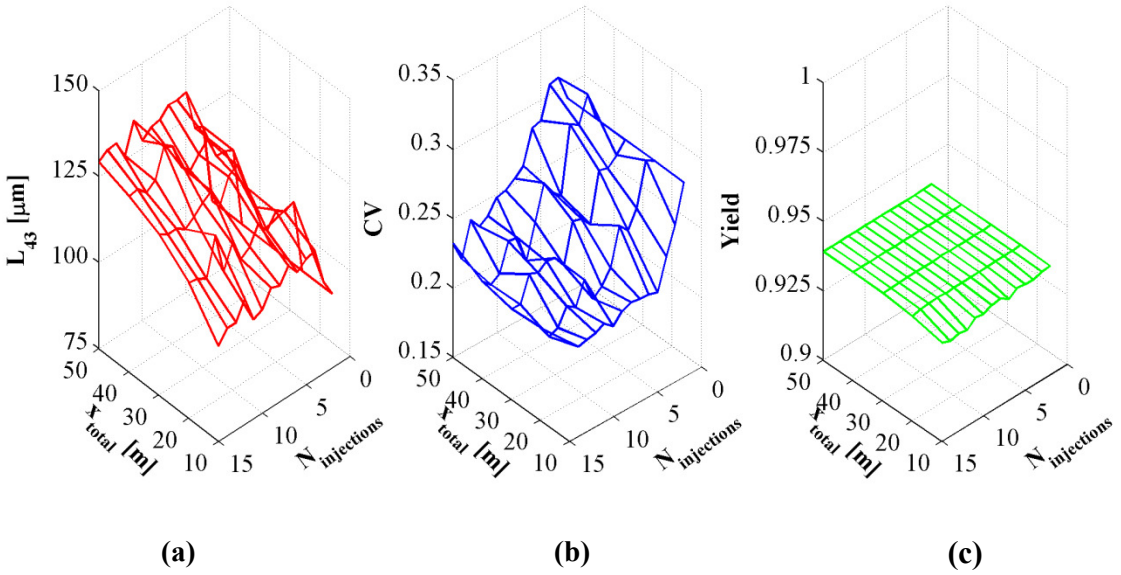

Figure 5.2: Results of the simultaneous design and control (SDC) optimization framework for the MSMA-PFC array over length, number of injections, and antisolvent profile, showing (a) the L_{43} crystal size, (b) coefficient of variation (CV), and (c) the solid crystal yield computed via equation (5.1).

5.3.2 Further Investigation of the Maximum Obtained L_{43} and Minimum Obtained CV

The maximum obtained L_{43} size was 135 μm at $x_{total} = 50$ meters and 11 injections. The CV for that point was 0.24. The minimum CV was 0.207, obtained at $x_{total} = 20$ meters and 14 injections. The L_{43} for that point was 114 μm. These points are explored in

greater detail in Figure 5.3. Figure 5.3a shows the volume CSD's for these two points. We can see the multimodal nature in the L_{43}^{max} distribution, which is indicative of some cyclic behavior in the process. This behavior is not present in the CV^{min} volume distribution. The explanation for this is seen in Figure 5.3b, which shows the antisolvent profiles. We can see the optimal profile for maximizing L_{43} produces a cyclic-type "bursting" of antisolvent. Physically, we interpret this as the optimization seeking to avoid unnecessary nucleation, and focus on growing a smaller number of crystals that were nucleated near the beginnings. On the other hand, the CV^{min} antisolvent profile indicates that most of the antisolvent is added in the second half to minimize variation in the size. In the former case the operation is characterized by a more aggressive nucleation generation in the initial part of the crystallizer to favor the formation of crystals as soon as possible maximizing the residence time available for growth, whereas in the latter the minimization of the CV requires more gentle nucleation control at the beginning to minimize the multi-modal nature of the CSD, and then gradual increase of the supersaturation. The results indicate that for optimal performance equipment should be designed to allow the implementation of the appropriate optimal control strategy depending on the objectives. Future continuous crystallizers therefore need to be designed to be flexible, reconfigurable and adaptable to allow optimal operation. This can be achieved by adopting the proposed SDC framework.

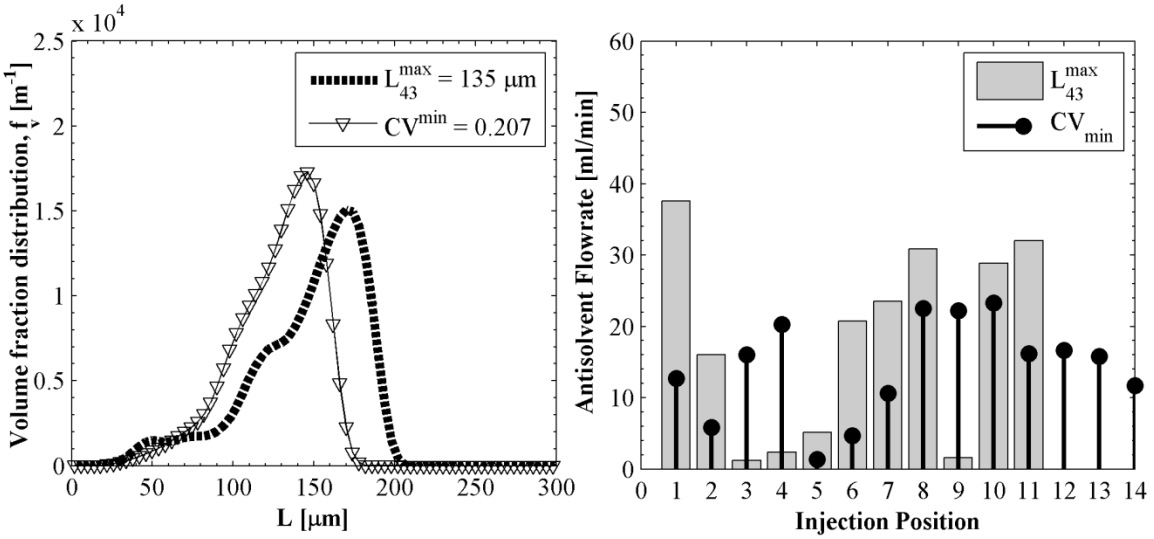

(a) **(b)**

Figure 5.3: Results for SDC over total length, number of injections, and antisolvent profile. We have chosen two points from the surfaces in Figure 5.2 for examination – one point corresponding to the maximum obtained L_{43}, and the other corresponding to the minimum obtained CV. (a) shows the volume CSD's for these two points. The antisolvent profiles that produced these distributions are shown in (b).

5.4 Problem Formulation for Case When Total Flowrates are Used as Decision Variables

In the prior results discussed in section 5.3, we used a fixed total antisolvent flowrate and a fixed feed volumetric flowrate. In the results in this section, these strictures have been removed and total antisolvent (A_{total}, ml/min) and feed flowrate (V_{feed}, ml/min) have become bounded decision variables. Much like in section 5.3, we have investigated how the results change whether the objective is to maximize L_{43} or the minimize CV. Landscapes were generated for various quantities of interest by iterating over total

MSMA-PFC length and the number of injections. The model equations, parameters, and solution methods are identical to those in CHAPTER 4. The two optimization problems solved independently (not multi-objective) were:

$$\max_{a_j, V_{feed}, A_{total}} \quad L_{43} \tag{5.2}$$

and

$$\min_{a_j, V_{feed}, A_{total}} \quad CV \tag{5.3}$$

Both of which were subject to:

$$10 \leq V_{feed} \leq 1000$$
$$10 \leq A_{total} \leq 1000$$
$$0 \leq a_j \leq 1$$

$$\sum_{i=1}^{N} a_j = 1 \tag{5.4}$$

$$C_{final} - 1.05 C_{final}^{sat} \leq 0$$

$$-C_{final} + C_{final}^{sat} \leq 0$$

The prior SDC results did not require a yield constraint, as using a fixed quantity of 200 ml/min antisolvent with 100 ml/min of feed would "lock-in" the final yield. However, with V_{feed} and A_{total} now free decision variables, a constraint on yield is now require to remove economically infeasible designs from consideration.

5.5 Results and Discussion for Case When Antisolvent Flowrate and Feed Flowrate are Decision Variables

5.5.1 Landscapes for Feed Flowrate

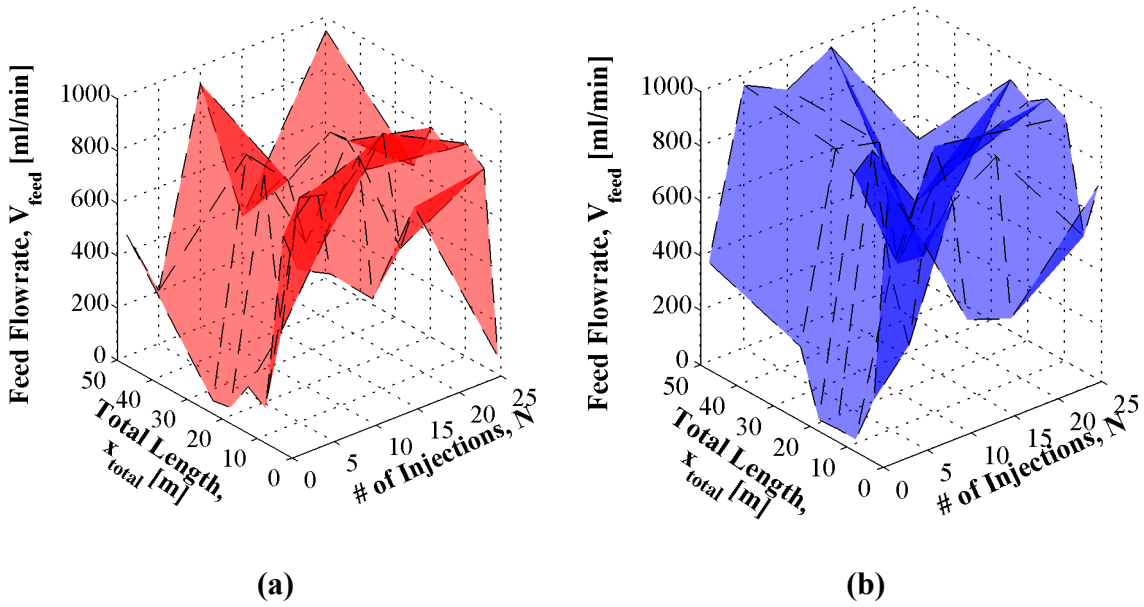

Figure 5.4 Optimized landscapes of feed volumetric flowrates (V_{feed}) against total length of PFC array and number of PFC injections. In (a) the objective was to maximize L_{43}. In (b) the objective was to minimize CV.

The results in Figure 5.4 are the optimal values of V_{feed} for various ordered pairs of total length and numbers of injections. In this section and all of the succeeding sections in this chapter, all data corresponding to the maximization of L_{43} is presented in red, and all data corresponding to the minimization of CV is presented in blue. While these data are somewhat noisy due to the use of the GA, some trends can be noticed. First, we observe that the optimal values of V_{feed} in both cases are generally higher than 100 ml/min,

suggesting longer arrays with more injections can handle a higher mass throughput. We furthermore see that the flowrates tend to be higher when minimizing CV.

5.5.2 Landscapes for Total Antisolvent Flowrate

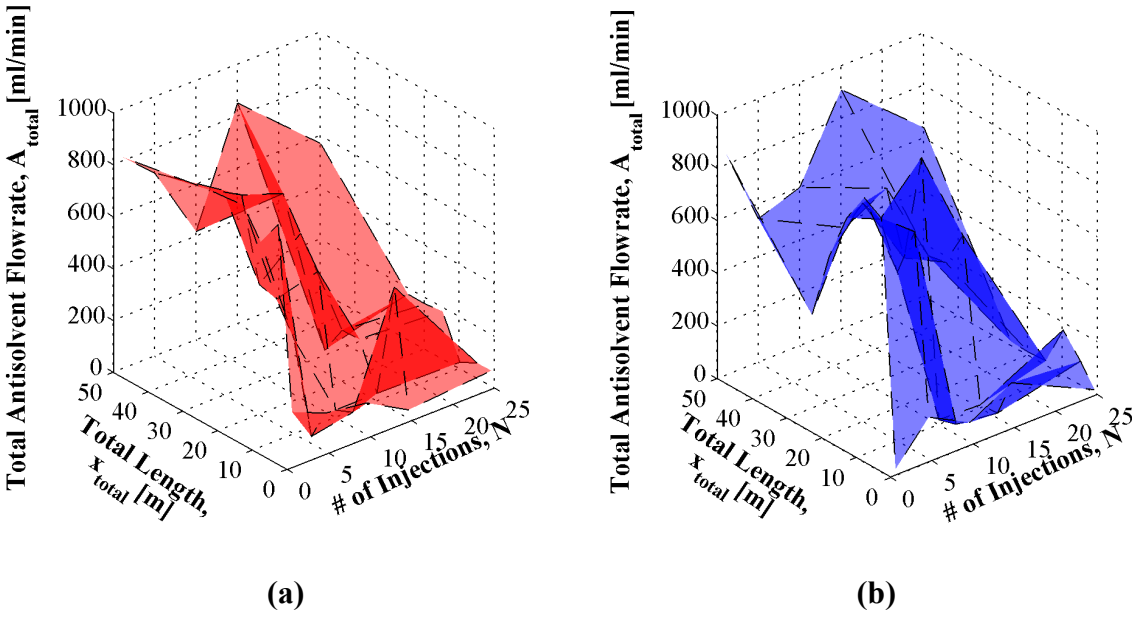

Figure 5.5 Optimized landscapes of total antisolvent volumetric flowrates (A_{total}) against total length of PFC array and number of PFC injections. In (a) the objective was to maximize L_{43}. In (b) the objective was to minimize CV.

Figure 5.5 shows the optimal values of A_{total} for the two optimization problems. These results however, are much closer to one another than the previous plot. A general trend we observe is that longer arrays tend to use more antisolvent than shorter ones. The

similarity in shape may be due to the fact that both optimizations are subjected to the same yield constraint. Thus, a higher feed flowrate would demand a higher antisolvent flowrate in order to deplete the supersaturation to within feasibility. This suggests that the distribution of the antisolvent impacts the process more subtly, though importantly.

5.5.3 Landscapes for Residence Time

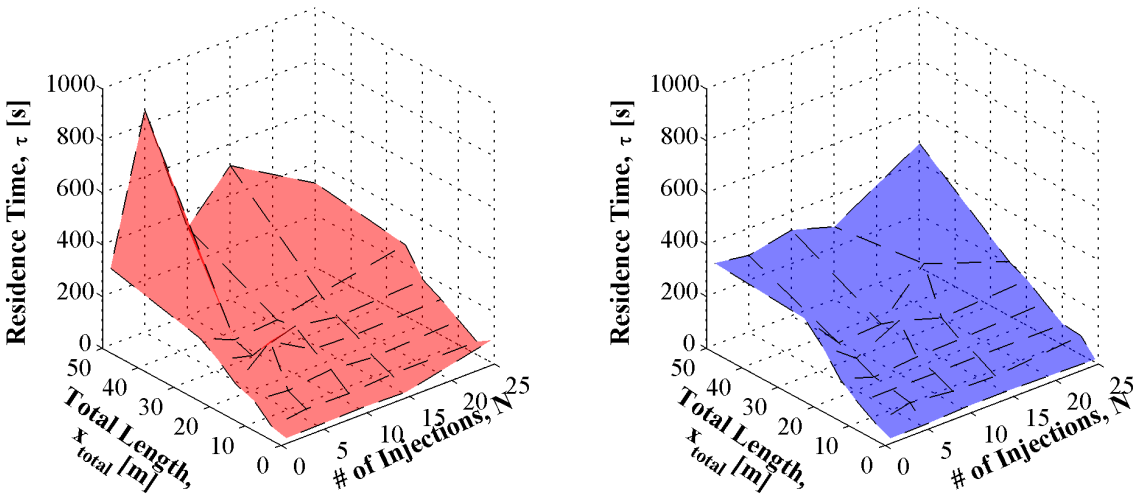

Figure 5.6 Optimized landscapes of residence time (τ) against total length of PFC array and number of PFC injections. In (a) the objective was to maximize L_{43}. In (b) the objective was to minimize CV.

Figure 5.6 shows the residence time landscapes. We can conclude than that optimal residence times follows a roughly linear trend with increasing total length, and is

independent of the number of injections. The similarity between the two plots suggests that total residence time is not precisely what differentiates the two control strategies arrived at by the optimization, and that the individual flowrates are much more important. The relative independence of residence time with the number of injections suggests that the optimal residence time is determined more by the yield constraint and tube geometry, rather than the individual flowrates of antisolvent or the feed flowrate.

5.5.4 Landscapes for Mass-Mean Crystal Size and Coefficient of Variation

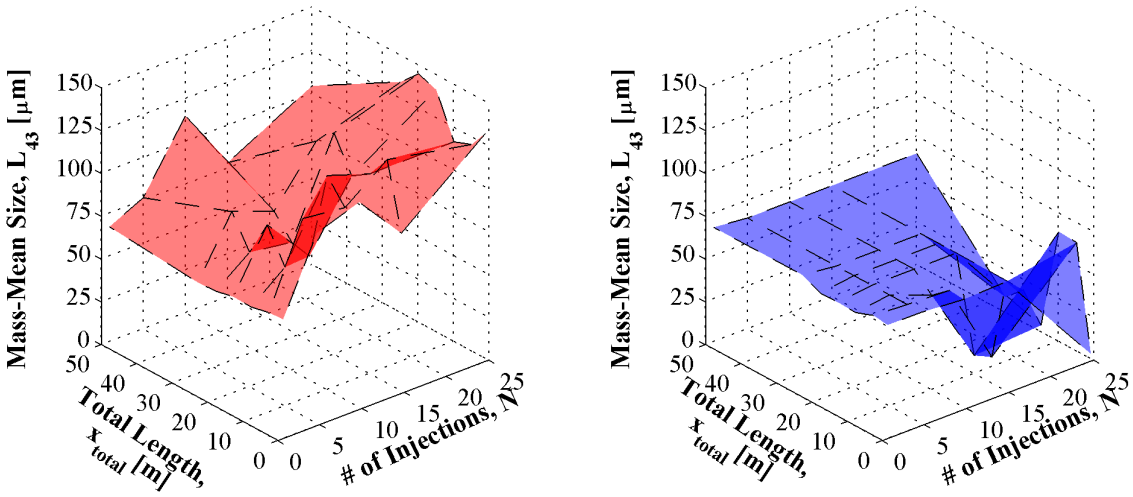

Figure 5.7 Optimized landscapes of mass-mean crystal size (L_{43}) against total length of PFC array and number of PFC injections. In (a) the objective was to maximize L_{43}. In (b) the objective was to minimize CV.

Figure 5.7 shows the landscapes for mass-mean crystal size. Clearly, maximizing L_{43} leads to much larger crystals than when minimizing CV. These results are in agreement

with the Pareto frontier results from section 4.5.2, which show that there is a significant tradeoff between these two quantities during optimization. We furthermore note that there is not much increase in the maximum obtained crystal size (about 140 μm) compared to the 135 μm in Figure 5.3. The landscapes for coefficient of variation are shown in Figure 5.8 below are somewhat puzzling in that the results in Figure 5.8a show generally lower CV than those in Figure 5.8b. This may be due to the greater complexity of the CV objective function causing improper convergence, as evidence by the landscape plot in section 4.5.1. However, certain points do show significantly higher CV when solely attempting to minimize L_{43}, suggesting again that a more aggressive crystallization leads to more growth, but also more nucleation.

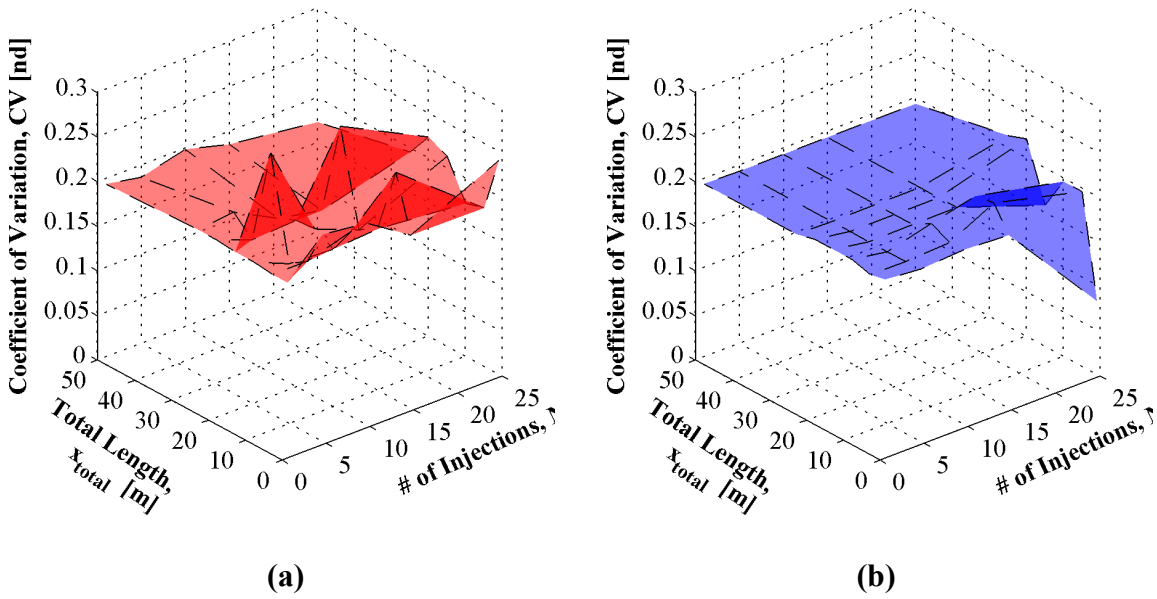

Figure 5.8 Optimized landscapes of coefficient of variation (CV) against total length of PFC array and number of PFC injections. In (a) the objective was to maximize L_{43}. In (b) the objective was to minimize CV.

5.5.5 Number Fraction Distributions for the Case of 25 Injections

Figure 5.9 shows the final exit distributions calculate using the finite-volume method for the case of 25 injections for the crystallizer lengths of 1 meter and 50 meters. The two distributions in each graph correspond to either attempting to maximize L_{43}, or minimize CV. We can see in Figure 5.9 two main features that stand out from this data. Maximizing L_{43} tends to lead to a multimodal distribution (Figure 5.9a red curve). This is because the objective was to maximize L_{43}, and L_{43} the calculation of L_{43} is dominated by larger crystal sizes. The distributions generated from minimizing CV are much smoother, and do

not tend to be multi-modal. We observe though the longest tube length of 50 meters, the multiple modes in the red curve die out.

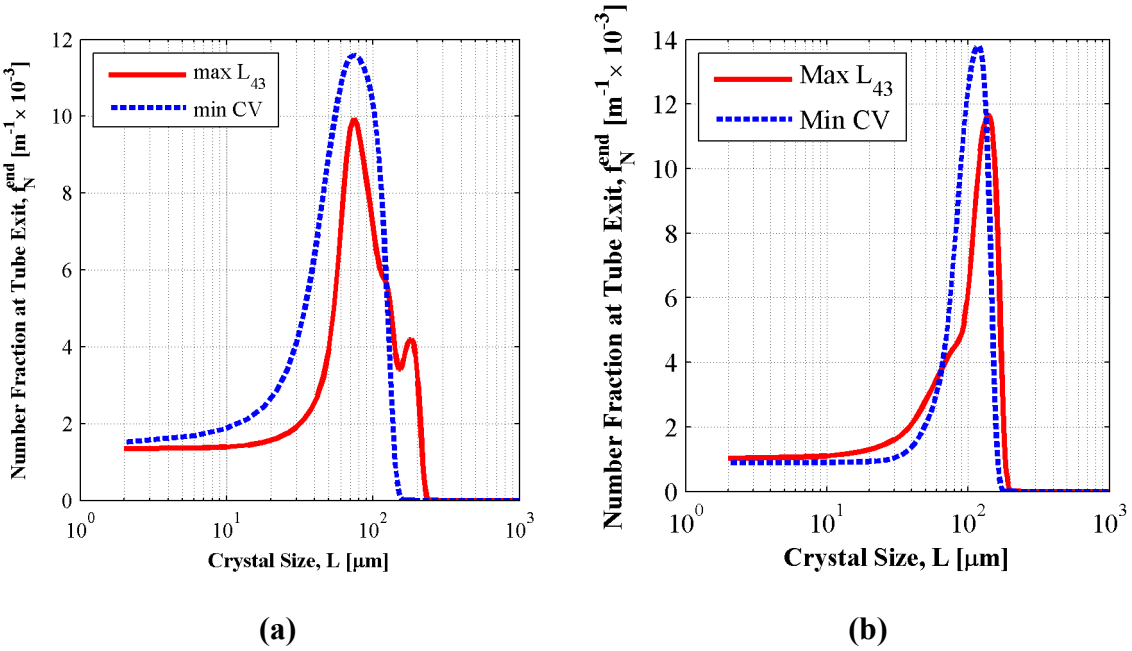

(a) **(b)**

Figure 5.9 Number fraction distributions for the case of 25 injections. Each plot corresponds to a different total length. (a) 1 meter and (b) 50 meters.

5.5.6 Antisolvent Profiles for the Case of 25 Injections

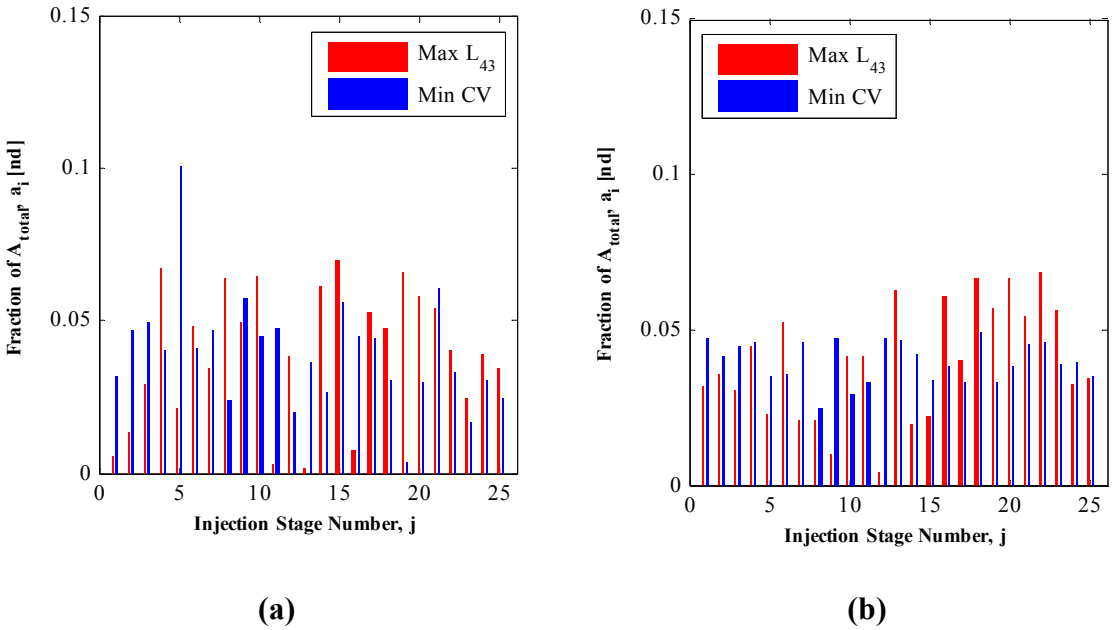

Figure 5.10 Antisolvent fraction profiles for the case of 25 injections. Each plot corresponds to a different total length. (a) 1 meter, (b) 50 meters.

Figure 5.10 above shows the antisolvent fraction profiles for the two optimization cases. Generally, it is difficult to discern noticeable features from these profiles, indicating that optimal or near-optimal solutions are not intuitive. Nearly all addition used less than 10% of the total antisolvent. The profiles are different from each other, agreeing with intuition that total length is a significant design variable that directly impacts the optimal possible performance, and also affects what the antisolvent addition profile should be.

5.5.7 Growth and Nucleation Profiles for the Case of 25-Injections

Figure 5.11 shows growth and nucleation rate profiles for the case of 1 meter and 50 meters total length when maximizing the mean crystal size. Figure 5.12 likewise shows the same type of figures for those same lengths, but for the case of minimizing the coefficient of variation.

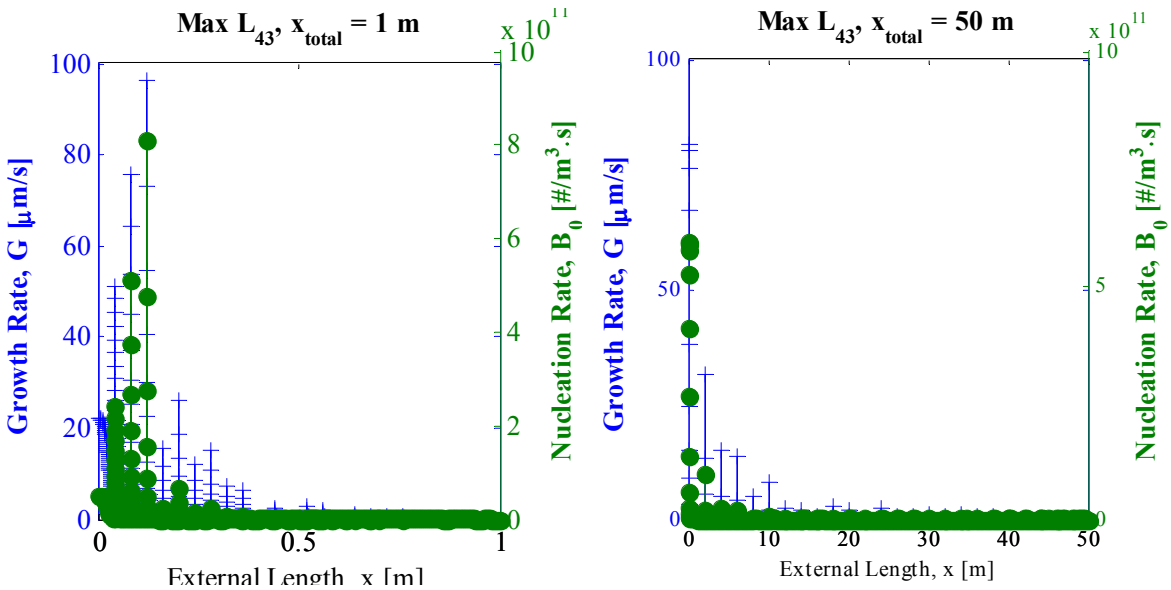

Figure 5.11 Growth and nucleation rate profiles for the case of maximizing mass-mean crystal size. (a) 1 m total length, (b) 50 m total length.

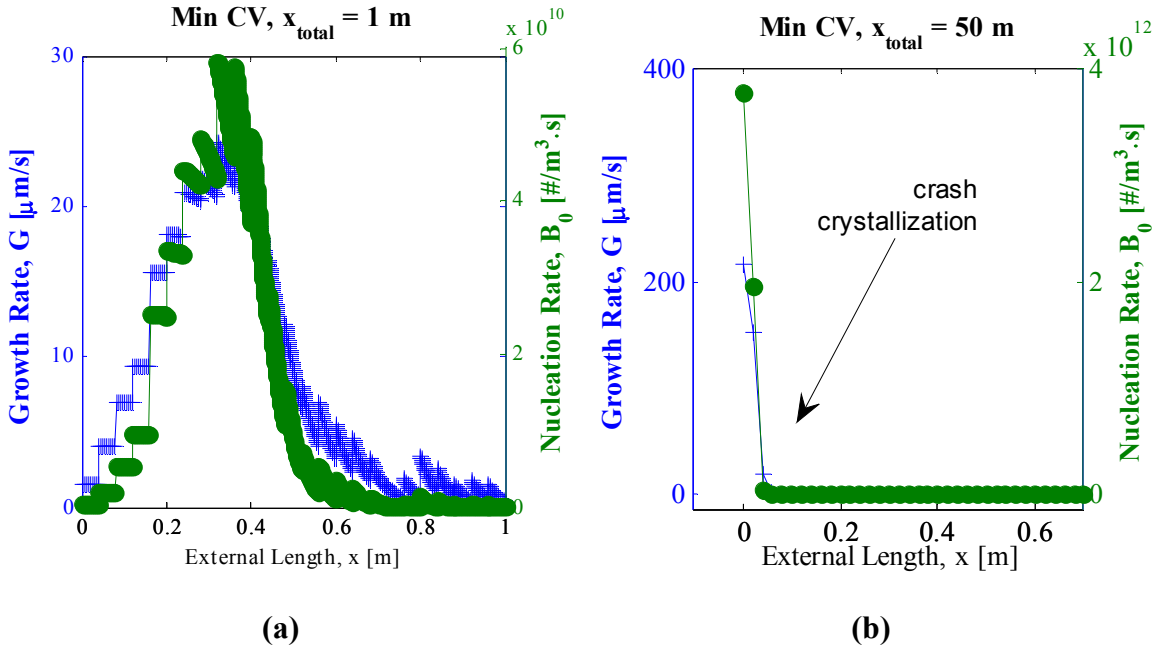

Figure 5.12 Growth and nucleation rate profiles for the case of minimizing coefficient of variation. (a) 1 m total length, (b) 50 m total length. Note the change of x-scale in (b).

For the case of maximizing mean size, generally, the optimization seeks to raise the growth and nucleation rates in a pulsing fashion. However, two of the plots show exception to this rule. Figure 5.12a shows a distinct "jagged hill" type profile which is not seen in any of the other plots. It is also worth noting that this profile scored a much lower CV than was typical (about 0.08) in Figure 5.8b. This suggests that many small segments are required to exert effective control over the fast-acting process of nucleation. Figure 5.12b shows that virtually all of the growth and nucleation occur in the first stage as a crash crystallization. Intuitively, growth and nucleation decline toward the end of the crystallizer. This is partly in order to satisfy the yield constraint, but also because available supersaturation is being consumed by growth and nucleation.

5.6 Summary and Conclusions

A simultaneous design and control (SDC) framework is proposed based on the complete optimization of the entire PFC array over total length, number of injections, feed flowrate, total antisolvent flowrate, and antisolvent profile. It is shown that, for the case of static feed and antisolvent flowrates, the typical optimal antisolvent addition protocol leads to a cyclic operation which promotes shifts between growth-dominated and nucleation-dominated regimes in the different PFC segments. This periodic operation yields to a strongly nonconvex search landscape motivating the use of genetic algorithm for the optimization. We have also investigated the performance of the MSMA-PFC when feed flowrate and total antisolvent flowrate are used as decision variables as well. The results indicate that there is little increase in maximum L_{43} crystal size compared to the results in CHAPTER 4, though significantly lower CV's can be obtained. However, higher flowrates are obtained by the optimization, indicating a higher mass flowrate can be used without reducing the mean size. The flow profiles have no discernible pattern, but do indicate that there is benefit to distributing antisolvent across the length of the crystallizer. The growth and nucleation rate profile plots indicate, for both optimizations, a general pattern of high supersaturation at the beginning of the crystallizer, with supersaturation being "pulsed" down the remainder of the length of the crystallizer. The SDC framework can be used to design flexible, reconfigurable and adaptive continuous crystallization systems that can achieve optimal performance by allowing the implementation of the best control strategy needed for a particular objective and under certain operating constraints.

CHAPTER 6. PARAMETRIC STUDY OF THE FEASIBILITY OF IN-SITU FINES DISSOLUTION IN THE MSMA-PFC

6.1 Abstract

We have investigated the use of an antisolvent MSMA-PFC , which can grow and keep extant large crystals while dissolving fines in-situ. By applying and extending the framework discussed in CHAPTER 5, we have shown that dissolution is rejected by the optimization and that dissolution is suboptimal. A reduced orthogonal array experimental design was used to avoid a high computation time. The results of the main-factor analysis show that nucleation rate imparts the greatest process sensitivity, followed by growth rate. High nucleation overwhelms the MSMA-PFC. The MSMA-PFC performs best under kinetic crystallization conditions in which a single PFC also works sufficiently well, indicating little benefit.

6.2 Introduction

While purification is the main motive behind crystallization, the crystal size distribution (CSD) affects downstream operations and the ameliorative properties of the final dosage form. Downstream processes affected by CSD shape include filtering, washing, and drying [53]. The presence of fine crystals encumbers these operations.

The curative properties of the final dosage form are dependent on the dissolution rate and bioavailability, which are strongly affected by the CSD and other particle properties [110], [195]. The typical method of removing fines is to classify the product crystals, re-dissolve the fines, separate the antisolvent when feasible, and recycle the mixture back to the crystallization system. However, this method is problematic. Classification, recycle, and stream separation require further process equipment, increasing capital and operating costs. Classification combined with recycle has been mathematically deduced (and subsequently observed) to impart oscillatory dynamics to the CSD. These oscillations make it difficult to obtain a consistent product. Furthermore, from a risk analysis viewpoint, extra equipment is generally "more things that can go wrong", and present another route by which microbes could contaminate the manufacturing process. Ideally, it would be good if we could eliminate fines altogether by an in-situ approach.

6.3 Prior Work on In-Situ Fines Removal

Previous work by Abu Bakar et al. [195] and Majumder and Nagy [113] explored the concept of "in-situ" fines removal, where the operation of the crystallizer actively eliminates fine crystals during the crystallization by means of dissolution. With this approach, classification, re-dissolving, and stream separation become (in theory) unnecessary. The work by Majumder and Nagy [113] most closely follows our work here. In that work, a constrained nonlinear optimization problem was solved to identify operating curves that would match a target distribution in a least-squares sense by

removing fine crystals. Majumder and Nagy [113] previously investigated computationally the use of multisegment cooling crystallization for in-situ fines dissolution. In that work, the decision variables were the jacket temperatures in each segment, which allowed the particular segment to go above or below solubility as necessary to dissolve the fine crystals and grow large ones. Ridder et al. [161], [162] have modeled and optimized a multi-segment antisolvent crystallizer for drug crystal production, but that work did not allow for dissolution to occur. This work is an extension of the previous works by Ridder et al. and Majumder and Nagy, as we are now using an antisolvent crystallization with the capability to dissolve crystals when below solubility. Figure 6.1 below depicts the path of information flow for a cooling PFC crystallization process, and an antisolvent PFC crystallization process. For an antisolvent crystallization, the decision variables are the flowrates of antisolvent into each segment. The cooling crystallization has no coupling between residence time and the control (jacket temperature), and residence time is constant within each segment. None of this is true in antisolvent crystallization, since the addition of antisolvent simultaneously affects the current concentration via dilution, and reduces the current residence time due to a mass balance argument. This coupling dramatically increases the difficulty in optimizing the process.

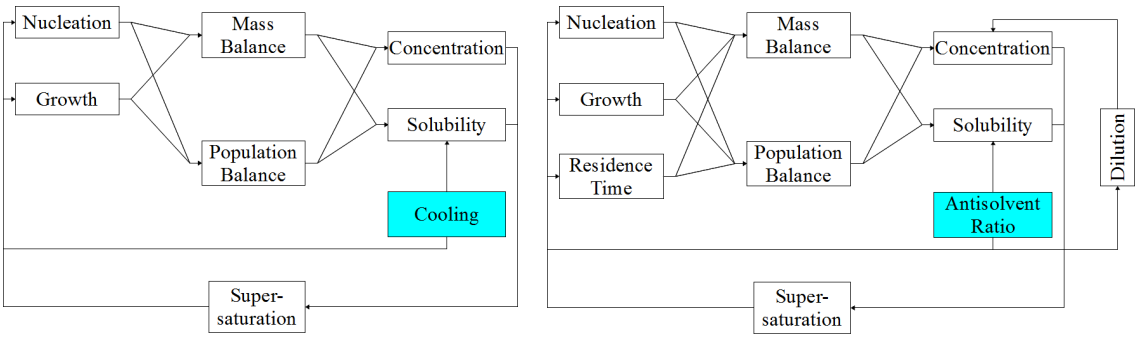

(a) **(b)**

Figure 6.1 Information flow diagrams in a multisegment crystallizer for (a) cooling crystallization and (b) antisolvent crystallization.

6.4 Parametric Study via Optimization of the Antisolvent Crystallizer

In this work, we present results for the steady-state operation of a multi-segment, multi-addition, plug-flow crystallizer MSMA-PFC which utilizes dissolution to eliminate fine crystals. We have explored the geometric design parameters of the crystallizer, as well as the kinetic parameters of crystallization. To reiterate, this work is an extension of that by Majumder and Nagy [113], but for the case of antisolvent crystallization as opposed to a cooling crystallization.

6.5 Model Framework

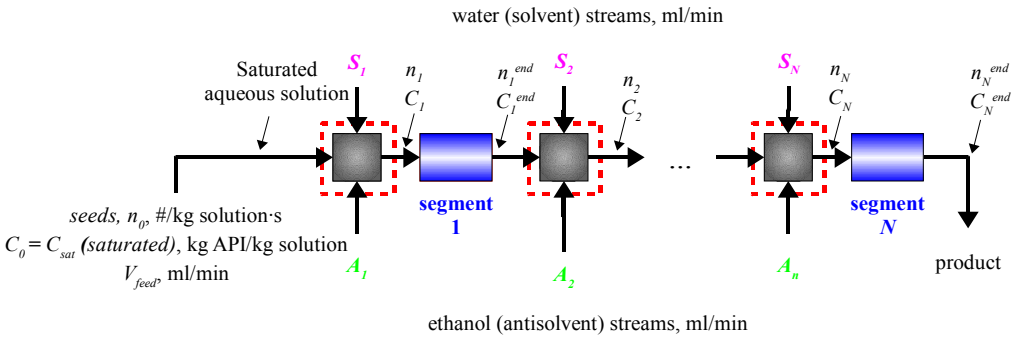

Figure 6.2 Diagram of the MSMA-PFC. Seeded liquid solvent, with solute concentration C_0 flows in from the left into a mixing chamber (gray box). The dilution correction factor, γ_j, is applied to the exit stream around each mixing point (red dashed boxes). The combined streams then flow into a plug-flow segment (blue rectangle). Antisolvent reduces solubility, triggering nucleation and growth. Streams of pure solvent are utilized to push the solution below solubility when necessary.

The model presented here is similar to that discussed in CHAPTER 4 and CHAPTER 5. Some important differences we mention immediately are:

- The greatest difference is that the model now accepts pure solvent additions in addition to antisolvent. The addition of pure solvent can permit the crystallization to go below solubility, thus inducing dissolution of the crystals. The idea is to dissolve the smallest crystals, while keeping the large ones relatively intact.
- Before, ethanol was the solvent and water the antisolvent. In this chapter, water is the solvent and ethanol is the antisolvent.
- Flufenamic acid was the solute in the first model, whereas here we have no drug in particular as the solute; this is a parametric study.

- In the prior model, concentration and number density were expressed on a *volume of solution* basis. In this chapter, concentration and number density are based on a *mass of solution* basis.
- The prior model was unseeded, with primary nucleation present. Here we are using a seeded process with secondary nucleation present.

The MSMA-PFC is based on the setup in Alvarez and Myerson [135]. It is modeled as a series of ideal plug flow elements, of equal length, and antisolvent is added at the beginning of each segment (Figure 6.2 above). Each of the *N* segments is a separate PFC, running in steady-state, isothermal operation. The inlet stream (far left) feeds saturated mother liquor at flowrate V_{feed} (ml/min), with an initial concentration of solute, C_0 (kg API/kg solution), and a seed CSD, n_0 (# of crystals/kg of solution·m). At each mixing point (gray boxes in Figure 6.2), antisolvent flowing at flowrate A_j (ml/min), and pure solvent at flowrate S_j (ml/min), for $j = 1,2, \dots, N$. We reiterate that we are using mass-intensive units for our state variables, n (#/kg solution) and C (kg API/kg solution). After mixing with the solvent and antisolvent streams, the mixture then flows into the j^{th} PFC segment, where nucleation and growth occur. We assume the streams mix on a time scale well below the induction time, and also attain plug-flow. At the exit of the segment, a new size distribution, $n(L, x_j^{end})$, and a reduced solute concentration, $C(x_j^{end})$, are obtained. We will abbreviate these quantities as n_j^{end} and C_j^{end}. We clarify to the reader that this is not the same as C_{j+1} or n_{j+1}; these quantities are created when the next solvent and antisolvent streams are added; the pattern of indexing is made clear in Figure 6.2 above. This process continues recursively until the product stream leaves the final,

N^{th} segment (product stream). The final crystal size distribution, n_N^{end}, is used for solving the least-squares optimization problem. Both n_N^{end} and C_N^{end} are used to calculate several constraints. Summation indices always use the letter i as a dummy index. The letter j always refers to "for the j^{th} PFC segment." When an index refers to a mixing point, j always refers to the mixing point immediately preceeding the j^{th} PFC segment (e.g. the $j = 1$ mixing point is the very first mixing point on the left hand side in Figure 6.2 above).

The addition of streams A_j and S_j to the process causes a decrease in C and n in the oncoming feed stream due to the effect of dilution. Concentration and number density are reduced is because the solute mass (and crystal mass) has remained the same, but total volume has increased. There is a double meaning of this term in the literature, as some authors refer to antisolvent crystallization as "dilution" [51]. We reiterate that in this paper, we refer to dilution as being the reduction in solute concentration due to the addition of liquid. To account for this effect, the number density of the j^{th} outgoing stream, n_j (# of crystals/kg of solution·m) about the j^{th} mixing point is multiplied by:

$$\gamma_j = \frac{\rho_j^{solution} V_j^{solution}}{\rho_{j+1}^{solution} V_{j+1}^{solution}} \tag{6.1}$$

Where $\rho_j^{solution}$ is the density of the solution, and V_j is the volumetric flow rate of the entire stream. V_j can be determined by dividing the total solution mass flow rate by the total solution density:

$$V_{j+1}^{solution} = \frac{\rho_{H_2O}\left(V_{feed} + \sum_{i=1}^{j} S_i\right) + \rho_{EtOH} \sum_{i=1}^{j} A_i}{\rho_{j+1}^{solution}} \tag{6.2}$$

Where ρ_{H_2O} and ρ_{EtOH} are the densities of water and ethanol (997 kg/m^3 and 785.22 kg/m^3, respectively). The total solution density, $\rho_{j+1}^{solution}$ (kg/m^3), is calculated numerically from a curve fit of the density of an ethanol-water mixture in terms of ethanol mass fraction. These expressions are derived by performing progressively wider mass balances about the mixing points and PFC segments. The method is more easily explained with a diagram (Figure 6.3 below). The colored boxes demonstrate the pattern one follows to ultimately derive (6.1) and (6.2).

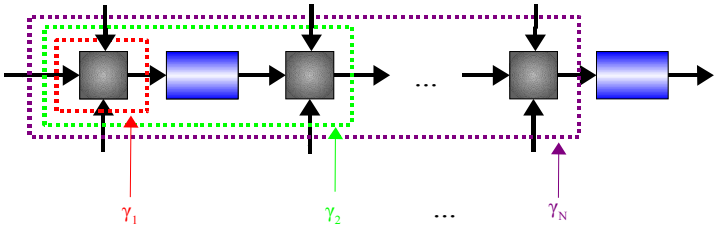

Figure 6.3 Mass balance envelopes that are used to derive γ dilution correction factor. Incoming streams are positive; outgoing are negative.

6.6 Crystal Population and Solute Mass Balance Equations

In order to properly model the crystallization, two equations need to be solved simultaneously: the population balance equation, and the mass balance equation.

The population balance equation is the same as (4.2). The mass balance on dissolved drug is given by:

$$\frac{dC_j}{dx} = -\frac{\rho_c k_v}{u_{x,j}}(3G\mu_{2,j} + B_{0,j}L_0^3) \tag{6.3}$$

The term μ_2 is the second moment of the crystal size distribution (m^2 of crystals/kg solution). C is the solute concentration in the liquid phase (kg API/kg solution), ρ_c is the density of crystalline API (assumed to be 1490 kg/m^3), L_0 is the minimum detectable crystal size (m), B_0 is the nucleation rate (# of nucleated crystals/kg solution·s), and k_v is the dimensionless crystal shape factor ($\pi/6$ for spheres) [196]. The units of the derivative reduce to (kg of crystals/kg solution·m external coordinate). In a pure mathematical treatment, L_0 would simply be set to zero; however, all instrumentation used in practice for experimentation and process control will have limits to observability. When the crystallization is *below* solubility, the mass balance becomes:

$$\frac{dC_j}{dx} = \frac{3\rho_c k_v D\mu_{2,j}}{u_{x,j}} \tag{6.4}$$

Where D is the dissolution rate, explained in the section 0.

6.6.1 Boundary Conditions

For the first segment ($j = 1$), the boundary conditions for these equations are:

$$n_1(L, x = 0) = \gamma_1 n_0$$
$$n_1(L = 0, x) = B_{0,1}/G_1 \tag{6.5}$$
$$C_1(x = 0) = \gamma_1 C_0$$

Where n_0 is the seed crystal size distribution, B_0 is the nucleation rate (#/kg of solution·s), and C_0 is the initial solute concentration. In subsequent segments ($j \geq 2$), the boundary conditions become:

$$n_j(L, x = 0) = \gamma_j n_{j-1}^{end}$$
$$n_j(L = 0, x) = B_{0,j}/G_j \tag{6.6}$$
$$C_j(x = 0) = \gamma_j C_{j-1}^{end}$$

A Gaussian bell curve was used for n_0 (#/kg of solution·m) in all cases, with mean δ_{seed} (meters) and standard deviation ω_{seed} (meters) (we would normally use the Greek letters μ and σ for the mean and standard deviation, but these letters already correspond in this work to the moments of the crystal size distribution and the supersaturation):

$$n_0(L) = \frac{N_{total}}{\omega_{seed}\sqrt{2\pi}} \exp\left(-\frac{(L - \delta_{seed})^2}{2{\omega_{seed}}^2}\right) \tag{6.7}$$

Where N_{total} is the total number density (# of crystals/kg solution). N_{total} can be interpreted in (6.7) as a constant that forces the seed distribution to agree with the specified seed mass loading, ξ (%, dimensionless). The mass balance on the seed distribution is closed by solving the algebraic equation for N_{total} such that:

$$\xi C_0 - \rho_c k_v \mu_{3,0} = 0 \tag{6.8}$$

Where $\mu_{3,0}$ is the third moment of the seed distribution. Equation (6.8) is closed by manipulating N_{total}, which is embedded in the integral term $\mu_{3,0}$:

$$\mu_{3,0} = \int_0^\infty n_0 L^3 dL \tag{6.9}$$

6.6.2 Growth, Nucleation, and Dissolution Rate Laws

The growth and nucleation laws are given by the equations (again, all j subscripts refer to the j^{th} segment):

$$\begin{gathered} G_j(S_j) = k_g S_j^g \\ B_{0,j}(S_j) = k_b \mu_2 S_j^b \\ D_j(S_j) = -\varphi k_g (1 - S_j)^d \\ S_j = C_j(x)/C_{sat,j} \end{gathered} \tag{6.10}$$

Where S is the supersaturation ratio, k_g is the growth rate constant, g is the growth rate order, k_b is the nucleation rate constant, b is the nucleation order, D is the dissolution rate, d is the dissolution order, and C_{sat} is the solubility concentration (kg API/kg solution). G is replaced by D in (6.3) for $S < 1$, and $d = 1$ always in this work. We use a modified version of the growth law for the dissolution rate law. The dissolution rate can be approximated by multiplying the modified version of the growth law by a constant $\varphi > 1$, which adjusts for the fact that dissolution is typically much faster than growth. The calculation of C_{sat} is discussed in section 6.6.3. A summary of all fixed parameters

related to equations (4.2) and (6.3) are given in Table 8 below. These variables were all kept fixed during the optimization; decision variables are delineated further ahead.

Table 8 Physical and chemical property data table used for modeling the antisolvent crystallization.

Parameter	**Value**
Initial concentration, C_0 [kg API/kg solution, always saturated]	0.030935
Shape factor, [-]	$\pi/6$
Solid API density, [kg/m^3]	1490
Dissolution acceleration, φ [-]	250
Number of segments, N [-]	50
Seed crystal mean size, δ_{seed} [μm]	50
Seed crystal standard deviation, ω_{seed} [μm]	10

6.6.3 Calculation of API Solubility

The solubility of the API in a water-ethanol (solvent-antisolvent) mixture was taken from the experimental data plot provided in Figure 2 of Luo et al. [196] for the case of the drug biapenem. Data points were extracted from the curve using the DataToGraph utility, and are given in Table 9 below [197]. Comparison with various curve fitting methods in MATLAB showed that linear interpolation provided the best fit. The data correspond to a minimum solubility in ethanol as 2.464 mg/ml, and a maximum solubility in water as 30.935 mg/ml.

Table 9 Solubility data for biapenem-water-ethanol system.

Water Mass Fraction, X_w	**C_{sat} x 10^3 (kg solute/kg solution)**
0.199	2.464
0.299	2.831
0.398	3.497
0.500	4.463
0.599	6.103
0.699	9.615
0.799	15.299
0.898	21.956
1.000	30.935

The water mass fraction in the j^{th} PFC is computed by:

$$X_{H_2O}^{j} = \frac{\rho_{H_2O} V_{feed} + \rho_{H_2O} \sum_{i=1}^{j} S_i}{\rho_{H_2O} V_{feed} + \rho_{H_2O} \sum_{i=1}^{j} S_i + \rho_{EtOH} \sum_{i=1}^{j} A_i} \tag{6.11}$$

Plugging $X_{H_2O}^{j}$ into the curve fit object created in MATLAB yields the solubility concentration of biapenem in segment j, $C_{sat,j}$.

6.7 Solution of Model Equations

A typical method used for solving equations (4.2) and (6.3) is to apply the method of moments (MOM), which reduces system to a set of coupled ordinary differential equations for the moments of the crystal size distribution. However, this method is useless here, since we need the full CSD to be able to match the target distribution. To

solve these equations, we have utilized a high-resolution finite volume (FV) technique, which is the combination of the semi-discrete FV technique with the van Leer flux limiter [113], [173]. This method provides $O(h^2)$ accuracy where the solution is smooth, without the oscillations found in other methods. Details on the finite volume method are given in Majumder and Nagy [113].

6.8 Optimization Problem Formulation

Our goal is to eliminate the production of fine crystals by utilizing dissolution. The quality of the elimination is ascertained by measuring how closely the attained number fraction distribution leaving the N^{th} PFC ($f_{N,end}$) matches a theoretically-best growth-only crystal size distribution, f_{target}. The target distribution is generated by simulating the crystallization with only one segment, with nucleation arbitrarily set to zero. With no nucleation, all solute depletion is solely due to crystal growth on the seeds, and no fine crystals are ever created. Thus, the target distribution is a hypothetical best-case scenario of pure growth achieved without nucleation. The closeness of matching can be expressed in a least-squares sense. By manipulation of the antisolvent and solvent flowrates in each segment (and other decision variables), we can make the fit between the model and the target distribution tighter. The population and mass balance equations are solved for each segment, and the output of one segment recursively becomes the input to the next segment. The procedure begins anew, with fresh antisolvent flowing into the main flow

stream. Population density and solute concentration are adjusted for the dilution induced by addition of antisolvent at each mixing point.

6.8.1 Least-Squares Objective Function

The final number fraction distribution, f_N, is used for formulating the least-squares problem:

$$\min_{\boldsymbol{d}} \quad \sum_{i=1}^{K} \left(f_{v,N,end}^{i} - f_{v,target}^{i}\right)^2 \tag{6.12}$$

Where $\boldsymbol{d}$ is the vector of decision variables (listed in Table 10), and $f_{v,N,end}$ is the volume fraction size distribution at the exit of the crystallizer. It is computed by:

$$f_{N,end} = \frac{n_N^{end}}{\int_0^{\infty} n_N^{end}\, dL} \tag{6.13}$$

The index i in (6.12) refers to a particular crystal size bin, with K total bins. Note that n integrates to n_{total} (the total number of crystals in the solution), while f integrates to 1. We use the number fraction distribution instead of the number density, since the addition of extra solvent and antisolvent causes dilution. In the previous work on cooling crystallization by Majumder and Nagy [113], the least-squares function was formulated in terms of volume density, n_v. In that work, there is no dilution effect, whereas in this work the effect of dilution reduces n_v monotonically with each liquid addition. If n_v were used to compute (6.12), it would be an "apples to oranges" comparison since total

volumetric flow rates are not the same. Using the volume fraction distribution, f_v, however, abrogates this difficulty.

6.8.2 List of Decision Variables and Bound Constraints

All $2N + 5$ decision variables in these optimizations had bound constraints. Table 10 below summarizes the decision variables and their lower/upper bounds.

Table 10 Decision variables and bound constraints for in-situ fines dissolution optimization.

Decision Variable	**Title**	**Units**	**Lower Bound**	**Upper Bound**
V_{feed}	Feed flowrate of saturated solvent	[ml/min]	0	300
A_{total}	Total flowrate of antisolvent	[ml/min]	0	300
S_{total}	Total flowrate of pure solvent	[ml/min]	0	150
d_{inner}	Inner diameter of crystallizer tube	[m]	10×10^{-3}	25×10^{-3}
ξ	Seed mass loading	[%, -]	2%	7%
$a_1, a_2, \ldots, a_N$	Antisolvent distribution fractions	[-]	0	1
$s_1, s_2, \ldots, s_N$	Pure solvent distribution fractions	[-]	0	1

The optimization of the MSMA-PFC is known to be highly non-convex, as shown by the landscape plots in Ridder et al. [161]. Such problems are not amenable to gradient search, and so we have opted for a stochastic approach to circumvent the nonconvexity. The genetic algorithm is a popular tool for solving optimization problems with this difficulty. To make the GA operate more smoothly, our decision variables were fractions of the total

antisolvent and total pure solvent. The flowrate into a segment j is the j^{th} fractional distribution variable multiplied by total flow allotment.

$$A_j = a_j A_{total}$$
$$S_j = s_j S_{total} \tag{6.14}$$

6.8.3 Linear and Nonlinear Constraints

There were no linear inequalities in this study. The only linear constraints in this work are two equalities, which require the apportionments of total liquid flows must each sum to unity. The remaining six constraints are nonlinear inequalities. Table 11 below summarizes these constraints.

Table 11 Linear and nonlinear constraints for in-situ fines dissolution optimization.

Name	Constraint	Description	Type
c_1	$\sum_{j=1}^{N} a_i = 1$	Total fractions of added liquid flows must sum to unity.	Linear
c_2	$\sum_{j=1}^{N} s_i = 1$		
c_3	$\sigma_N^{end} - 1.05 \leq 0$	Final supersaturation is bracketed between 0.85 and 1.05.	Nonlinear
c_4	$0.85 - \sigma_N^{end} \leq 0$		
c_5	$\tau_{total} - 3600 \leq 0$	Total residence time under 3600 seconds (1 hour).	
c_6	$0.30 - Y \leq 0$	Minimum required crystal mass yield of 30%.	

We require residence times of under 1 hour. In the multiple-cooling segment PFC array, residence time is constant, since flowrate of liquor into each segment is always the same.

However, the addition of antisolvent and pure solvent to the liquor flow changes residence time into a nonlinear function:

$$\tau_{total} = \sum_{j=1}^{N} \tau_j$$
$$= \frac{\pi d_{inner}^2 (x_{total}/N)}{4} \sum_{j=1}^{N} \frac{1}{V_{feed} + A_{total} \sum_{i=1}^{j} a_i + S_{total} \sum_{i=1}^{j} s_i} \tag{6.15}$$

Where x_{total}/N is the length of a single segment. The j^{th} summand in (6.15) is the residence time for the j^{th} segment, which is the segment's volume divided by the total flow rate through that segment. The total residence time is found by summing over all j individual residence times. Since each PFC volume is the same, it is taken out of the summation distributively.

Drug API products are typically expensive, making wasted API a serious expense. We require a crystal yield of at least 30% to trim unwise crystallization strategies from consideration. Yield is calculated in the following manner:

$$Y = \frac{V_{feed}\rho_{H_2O} C_0 - (V_{feed}\rho_{H_2O} + S_{total}\rho_{H_2O} + A_{total}\rho_{EtOH}) C_N^{end}}{V_{feed}\rho_{H_2O} C_0} \tag{6.16}$$

If $C_N^{end} = 0$, then all of the solute has been crystallized, and thus $Y = 1$. If no crystallization has occurred, the numerator will be zero, and thus $Y = 0$. If seed crystals have been dissolved due to excessive dissolution, then Y becomes negative.

6.9 Solution of Least-Squares Problem by the Genetic Algorithm

The GA is less efficient compared to gradient-based methods, such as sequential quadratic programming (SQP). However, algorithms like SQP are not robust to initial

guess, and can become trapped in a sub-optimal local minimum [198], [199]. This is true when the objective function and/or constraints are non-convex. Stochastic methods, such as the GA or simulated annealing, are appropriate for nonconvex optimization. The problem was solved by manipulating the $2N + 5$ decision variables with the genetic algorithm (GA). Each set of kinetic parameters and crystallizer lengths listed in Table 13 were optimized over to minimize the sum of the squares in (6.12). The GA initial population was created by randomly sampling over the bounds given in Table 10 above. The number of injections could not be used as a decision variable, as MATLAB's genetic algorithm cannot solve mixed-integer nonlinear programming (MINLP) problems that have any type of equality constraint. The number of injections used was 50, which gave a good tradeoff between curve fit and computation time. The population size was 750, repeated for 25 generations. The MATLAB integrator, depending on the particular run, was chosen for the quickest solution time. Either ode45, ode15s, or ode23 were used.

6.10 Results and Discussion

6.10.1 Experimental Design Array

To investigate the crystallizer's performance for various kinetic parameters, a reduced orthogonal array experimental design was used, with five factors, four levels, and 16 total runs. The five factors are the nucleation and growth parameters, and the total crystallizer length. The five factors and the four levels used are shown in Table 12 below.

Table 12 Table of the five factors and four levels used for examining parameter space.

Level	**Nucleation rate constant, k_b [#/m^2·s]**	**Nucleation order, b [nd]**	**Growth rate constant k_g [µm/s]**	**Growth order g [nd]**	**Total length of crystallizer, x_{total} [m]**
1	1×10^6	1	1×10^{-7}	1	5
2	1×10^7	2	5×10^{-7}	1.333	10
3	1×10^8	3	1×10^{-6}	1.667	15
4	1×10^9	4	5×10^{-6}	2	20

A reduced design was used, since exhaustive search over 4^5 = 1024 different optimizations was computationally prohibitive. This experimental table is given in Table 13 below. The orthogonal array table allows for a good sampling of the search space with only 16 samples instead of 1024.

Table 13 Experimental design table of factors and levels for the curve fit optimizations conducted. The numbers correspond to the level column in Table 12. The sum of the squares of the errors (SSE) and total amount of pure solvent added (S_{total}) are given for each run.

Run #	k_b	b	k_g	g	x_{total}	**SSE**	S_{total}
1	1	1	1	1	1	2.67E+07	80
2	1	2	2	2	2	4.71E+06	0
3	1	3	3	3	3	1.25E+07	1
4	1	4	4	4	4	7.58E+05	1
5	2	1	2	3	4	5.62E+08	3
6	2	2	1	4	3	7.42E+08	0
7	2	3	4	1	2	2.25E+07	2
8	2	4	3	2	1	6.93E+07	0
9	3	1	3	4	2	2.22E+09	8
10	3	2	4	3	1	2.10E+08	2
11	3	3	1	2	4	6.08E+09	0
12	3	4	2	1	3	3.10E+09	9
13	4	1	4	2	3	3.41E+09	11
14	4	2	3	1	4	7.82E+09	24
15	4	3	2	4	1	8.28E+09	25
16	4	4	1	3	2	1.27E+10	16

Table 13 shows the experimental design matrix, as well as the resulting sum of the squared errors for each curve fit to the zero-nucleation target distribution.

6.10.2 Volume Fraction Distributions for Optimized Cases

The data in Table 13 show that run #1 gave the tightest curve fit (Figure 6.4). The reason for this tight curve fit is due to the system exhibiting low nucleation (the k_b level is at the lowest level). Also in Figure 6.4 we show the performance of a single segment *with nucleation turned back on* ($B_0 > 0$). We can see there is little improvement observed between MSMA-PFC and using a single segment.

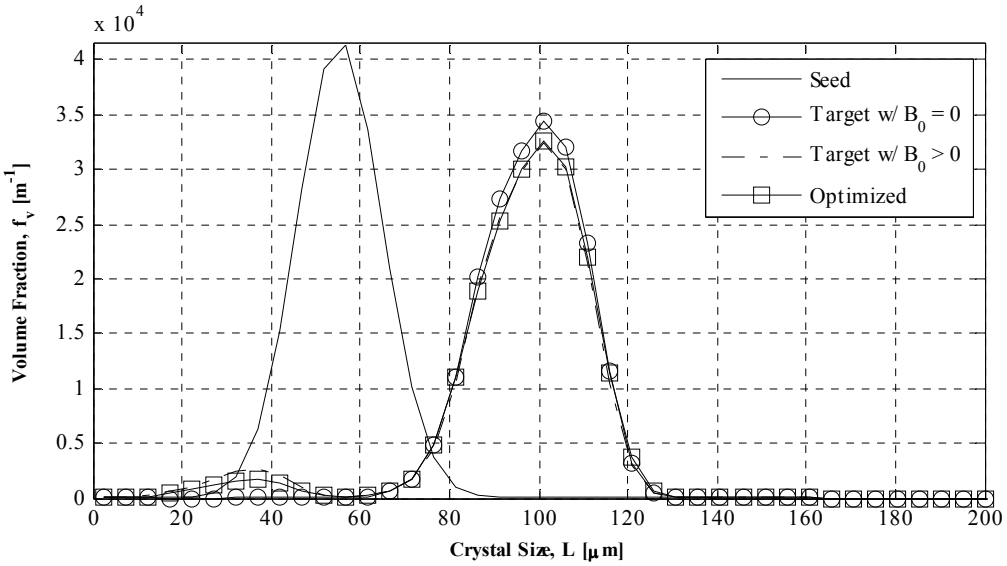

Figure 6.4 Volume-fraction distribution for run #1.

Increasing values of k_b rapidly degrade the curve fit due to overwhelming nucleation. Run #11 is representative of runs which are nucleation-dominated. As shown in Figure 6.5, there is a large amount of fines created, and the optimal result fails to hit the target distribution. While we have improved the volume fraction distribution over the single-segment case by producing less fines at the exit, there is still a great deal of fines produced. The nucleation rate constant has the greatest effect upon the performance of the crystallizer, indicating significant sensitivity to nucleation rate.

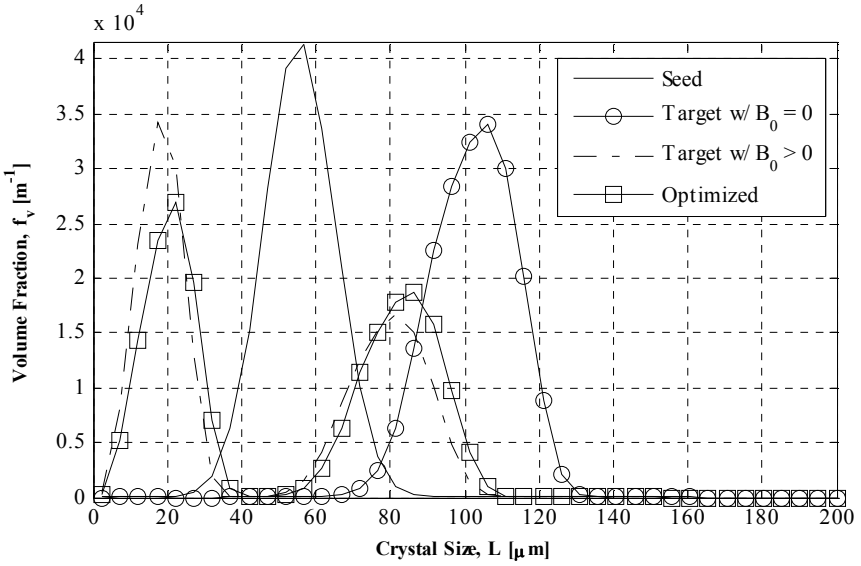

Figure 6.5 Volume-fraction distribution for run #11, a nucleation-dominated case.

6.10.3 Main-Factor Analysis

The results in section 6.10.2 suggest to us that the best results, intuitively, are obtained when the system is growth-dominated. Main-factor analysis of the experimental matrix confirms this suspicion. Main-factor analysis is done by taking the average of all SSE for a given factor at the same level. For example, the average for the factor k_b at level 2 would take the average SSE of runs 5, 6, 7, and 8. This process is repeated for all five factors and all four levels, which generates Table 14 below.

Table 14 Level-wise averages of SSE for each corresponding level and factor pair.

SSE	k_b	b	k_g	g	x_{total}
L1	**1.12E+07**	**1.56E+09**	4.89E+09	2.74E+09	2.15E+09
L2	3.49E+08	2.20E+09	2.99E+09	**2.39E+09**	3.74E+09
L3	2.90E+09	3.60E+09	2.53E+09	3.38E+09	**1.82E+09**
L4	8.06E+09	3.97E+09	**9.11E+08**	2.81E+09	3.62E+09

This analysis reveals to us what the most sensitive parameters are, and also what combination of levels will theoretically provide the best curve fit – which we hypothesized would be the growth-dominated case. We can see in Table 14 that the factor k_b spans the widest range of SSE values over the level averages. We thus conclude that k_b is the most sensitive parameter. Following the same line of reasoning, the second-

most sensitive parameter is k_g. The optimal curve fit is projected to be the set of levels for which SSE is a minimum for each corresponding factor. These values are shown in boldface in Table 14 (they are the minimum values within each column). The main-factor analysis projects that the tightest curve fit will be observed at a k_b of level 1, a b of level 1, a k_g of level 4, a g of level 2, and an x_{total} of level 3. We term this the "projected optimum." Note that this set of factors and levels is not present in Table 13. Solving the optimization problem with this new set of parameters generates the volume fraction distributions in Figure 6.6, which had an SSE of 4.83×10^5, which is less than the minimum of 7.58×10^5 in Table 13.

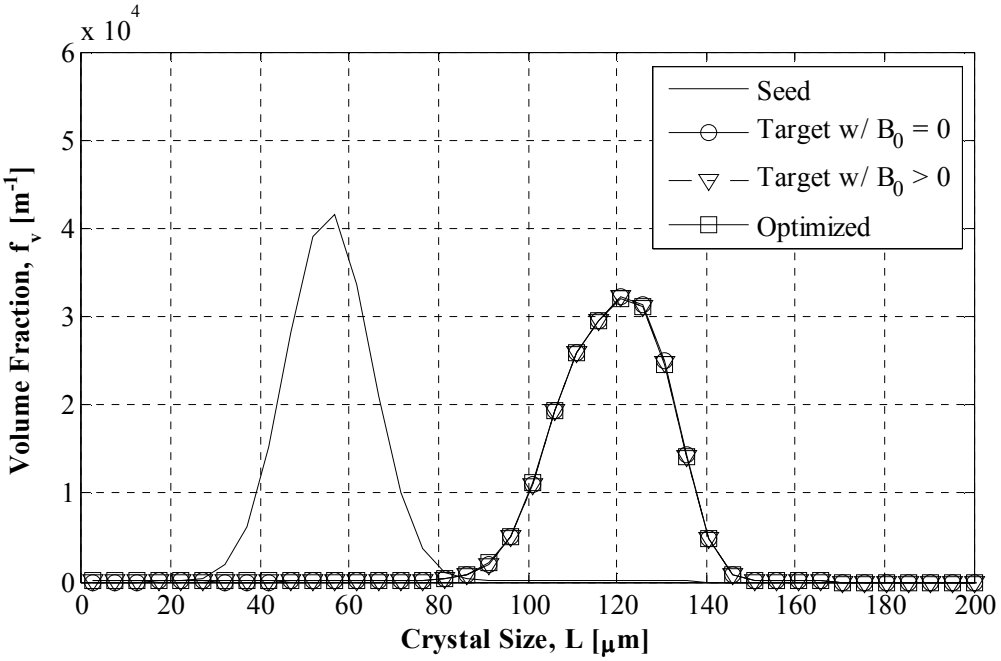

Figure 6.6 Optimal fit predicted by analysis of the orthogonal array design.

This result matches our intuition that the best result is obtained when nucleation is slow and growth is fast. However, this has the effect of "cancelling out" the benefits of using multiple injections, as we obtain a very tight fit to the curve anyways when using a single injection for this set of kinetic parameters. There was no discernible trend observed with respect to the optimized tube diameter. However, seed loading was typically between 5.0%-6.5%.

6.10.4 No Dissolution is Used to Control Fines

It is interesting (even if a bit disappointing) to observe that the optimization does not want to use dissolution to get rid of fine crystals. The total amount of pure solvent added during each optimization is given as the rightmost column in Table 13. Observe that little to no pure solvent is ever added to the system for the optimal curve fits (observe in Table 10 that $S_{total}$is bounded on the left by zero). The supersaturation profiles (S vs. x plots) show barely any dissolution occurring. The supersaturation profile for the "project optimum" is representative (Figure 6.7).

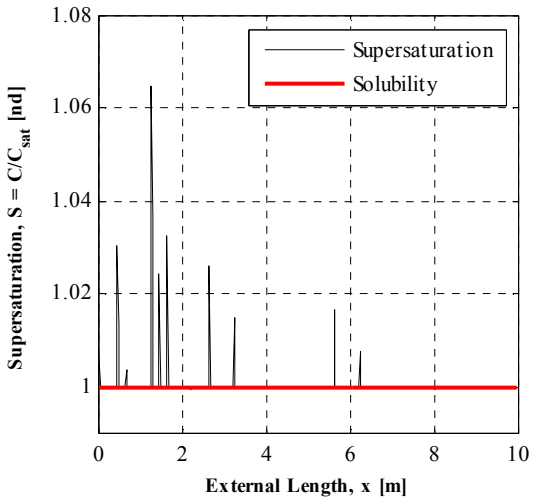

Figure 6.7 Supersaturation profile for project optimum, representative of the other supersaturation profiles.

Note how the supersaturation does not significantly (or at all) go below 1 anywhere in Figure 6.7. This indicates to us that the situations in which the curve fit is superior to the single-segment case (Figure 6.4 and Figure 6.5) is more likely due to the better control offered by using multiple segments (and thus having finer control over supersaturation), rather than making use of fines dissolution. The reason the optimization refuses to add pure solvent in significant amounts is due to the fact that adding pure solvent reduces the concentration (via dilution) and reduces available residence time (via equation (6.15)). Reduced concentration reduces the available supersaturation, and reducing the residence time reduces the time available for growth inside the MSMA-PFC. Thus, despite the potential for dissolving fines, the benefit of adding pure solvent does not counterbalance the other two negative phenomena.

6.11 Summary and Conclusions

We have investigated the use of the MSMA-PFC, run in antisolvent mode, for the growing of crystals while dissolving fines in-situ. The model equations solved were the partial differential population balance equation and the integro-differential mass balance equation. The solution method used was the finite volume method, since the entire CSD was required to calculate the sum of the squared errors for the curve fit. The final CSD was compared to a target CSD generated by arbitrarily setting nucleation to zero. A reduced orthogonal array experimental design was used to examine the effect of several kinetic parameters and total crystallizer length. The genetic algorithm was used to optimize over the decision variables, with the parameters from the experimental design held constant. The results indicate that k_b is the most sensitive parameter, followed by k_g. As k_b increases, the curve fit degrades rapidly due to becoming overwhelmed by nucleation. Examination of the supersaturation profiles shows that dissolution is not occurring appreciably for any of the optimizations performed. The MSMA-PFC performs best under kinetic crystallization conditions in which a single PFC also works sufficiently well. There are situations where using multiple additions does improve the curve fit versus the single-segment case, but excessive fines still exist. The reason the optimization does not add any pure solvent is likely due to the addition of pure solvent causing a simultaneous decrease in concentration and decrease in residence time. Both of these cause the optimization to take “one step forward and two steps back”, thus adding pure solvent is judged to be sub-optimal.

CHAPTER 7. SUMMARY, CONCLUSIONS, AND FUTURE DIRECTIONS

7.1 Summary and Conclusions

The aim of this research was to investigate a new methods of producing pharmaceutical drugs using computational methods. The drug industry is undergoing a major shift in the way it thinks about manufacturing. Prior batch methods of manufacturing are expensive and wasteful, while continuous methods are much more efficient. This motivates the study of novel crystallizers. As an example, we have investigated the optimal operation and optimal design of a new type of crystallizer, the multi-segment, multi-addition plug flow crystallizer, or MSMA-PFC.

The literature review began our work. We started with a general overview of current problems in drug manufacture, and new technologies being investigated to address these problems. We discussed many of the interesting new technologies being pursued in the areas of synthesis, purification, and formulation of pharmaceuticals.

An especially important unit operation is crystallization, from which the vast majority of drugs are separated and purified. As discussed in CHAPTER 3, many new technologies

for continuous crystallization are being investigated for application toward pharmaceutical purification.

In CHAPTER 4, we discuss one such technology in great detail. This crystallizer uses multiple plug-flow elements in series, which allows for finer control of supersaturation in one dimension. We have investigated the use of a multi-segment, multi-addition plug flow crystallizer (MSMA-PFC) for the production of pharmaceutical API crystals via computational methods. We have also shown that the optimization is nonconvex, and is not amenable to gradient search methods. Instead, we have utilized the genetic algorithm to optimize the decision variables. A multiobjective optimization problem was solved to investigate the performance of the crystallizer. The crystallization system was simulated by solving the population balance and mass balance equations using, depending on circumstance, either the method-of-moments or the finite-volume method. The system is run exclusively at steady-state as an antisolvent crystallization. The decision variables (among others) are the flowrates of antisolvent (and if applicable, pure solvent) into each distinct segment. In this simplified case, we have examined the tradeoff between mass-mean crystal size and coefficient of variation – though a variety of other objective functions could be used to extend the framework further. Our results showed that rigorous optimization was able to generate superior designs to what was shown in prior literature. Using the Monte-Carlo method, we examined in greater detail the robustness of the crystallizer with respect to error in kinetic parameters and antisolvent flowrate. The results indicate that there is significant sensitivity to kinetic parameters, though the relationship to the nucleation rate constant is somewhat counterintuitive. We furthermore

find significant sensitivity with respect to antisolvent flowrate. Error is magnified when multiple stages are in error simultaneously.

In CHAPTER 5 We have introduced in this work a new framework for optimizing plug flow crystallization systems, which was lacking previously in the literature. Specifically, we have developed a combined model and optimization framework for identifying optimal designs of the MSMA-PFC. The methodology worked by splitting the MSMA-PFC into progressively greater numbers of segments, and optimizing mass-mean crystal size (or coefficient of variation) over the antisolvent profile. Our first study in this chapter used the same total flowrates as in CHAPTER 4 Results show that multiple modes in the distribution are observed when maximizing L_{43}, but generally a much smoother distribution is obtained when minimizing CV. This behavior persists when feed flowrate and total antisolvent are incorporated as decision variables as well. For the second part of our study, we permitted total antisolvent flowrate and feed flowrate to be decision variables. Under these circumstances, residence time tends to be independent of optimization objective. Using the finite volume method, the crystal size distributions show multiple modes are present when maximizing L_{43}, but typically unimodal when minimizing CV. Greatest control (tending toward larger crystal size) was observed when using 25 injections, as agrees with intuition. Antisolvent distribution is different when maximizing either L_{43} or CV, though in both cases antisolvent sends to be distributed in a wide manner across the injections, with almost no injections receiving > 10% of the total antisolvent.

In CHAPTER 6, we examined the use of the MSMA-PFC for the production crystals while dissolving fine crystals in-situ. The results show that the optimization actually does not want to dissolve the fine crystals in order to match the CSD. Optimization results routinely set pure solvent flow to either zero or small values compared to the feed flowrate and total antisolvent flowrate. We have used an orthogonal array experimental design to sample the parameter space over the nucleation and growth rate parameters, as well as the total crystallizer length. Single-factor analysis of the orthogonal array predicted the intuitive result that the best performance would be observed for the case of slow nucleation and fast growth. Using the parameters predicted from the single-factor analysis, we find that the best results are obtained for smallest values of k_b (low nucleation) and highest values of the growth constant, k_g. The most sensitive parameter is k_b, followed by k_g. The problem with this situation, is that when compared to using a single segment, there is virtually no improvement in performance, e.g. the system was already well-behaved to begin with. The best use of in-situ fines dissolution would be for the crystallization of low-nucleation systems. For moderate nucleation cases, the MSMA-PFC results do show improvement over the nucleating case, but still exhibit large amounts of fine crystals. At higher levels of nucleation, the systems becomes overwhelmed with fines. Examination of the supersaturation profiles reveals that the optimization does not make use of dissolution in any of the cases for fines removal. This is in contrast to the work by Majumder and Nagy [113] on in-situ fines dissolution using a cooling crystallization, which clearly showed the dissolution of fine crystals. The reason we believe that antisolvent crystallization fails to make use of dissolution by the addition of pure solvent is because the addition of pure solvent causes too much loss of

supersaturation due to the effect of dilution. Furthermore, the addition of pure solvent simultaneously decreases the available residence time for crystallization. Thus, the addition of pure solvent causes us to "take one step forward and two steps back."

7.2 Future Directions

A variety of extensions of this work are possible. An important next step would be experimental verification of the optimal result found in CHAPTER 4 using a lab-scale plug flow crystallization system. Another possible direction is robust optimization of the flufenamic acid crystallization using a minimax framework. The idea here is to attempt to maximize the mean crystal size, but also to simultaneously minimize the mean size by manipulating experimental parameters over their uncertainty bounds. The results of this study would indicate how robust the crystallization process is to parametric uncertainty. Unsteady-state simulation and optimization of the plug flow crystallizer. In this study, time-optimal control could be used to optimize a variety of objectives for optimizing the startup of the PFC, e.g. minimizing the mass of wasted API. Dynamical analysis of the unsteady state MSMA-PFC is another future direction. In this study, variations in important parameters could reveal the presence of dynamical anomalies and bifurcations, or even chaotic behavior. Residence time effects are also of great importance. Our simulations always assumed plug flow, but incorporating a residence time distribution model into the framework would allow for better predictive capabilities. Chemical fouling is a known problem in the operation of plug flow crystallizers. This is when API

begins to crystallize and accumulate on the vessel walls. This interferes with heat transfer, and over the long term can reduce residence time by reducing total volume. A strategy is needed for the removal of fouling areas once they begin to accumulate, or for a way to operate the crystallization such that fouling does not occur. Economic analysis of a plant using an MSMA-PFC array is another future direction. A comparison between conventional batch technology and MSMPR modes would clearly show which technology was more economically viable. Such analysis for the case of MSMPR crystallization has already been done by Schaber et al. [5]. In this work, we have investigated solely antisolvent crystallization, but it is possible to utilize cooling and antisolvent crystallization simultaneously. Instead of a solubility curve, we now have a solubility surface with respect to temperature and antisolvent ratio. This allows for a new, independent actuator for the control of supersaturation. Polymorphism and chirality are of serious concern in drug crystallization. Synthesis of the incorrect solid or optical form will, in the best case scenario, lead to an inactive medication. In the worst case scenario, the resulting compound will be a deadly toxin. The extension of the framework in this work for the optimization of polymorphic form content and of optical form are another possible future direction. Significant interaction is known to exist between upstream and downstream processes in pharmaceutical manufacture. Another possible future direction would be to integrate other unit operations into the crystallization, such as filtration, washing, and drying. The final goal would be to optimize the properties of the final dry crystals produced at the exit of the crystallization section. Crystal shape is also of great importance in drug manufacture. In this work, we have only used a 1-dimension

population balance. However, two-dimensional population balances are becoming more commonly applied to shape control.

LITERATURE CITED

LITERATURE CITED

[1] K. V. Gernaey, A. E. Cervera-Padrell, and J. M. Woodley, "A perspective on PSE in pharmaceutical process development and innovation," *Comput. Chem. Eng.*, 2012.

[2] A. Rusu, K. Kuokkanen, and A. Heier, "Current trends in the pharmaceutical industry–A case study approach," *Eur. J. Pharm. Sci.*, vol. 44, no. 3, pp. 437–440, 2011.

[3] M. Kessel, "The problems with today's pharmaceutical business - an outsider's view," *Nat Biotech*, vol. 29, no. 1, pp. 27–33, Jan. 2011.

[4] K. V. Gernaey, A. E. Cervera-Padrell, and J. M. Woodley, "Development of continuous pharmaceutical production processes supported by process systems engineering methods and tools," *Future*, vol. 4, no. 11, pp. 1371–1374, 2012.

[5] S. D. Schaber, D. I. Gerogiorgis, R. Ramachandran, J. M. B. Evans, P. I. Barton, and B. L. Trout, "Economic Analysis of Integrated Continuous and Batch Pharmaceutical Manufacturing: A Case Study," *Ind. Eng. Chem. Res.*, vol. 50, no. 17, pp. 10083–10092, Jul. 2011.

[6] A. S. A. Roy, "Project FDA Report 5 | Stifling New Cures: The True Cost of Lengthy Clinical Drug Trials," *The Manhattan Institute*. [Online]. Available: http://www.manhattan-institute.org/html/fda_05.htm. [Accessed: 08-Feb-2013].

[7] L. Abboud and S. Hensley, "New Prescription For Drug Makers: Update the Plants - WSJ.com," *Wall Street Journal*, New York, 03-Sep-2003.

[8] J. Evans, "A paradigm shift," *TCE*, no. 860, pp. 32–34, Feb-2013.

[9] H. Wu, M. A. Khan, and A. S. Hussain, "PROCESS CONTROL PERSPECTIVE FOR PROCESS ANALYTICAL TECHNOLOGY: INTEGRATION OF CHEMICAL ENGINEERING PRACTICE INTO SEMICONDUCTOR AND PHARMACEUTICAL INDUSTRIES," *Chem. Eng. Commun.*, vol. 194, no. 6, pp. 760–779, Mar. 2007.

[10] S. Houlton, "Pharma braces for patent cliff impact," *RSC*, Dec-2011. [Online]. Available: http://www.rsc.org/chemistryworld/News/2011/December/pharma-braces-patent-cliff-impact.asp. [Accessed: 04-Nov-2012].

[11] P. Basu, G. Joglekar, S. Rai, P. Suresh, and J. Vernon, "Analysis of Manufacturing Costs in Pharmaceutical Companies," *J. Pharm. Innov.*, vol. 3, no. 1, pp. 30–40, Mar. 2008.

[12] U. S. F. G. Food and Drug Administration, "Current Good Manufacturing Practices for Drugs: Reports, Guidances and Additional Information > Pharmaceutical cGMPs for the 21st Century - A Risk-Based Approach," *fda.gov*, 2004. [Online]. Available: http://www.fda.gov/downloads/Drugs/DevelopmentApprovalProcess/Manufacturing/QuestionsandAnswersonCurrentGoodManufacturingPracticescGMPforDrugs/UCM176374.pdf. [Accessed: 29-Oct-2012].

[13] D. Hinz, "Process analytical technologies in the pharmaceutical industry: the FDA's PAT initiative," *Anal. Bioanal. Chem.*, vol. 384, no. 5, pp. 1036–1042, Mar. 2006.

[14] J. A. DiMasi, R. W. Hansen, and H. G. Grabowski, "The price of innovation: new estimates of drug development costs," *J. Health Econ.*, vol. 22, no. 2, pp. 151–185, Mar. 2003.

[15] G. V. Reklaitis, J. Khinast, and F. Muzzio, "Pharmaceutical engineering science—New approaches to pharmaceutical development and manufacturing," *Pharm. Eng. Sci.- Key Tomorrows Drugs*, vol. 65, no. 21, pp. iv–vii, Nov. 2010.

[16] R. Lakerveld, H. J. M. Kramer, A. I. Stankiewicz, and J. Grievink, "Application of generic principles of process intensification to solution crystallization enabled by a task-based design approach," *Sel. Pap. Eur. Process Intensif. Conf. EPIC 2009 Venice17 - 18 June 2009*, vol. 49, no. 9, pp. 979–991, Sep. 2010.

[17] T. Vetter, C. L. Burcham, and M. F. Doherty, "Regions of attainable particle sizes in continuous and batch crystallization processes," *Chem. Eng. Sci.*, vol. 106, no. 0, pp. 167–180, Mar. 2014.

[18] D. L. Ma, S. H. Chung, and R. D. Braatz, "Worst-case performance analysis of optimal batch control trajectories," *AIChE J.*, vol. 45, no. 7, pp. 1469–1476, 1999.

[19] K. Plumb, "Continuous Processing in the Pharmaceutical Industry: Changing the Mind Set," *7th World Congr. Chem. Eng.*, vol. 83, no. 6, pp. 730–738, Jun. 2005.

[20] B. Benyahia, R. Lakerveld, and P. I. Barton, "A Plant-Wide Dynamic Model of a Continuous Pharmaceutical Process," *Ind. Eng. Chem. Res.*, vol. 51, no. 47, pp. 15393–15412, Oct. 2012.

[21] B. Y. Shekunov and P. York, "Crystallization processes in pharmaceutical technology and drug delivery design," *J. Cryst. Growth*, vol. 211, no. 1–4, pp. 122–136, Apr. 2000.

[22] S. M. Reutzel-Edens, "Achieving polymorph selectivity in the crystallization of pharmaceutical solids: basic considerations and recent advances.," *Curr. Opin. Drug Discov. Devel.*, vol. 9, no. 6, p. 806, 2006.

[23] S. Mascia, P. L. Heider, H. Zhang, R. Lakerveld, B. Benyahia, P. I. Barton, R. D. Braatz, C. L. Cooney, J. M. B. Evans, T. F. Jamison, K. F. Jensen, A. S. Myerson, and B. L. Trout, "End-to-End Continuous Manufacturing of Pharmaceuticals: Integrated Synthesis, Purification, and Final Dosage Formation," *Angew. Chem. Int. Ed.*, vol. 52, no. 47, pp. 12359–12363, 2013.

[24] J. Chen, B. Sarma, J. M. B. Evans, and A. S. Myerson, "Pharmaceutical Crystallization," *Cryst. Growth Des.*, vol. 11, no. 4, pp. 887–895, Feb. 2011.

[25] D. Barrasso and R. Ramachandran, “A comparison of model order reduction techniques for a four-dimensional population balance model describing multi-component wet granulation processes,” *Chem. Eng. Sci.*, vol. 80, no. 0, pp. 380–392, Oct. 2012.

[26] M. M. Crowley, F. Zhang, M. A. Repka, S. Thumma, S. B. Upadhye, S. Kumar Battu, J. W. McGinity, and C. Martin, “Pharmaceutical Applications of Hot-Melt Extrusion: Part I,” *Drug Dev. Ind. Pharm.*, vol. 33, no. 9, pp. 909–926, 2007.

[27] M. A. Repka, S. K. Battu, S. B. Upadhye, S. Thumma, M. M. Crowley, F. Zhang, C. Martin, and J. W. McGinity, “Pharmaceutical Applications of Hot-Melt Extrusion: Part II,” *Drug Dev. Ind. Pharm.*, vol. 33, no. 10, pp. 1043–1057, 2007.

[28] P. Kleinebudde, “Roll compaction/dry granulation: pharmaceutical applications,” *Int. Assoc. Pharm. Technol. APV*, vol. 58, no. 2, pp. 317–326, Sep. 2004.

[29] M. N. C. Cipich, “Real time steady-state data reconciliation and gross error detection in continuous pharmaceutical manufacturing,” Master’s, Purdue University, West Lafayette, Indiana, 2009.

[30] D. Sperger and E. Munson, “Analysis of Structural Variability in Pharmaceutical Excipients Using Solid-State NMR Spectroscopy,” *AAPS PharmSciTech*, vol. 12, no. 3, pp. 821–833, Sep. 2011.

[31] C. Vervaet and J. P. Remon, “Continuous granulation in the pharmaceutical industry,” *Granulation Length Scales - 2nd Int. Workshop Granulation Granulation Length Scales - 2nd Int. Workshop Granulation*, vol. 60, no. 14, pp. 3949–3957, Jul. 2005.

[32] B. Scott and A. Wilcock, “Process Analytical Technology in the Pharmaceutical Industry: A Toolkit for Continuous Improvement,” *PDA J. Pharm. Sci. Technol.*, vol. 60, no. 1, pp. 17–53, 2006.

[33] A. A. Levis and L. G. Papageorgiou, “A hierarchical solution approach for multi-site capacity planning under uncertainty in the pharmaceutical industry,” *ESCAPE 13*, vol. 28, no. 5, pp. 707–725, May 2004.

[34] R. W. Bondi Jr. and J. K. Drennen III, “5 - Quality by Design and the Importance of PAT in QbD,” in *Separation Science and Technology*, vol. Volume 10, Satinder Ahuja and Stephen Scypinski, Ed. Academic Press, 2011, pp. 195–224.

[35] U. FDA, “Pharmaceutical cGMPs for the 21st Century - A Risk-Based Approach.” US Federal Government, Sep-2004.

[36] FDA, “Guidance for Industry PAT — A Framework for Innovative Pharmaceutical Development, Manufacturing, and Quality Assurance.” Sep-2004.

[37] R. D. Braatz, “Advanced control of crystallization processes,” *Annu. Rev. Control*, vol. 26, no. 1, pp. 87–99, 2002.

[38] P. A. Larsen, D. B. Patience, and J. B. Rawlings, “Industrial crystallization process control,” *Control Syst. IEEE*, vol. 26, no. 4, pp. 70–80, 2006.

[39] W. J. Genck, “Optimizing Crystallizer Scaleup,” *Chem. Eng. Prog.*, pp. 36–44, Jun. 2003.

[40] A. G. Jones, *Crystallization process systems*. Oxford: Butterworth-Heinemann, 2002.

[41] P.-H. Jézéquel, “The concept of ‘scaleable reactor’ in the precipitation of silver halide photographic microcrystals,” *Ind. Cryst.*, vol. 56, no. 7, pp. 2399–2408, Apr. 2001.

[42] A. Mersmann and F. W. Rennie, “Design of Crystallizers and Crystallization Processes,” in *Crystallization Technology Handbook*, 1st ed., A. Mersmann, Ed. New York: Marcel-Dekker, 1995, pp. 242–243.

[43] H.-H. Tung, “Industrial Perspectives of Pharmaceutical Crystallization,” *Org. Process Res. Dev.*, vol. 17, no. 3, pp. 445–454, Mar. 2013.

[44] B. Schmidt, J. Patel, F. X. Ricard, C. M. Brechtelsbauer, and N. Lewis, “Application of Process Modelling Tools in the Scale-Up of Pharmaceutical Crystallisation Processes,” *Org. Process Res. Dev.*, vol. 8, no. 6, pp. 998–1008, Nov. 2004.

[45] H. Wei, “Computer-aided design and scale-up of crystallization processes: Integrating approaches and case studies,” *Chem. Eng. Res. Des.*, vol. 88, no. 10, pp. 1377–1380, Oct. 2010.

[46] S. M. Peker and S. S. Helvaci, *Solid-liquid two phase flow*, 1st ed. Amsterdam: Elsevier, 2008.

[47] J. B. Rawlings, S. M. Miller, and W. R. Witkowski, “Model identification and control of solution crystallization processes: A review,” *Ind. Eng. Chem. Res.*, vol. 32, no. 7, pp. 1275–1296, 1993.

[48] B. Igne, Z. Shi, J. K. Drennen, and C. A. Anderson, “Effects and Detection of Raw Material Variability on the Performance of Near-Infrared Calibration Models for Pharmaceutical Products,” *J. Pharm. Sci.*, vol. 103, no. 2, pp. 545–556, 2014.

[49] Y. Pathak and D. Thassu, “Scale Up and Technology Transfer of Pharmaceutical Suspensions,” in *Pharmaceutical Suspensions*, A. K. Kulshreshtha, O. N. Singh, and G. M. Wall, Eds. Springer New York, 2010, pp. 245–264.

[50] T. Chiu and P. D. Christofides, “Nonlinear control of particulate processes,” *AIChE J.*, vol. 45, no. 6, pp. 1279–1297, 1999.

[51] N. S. Tavare, *Industrial Crystallization: Process Simulation, Analysis, and Design*. New York: Plenum, 1995.

[52] U. Vollmer and J. Raisch, “Population balance modelling and H∞—controller design for a crystallization process,” *Part. Process.*, vol. 57, no. 20, pp. 4401–4414, Oct. 2002.

[53] M. Sen, A. Chaudhury, R. Singh, J. John, and R. Ramachandran, “Multi-scale flowsheet simulation of an integrated continuous purification–downstream pharmaceutical manufacturing process,” *Int. J. Pharm.*, vol. 445, no. 1–2, pp. 29–38, Mar. 2013.

[54] R. Lakerveld, B. Benyahia, P. L. Heider, H. Zhang, R. D. Braatz, and P. I. Barton, “Averaging Level Control to Reduce Off-Spec Material in a Continuous Pharmaceutical Pilot Plant,” *Processes*, vol. 1, no. 3, pp. 330–348, 2013.

[55] “MIT Engineering: Labs, Centers & Programs: Novartis-MIT Center for Continuous Manufacturing.” [Online]. Available: http://engineering.mit.edu/research/labs_centers_programs/novartis.php. [Accessed: 28-May-2013].

[56] "Engineering Research Center for Structured Organic Particulate Systems (C-SOPS)." [Online]. Available: http://ercforsops.org/. [Accessed: 28-May-2013].

[57] L. Pernenkil and C. L. Cooney, "A review on the continuous blending of powders," *Chem. Eng. Sci.*, vol. 61, no. 2, pp. 720–742, Jan. 2006.

[58] J. F. Gamble, W.-S. Chiu, V. Gray, H. Toale, M. Tobyn, and Y. Wu, "Investigation into the Degree of Variability in the Solid State Properties of Common Pharmaceutical Excipients - Microcrystalline Cellulose," in *Particulate Materials: Synthesis, Characterisation, Processing and Modelling*, The Royal Society of Chemistry, 2012, pp. 82–91.

[59] E. Tomba, M. De Martin, P. Facco, J. Robertson, S. Zomer, F. Bezzo, and M. Barolo, "General procedure to aid the development of continuous pharmaceutical processes using multivariate statistical modeling – An industrial case study," *Int. J. Pharm.*, vol. 444, no. 1–2, pp. 25–39, Feb. 2013.

[60] C. Graffner, "Workshop: Quality by Design in pharmaceutical development and manufacture," presented at the ICH Q8 Pharmaceutical Development - Lakemedelsverket Medical Products Agency, Stockholm, 28-Mar-2006.

[61] M. Staples, "The Concept of Quality-by-Design," in *Pharmaceutical Stability Testing to Support Global Markets*, vol. XII, K. Huynh-Ba, Ed. Springer New York, 2010, pp. 101–106.

[62] Yubing Tang, "Quality by Design Approaches to Analytical Methods - FDA Perspective," presented at the AAPS, Washington D.C., 25-Oct-2011.

[63] J. Claridge and T. Fabian, "History and Development of Evidence-based Medicine," *World J. Surg.*, vol. 29, no. 5, pp. 547–553, May 2005.

[64] L. X. Yu, R. A. Lionberger, A. S. Raw, R. D'Costa, H. Wu, and A. S. Hussain, "Applications of process analytical technology to crystallization processes," *Pharm. Solid Polymorph. Drug Dev. Regul.*, vol. 56, no. 3, pp. 349–369, Feb. 2004.

[65] X. Liu, D. Sun, F. Wang, Y. Wu, Y. Chen, and L. Wang, "Monitoring of antisolvent crystallization of sodium scutellarein by combined FBRM–PVM–NIR," *J. Pharm. Sci.*, vol. 100, no. 6, pp. 2452–2459, 2011.

[66] K. A. Bakeev, *Process analytical technology: spectroscopic tools and implementation strategies for the chemical and pharmaceutical industries*. Wiley, 2010.

[67] A. Shukla, A. Prakash, and S. Rohani, "Online measurement of particle size distribution during crystallization using ultrasonic spectroscopy," *Chem. Eng. Sci.*, vol. 65, no. 10, pp. 3072–3079, May 2010.

[68] O. Suleiman Ahmad, J. Debayle, N. Gherras, B. Presles, G. Févotte, and J.-C. Pinoli, "Recognizing overlapped particles during a crystallization process from in situ video images for measuring their size distributions," pp. 800005–800005, Jun. 2011.

[69] N. Gherras, E. Serris, and G. Fevotte, "Monitoring industrial pharmaceutical crystallization processes using acoustic emission in pure and impure media," *Int. J. Pharm.*, vol. 439, no. 1–2, pp. 109–119, Dec. 2012.

[70] Z. K. Nagy, G. Fevotte, H. Kramer, and L. L. Simon, "Recent advances in the monitoring, modelling and control of crystallization systems," *60th Anniv. Eur. Fed. Chem. Eng. EFCE*, vol. 91, no. 10, pp. 1903–1922, Oct. 2013.

[71] M. L. Balboni, “Process Analytical Technology: Concepts and Principles,” *Pharm. Technol.*, Oct. 2003.
[72] L. Gradinarsky, H. Brage, B. Lagerholm, I. Niklasson Björn, and S. Folestad, “In situ monitoring and control of moisture content in pharmaceutical powder processes using an open-ended coaxial probe,” *Meas. Sci. Technol.*, vol. 17, no. 7, p. 1847, 2006.
[73] Anonymous, “Guideline on Real Time Release Testing (formerly Guideline on Parametric Release).” European Medicines Agency, 25-Feb-2010.
[74] V. Venkatasubramanian, “DROWNING IN DATA: Informatics and modeling challenges in a data-rich networked world,” *AIChE J.*, vol. 55, no. 1, pp. 2–8, 2009.
[75] R. F. Stengel, *Optimal Control and Estimation*, 1st Edition. New York: Dover, 1994.
[76] S. Y. Wong, R. K. Bund, R. K. Connelly, and R. W. Hartel, “Modeling the Crystallization Kinetic Rates of Lactose via Artificial Neural Network,” *Cryst. Growth Des.*, vol. 10, no. 6, pp. 2620–2628, May 2010.
[77] H. Wu, M. White, and M. A. Khan, “Quality-by-Design (QbD): An integrated process analytical technology (PAT) approach for a dynamic pharmaceutical co-precipitation process characterization and process design space development,” *Int. J. Pharm.*, vol. 405, no. 1–2, pp. 63–78, Feb. 2011.
[78] C. M. V. Moore, “Continuous Manufacturing - FDA Perspective on Submissions and Implementation,” presented at the PQRI Workshop on Sample Sizes for Decision Making in New Manufacturing Paradigms, Bethesda, Maryland, USA, 13-Sep-2011.
[79] L. X. Yu, “Pharmaceutical quality by design: product and process development, understanding, and control,” *Pharm. Res.*, vol. 25, no. 4, pp. 781–791, 2008.
[80] I. M. Hamdan, “Exceptional events management applied to continuous pharmaceutical manufacturing,” Purdue University, West Lafayette, Indiana, 2010.
[81] F. Boukouvala, R. Ramachandran, A. Vanarase, F. J. Muzzio, and M. G. Ierapetritou, “Computer Aided Design and Analysis of Continuous Pharmaceutical Manufacturing Processes,” in *Computer Aided Chemical Engineering*, vol. Volume 29, M. C. G. and A. C. K. E.N. Pistikopoulos, Ed. Elsevier, 2011, pp. 216–220.
[82] A. Kalbag and C. Wassgren, “Inter-tablet coating variability: Tablet residence time variability,” *Chem. Eng. Sci.*, vol. 64, no. 11, pp. 2705–2717, Jun. 2009.
[83] B. Freireich and C. Wassgren, “Intra-particle coating variability: Analysis and Monte-Carlo simulations,” *Chem. Eng. Sci.*, vol. 65, no. 3, pp. 1117–1124, Feb. 2010.
[84] B. Freireich, W. R. Ketterhagen, and C. Wassgren, “Intra-tablet coating variability for several pharmaceutical tablet shapes,” *Chem. Eng. Sci.*, vol. 66, no. 12, pp. 2535–2544, Jun. 2011.
[85] T. Sinha, R. Bharadwaj, J. S. Curtis, B. C. Hancock, and C. Wassgren, “Finite element analysis of pharmaceutical tablet compaction using a density dependent material plasticity model,” *Powder Technol.*, vol. 202, no. 1–3, pp. 46–54, Aug. .
[86] Z. K. Nagy and R. D. Braatz, “Advances and New Directions in Crystallization Control,” *Annu. Rev. Chem. Biomol. Eng.*, vol. 3, pp. 55–75, 2012.

[87] V. Venkatasubramanian, C. Zhao, G. Joglekar, A. Jain, L. Hailemariam, P. Suresh, P. Akkisetty, K. Morris, and G. V. Reklaitis, "Ontological informatics infrastructure for pharmaceutical product development and manufacturing," *Pap. Form Chem. Process Control VII CPC VII Seventh Int. Conf. Ser.*, vol. 30, no. 10–12, pp. 1482–1496, Sep. 2006.

[88] C. Zhao, G. Joglekar, A. Jain, V. Venkatasubramanian, and G. V. Reklaitis, "Pharmaceutical informatics: A novel paradigm for pharmaceutical product development and manufacture," in *Computer Aided Chemical Engineering*, vol. Volume 20, Luis Puigjaner and Antonio Espuña, Ed. Elsevier, 2005, pp. 1561–1566.

[89] M. Fujiwara, Z. K. Nagy, J. W. Chew, and R. D. Braatz, "First-principles and direct design approaches for the control of pharmaceutical crystallization," *J. Process Control*, vol. 15, no. 5, pp. 493–504, 2005.

[90] Z. K. Nagy and R. D. Braatz, "Robust nonlinear model predictive control of batch processes," *AIChE J.*, vol. 49, no. 7, pp. 1776–1786, 2004.

[91] J. D. Ward, C.-C. Yu, and M. F. Doherty, "Plantwide dynamics and control of processes with crystallization," *Comput. Chem. Eng.*, vol. 34, no. 1, pp. 112–121, Jan. 2010.

[92] S. Skogestad, "Economic Plantwide Control," in *Plantwide Control*, John Wiley & Sons, Ltd, 2012, pp. 229–251.

[93] S. Vasudevan and G. P. Rangaiah, "A Review of Plantwide Control Methodologies and Applications," in *Plantwide Control*, John Wiley & Sons, Ltd, 2012, pp. 179–201.

[94] M. J. Abel, "Process systems engineering of continuous pharmaceutical manufacturing," Dissertation, MIT, Cambridge, MA, 2010.

[95] J. A. Dirksen and T. A. Ring, "Fundamentals of crystallization: Kinetic effects on particle size distributions and morphology," *Chem. Eng. Sci.*, vol. 46, no. 10, pp. 2389–2427, 1991.

[96] G. R. Desiraju, J. J. Vittal, and A. Ramanan, *Crystal Engineering: A Textbook*. World Scientific Publishing Company, 2011.

[97] R. Davey and J. Garside, *From Molecules to Crystallizers*, 1st ed. New York: Oxford, 2000.

[98] M. Giulietti and A. Bernardo, "Chapter 14 - Crystallization by Antisolvent Addition and Cooling," in *Crystallization - Science and Technology*, Internet: InTech, 2012.

[99] A. Llinàs and J. M. Goodman, "Polymorph control: past, present and future," *Drug Discov. Today*, vol. 13, no. 5–6, pp. 198–210, Mar. 2008.

[100] I. Dohgane, H. Hosaka, and A. Tasaka, "Method for Separation of m-or p-cresol," 4032581, 28-Jun-1977.

[101] T. Rungsimanon, K. Yuyama, T. Sugiyama, and H. Masuhara, "Crystallization in Unsaturated Glycine/D2O Solution Achieved by Irradiating a Focused Continuous Wave Near Infrared Laser," *Cryst. Growth Des.*, vol. 10, no. 11, pp. 4686–4688, Sep. 2010.

[102] T. Rungsimanon, K. Yuyama, T. Sugiyama, H. Masuhara, N. Tohnai, and M. Miyata, "Control of Crystal Polymorph of Glycine by Photon Pressure of a Focused Continuous Wave Near-Infrared Laser Beam," *J. Phys. Chem. Lett.*, vol. 1, no. 3, pp. 599–603, Jan. 2010.
[103] K. Yuyama, C.-S. Wu, T. Sugiyama, and H. Masuhara, "Laser trapping-induced crystallization of l-phenylalanine through its high-concentration domain formation," *Photochem. Photobiol. Sci.*, vol. 13, no. 2, pp. 254–260, 2014.
[104] J. E. Aber, S. Arnold, B. A. Garetz, and A. S. Myerson, "Strong dc Electric Field Applied to Supersaturated Aqueous Glycine Solution Induces Nucleation of the γ Polymorph," *Phys. Rev. Lett.*, vol. 94, no. 14, p. 145503, Apr. 2005.
[105] B. C. Knott, J. L. LaRue, A. M. Wodtke, M. F. Doherty, and B. Peters, "Communication: Bubbles, crystals, and laser-induced nucleation," *J. Chem. Phys.*, vol. 134, no. 17, 2011.
[106] O. Narducci, A. G. Jones, and E. Kougoulos, "An Assessment of the Use of Ultrasound in the Particle Engineering of Micrometer-Scale Adipic Acid Crystals," *Cryst. Growth Des.*, vol. 11, no. 5, pp. 1742–1749, Mar. 2011.
[107] O. Sohnel and J. Garside, *Precipitation: Basic Principles and Industrial Applications*, 1st ed. Oxford: Butterworth-Heinemann, 1992.
[108] A. Mersmann, "Crystallization and precipitation," *Chem. Eng. Process. Process Intensif.*, vol. 38, no. 4, pp. 345–353, 1999.
[109] J. J. De Yoreo and P. G. Vekilov, "Principles of Crystal Nucleation and Growth," *Rev. Mineral. Geochem.*, vol. 54, no. 1, pp. 57–93, 2003.
[110] N. Rodríguez-hornedo and D. Murphy, "Significance of controlling crystallization mechanisms and kinetics in pharmaceutical systems," *J. Pharm. Sci.*, vol. 88, no. 7, pp. 651–660, 1999.
[111] A. D. Randolph and M. A. Larson, *Theory of Particulate Processes: Analysis and Techniques of Continuous Crystallization*. New York: Academic Press, 1971.
[112] A. Mersmann, "Fundamentals of Crystallization," in *Crystallization Technology Handbook*, New York: Marcel-Dekker, 1995, p. 41.
[113] A. Majumder and Z. K. Nagy, "Fines removal in a continuous plug flow crystallizer by optimal spatial temperature profiles with controlled dissolution," *AIChE J.*, vol. 59, no. 12, pp. 4582–4594, 2013.
[114] A. A. Lonare and S. R. Patel, "Antisolvent Crystallization of Poorly Water Soluble Drugs," *Int. J. Chem. Eng. Appl.*, vol. 4, no. 5, pp. 337–341, Oct. 2014.
[115] A. Caillet, N. Sheibat-Othman, and G. Fevotte, "Crystallization of Monohydrate Citric Acid. 2. Modeling through Population Balance Equations," *Cryst. Growth Des.*, vol. 7, no. 10, pp. 2088–2095, Oct. 2007.
[116] M. O. Besenhard, R. Hohl, A. Hodzic, R. J. P. Eder, and J. G. Khinast, "Modeling a seeded continuous crystallizer for the production of active pharmaceutical ingredients," *Cryst. Res. Technol.*, vol. 49, no. 2–3, pp. 92–108, 2014.
[117] A. Nangia, "Conformational Polymorphism in Organic Crystals," *Acc. Chem. Res.*, vol. 41, no. 5, pp. 595–604, Mar. 2008.
[118] M. Kitamura, "Strategy for control of crystallization of polymorphs," *CrystEngComm*, vol. 11, no. 6, pp. 949–964, 2009.

[119] J. Ulrich and P. Frohberg, “Problems, potentials and future of industrial crystallization,” *Front. Chem. Sci. Eng.*, pp. 1–8, 2013.
[120] S. A. Bhat and B. Huang, “Preferential crystallization: Multi-objective optimization framework,” *AIChE J.*, vol. 55, no. 2, pp. 383–395, 2009.
[121] S. Qamar, M. Peter Elsner, I. Hussain, and A. Seidel-Morgenstern, “Seeding strategies and residence time characteristics of continuous preferential crystallization,” *Chem. Eng. Sci.*, vol. 71, pp. 5–17, Mar. 2012.
[122] C. Groom, “Industrial problems from polymorphism and how we might avoid them,” Cambridge Crystallographic Data Centre.
[123] M. Wang, G. C. Rutledge, A. S. Myerson, and B. L. Trout, “Production and characterization of carbamazepine nanocrystals by electrospraying for continuous pharmaceutical manufacturing,” *J. Pharm. Sci.*, vol. 101, no. 3, pp. 1178–1188, 2012.
[124] S. M. Miller and J. B. Rawlings, “Model identification and control strategies for batch cooling crystallizers,” *AIChE J.*, vol. 40, no. 8, pp. 1312–1327, 1994.
[125] C. Schaefer, C. Lecomte, D. Clicq, A. Merschaert, E. Norrant, and F. Fotiadu, “On-line near infrared spectroscopy as a Process Analytical Technology (PAT) tool to control an industrial seeded API crystallization,” *J. Pharm. Biomed. Anal.*, no. 0.
[126] R. B. Bird, W. E. Stewart, and E. N. Lightfoot, *Transport phenomena*. Wiley, 2006.
[127] G. Hetsroni, Ed., *Handbook of Multiphase Systems*. Washington D.C.: Hemisphere Publishing, 1982.
[128] R. M. Felder and R. W. Rousseau, *Elementary Principles of Chemical Processes*, 3rd ed. New York: Wiley, 2000.
[129] W. Pietsch, *Agglomeration in industry: occurence and applications*, vol. 1. Weinheim: Wiley-VCH, 2005.
[130] J. D. Litster, “Lecture Notes for Particle Design Course.” Purdue University, 2012.
[131] D. Ramkrishna and A. W. Mahoney, “Population balance modeling. Promise for the future,” *Chem. Eng. Sci.*, vol. 57, no. 4, pp. 595–606, Feb. 2002.
[132] D. Ramkrishna, *Population balances: Theory and applications to particulate systems in engineering*. San Diego: Academic press, 2000.
[133] H. M. Hulburt and S. Katz, “Some problems in particle technology: A statistical mechanical formulation,” *Chem. Eng. Sci.*, vol. 19, no. 8, pp. 555–574, Aug. 1964.
[134] M. Attarakih, “Integral formulation of the population balance equation: Application to particulate systems with particle growth,” *Comput. Chem. Eng.*, vol. 48, no. 0, pp. 1–13, Jan. 2013.
[135] A. J. Alvarez and A. S. Myerson, “Continuous plug flow crystallization of pharmaceutical compounds,” *Cryst. Growth Des.*, vol. 10, no. 5, pp. 2219–2228, 2010.
[136] X. Y. Woo, R. B. H. Tan, and R. D. Braatz, “Modeling and Computational Fluid Dynamics−Population Balance Equation−Micromixing Simulation of Impinging Jet Crystallizers,” *Cryst. Growth Des.*, vol. 9, no. 1, pp. 156–164, Dec. 2008.
[137] X. Y. Woo, R. B. H. Tan, and R. D. Braatz, “Precise tailoring of the crystal size distribution by controlled growth and continuous seeding from impinging jet crystallizers,” *CrystEngComm*, vol. 13, no. 6, pp. 2006–2014, 2011.

[138] X. Y. Woo, R. B. H. Tan, P. S. Chow, and R. D. Braatz, "Simulation of Mixing Effects in Antisolvent Crystallization Using a Coupled CFD-PDF-PBE Approach," *Cryst. Growth Des.*, vol. 6, no. 6, pp. 1291–1303, Apr. 2006.
[139] M. Smith and T. Matsoukas, "Constant-number Monte Carlo simulation of population balances," *Chem. Eng. Sci.*, vol. 53, no. 9, pp. 1777–1786, May 1998.
[140] Y. Lin, K. Lee, and T. Matsoukas, "Solution of the population balance equation using constant-number Monte Carlo," *Popul. Balance Model. Part. Syst.*, vol. 57, no. 12, pp. 2241–2252, Jun. 2002.
[141] D. Ramkrishna, "Analysis of population balance—IV: The precise connection between Monte Carlo simulation and population balances," *Chem. Eng. Sci.*, vol. 36, no. 7, pp. 1203–1209, 1981.
[142] R. T. Marler and J. S. Arora, "Survey of multi-objective optimization methods for engineering," *Struct. Multidiscip. Optim.*, vol. 26, no. 6, pp. 369–395, Apr. 2004.
[143] M. Ehrgott, "Multiobjective optimization," *AI Mag.*, vol. 29, no. 4, p. 47, 2009.
[144] T. Stewart, O. Bandte, H. Braun, N. Chakraborti, M. Ehrgott, M. Göbelt, Y. Jin, H. Nakayama, S. Poles, and D. Stefano, "Real-World Applications of Multiobjective Optimization," in *Multiobjective Optimization*, J. Branke, K. Deb, K. Miettinen, and R. Slowinski, Eds. Springer-Verlag, 2008, pp. 285–327.
[145] M. Trifkovic, M. Sheikhzadeh, and S. Rohani, "Kinetics Estimation and Single and Multi-Objective Optimization of a Seeded, Anti-Solvent, Isothermal Batch Crystallizer," *Ind. Eng. Chem. Res.*, vol. 47, no. 5, pp. 1586–1595, Feb. 2008.
[146] D. Sarkar, S. Rohani, and A. Jutan, "Multi-objective optimization of seeded batch crystallization processes," *Chem. Eng. Sci.*, vol. 61, no. 16, pp. 5282–5295, Aug. 2006.
[147] K. Deb, *Multi-Objective Optimization Using Evolutionary Algorithms*, 1st ed. New York: Wiley, 2001.
[148] L. Chambers, Ed., *The Practical Handbook of Genetic Algorithms*, 2nd ed. Boca Raton: Chapman & Hall/CRC, 2001.
[149] J. L. Quon, H. Zhang, A. Alvarez, J. Evans, A. S. Myerson, and B. L. Trout, "Continuous Crystallization of Aliskiren Hemifumarate," *Cryst. Growth Des.*, vol. 12, no. 6, pp. 3036–3044, May 2012.
[150] H. Zhang, J. Quon, A. J. Alvarez, J. Evans, A. S. Myerson, and B. Trout, "Development of Continuous Anti-Solvent/Cooling Crystallization Process using Cascaded Mixed Suspension, Mixed Product Removal Crystallizers," *Org. Process Res. Dev.*, vol. 16, no. 5, pp. 915–924, Mar. 2012.
[151] A. J. Alvarez, A. Singh, and A. S. Myerson, "Crystallization of Cyclosporine in a Multistage Continuous MSMPR Crystallizer," *Cryst. Growth Des.*, vol. 11, no. 10, pp. 4392–4400, Aug. 2011.
[152] D. L. Browne, B. J. Deadman, R. Ashe, I. R. Baxendale, and S. V. Ley, "Continuous Flow Processing of Slurries: Evaluation of an Agitated Cell Reactor," *Org. Process Res. Dev.*, vol. 15, no. 3, pp. 693–697, Mar. 2011.
[153] O. Narducci, A. G. Jones, and E. Kougoulos, "Continuous crystallization of adipic acid with ultrasound," *Chem. Eng. Sci.*, vol. 66, no. 6, pp. 1069–1076, 2011.
[154] O. Levenspiel, *Chemical reaction engineering*, vol. 2. Wiley New York etc., 1972.

[155] S. Ferguson, G. Morris, H. Hao, M. Barrett, and B. Glennon, "In-situ monitoring and characterization of plug flow crystallizers," *18th Int. Symp. Ind. Cryst.*, vol. 77, no. 0, pp. 105–111, Jul. 2012.

[156] M. Midler Jr, E. L. Paul, E. F. Whittington, M. Futran, P. D. Liu, J. Hsu, and S.-H. Pan, "Crystallization method to improve crystal structure and size," 5,314,506, 1994.

[157] R. K. Thakur, C. Vial, K. D. P. Nigam, E. B. Nauman, and G. Djelveh, "Static Mixers in the Process Industries—A Review," *React. Eng. Microstruct. React.*, vol. 81, no. 7, pp. 787–826, Aug. 2003.

[158] R. J. P. Eder, S. Radl, E. Schmitt, S. Innerhofer, M. Maier, H. Gruber-Woelfler, and J. G. Khinast, "Continuously Seeded, Continuously Operated Tubular Crystallizer for the Production of Active Pharmaceutical Ingredients," *Cryst. Growth Des.*, vol. 10, no. 5, pp. 2247–2257, 2010.

[159] R. J. P. Eder, E. K. Schmitt, J. Grill, S. Radl, H. Gruber-Woelfler, and J. G. Khinast, "Seed loading effects on the mean crystal size of acetylsalicylic acid in a continuous-flow crystallization device," *Cryst. Res. Technol.*, vol. 46, no. 3, pp. 227–237, 2011.

[160] S. Lawton, G. Steele, P. Shering, L. Zhao, I. Laird, and X.-W. Ni, "Continuous Crystallization of Pharmaceuticals Using a Continuous Oscillatory Baffled Crystallizer," *Org. Process Res. Dev.*, vol. 13, no. 6, pp. 1357–1363, Oct. 2009.

[161] B. J. Ridder, A. Majumder, and Z. K. Nagy, "Population Balance Model-Based Multiobjective Optimization of a Multisegment Multiaddition (MSMA) Continuous Plug-Flow Antisolvent Crystallizer," *Ind. Eng. Chem. Res.*, vol. 53, no. 11, pp. 4387–4397, Feb. 2014.

[162] B. J. Ridder, A. Majumder, and Z. K. Nagy, "Population balance model based multi-objective optimization and robustness analysis of a continuous plug flow antisolvent crystallizer," *Am. Control Conf. ACC 2014*, pp. 3530–3535, Jun. 2014.

[163] A.-T. Nguyen, Y. L. Joo, and W.-S. Kim, "Multiple Feeding Strategy for Phase Transformation of GMP in Continuous Couette–Taylor Crystallizer," *Cryst. Growth Des.*, vol. 12, no. 6, pp. 2780–2788, Apr. 2012.

[164] N. Kockmann, M. Gottsponer, B. Zimmermann, and D. M. Roberge, "Enabling Continuous-Flow Chemistry in Microstructured Devices for Pharmaceutical and Fine-Chemical Production," *Chem. – Eur. J.*, vol. 14, no. 25, pp. 7470–7477, 2008.

[165] T. Van Gerven and A. Stankiewicz, "Structure, Energy, Synergy, Time—The Fundamentals of Process Intensification," *Ind. Eng. Chem. Res.*, vol. 48, no. 5, pp. 2465–2474, Feb. 2009.

[166] N. M. Nikačević, A. E. M. Huesman, P. M. J. Van den Hof, and A. I. Stankiewicz, "Opportunities and challenges for process control in process intensification," *Chem. Eng. Process. Process Intensif.*, vol. 52, no. 0, pp. 1–15, Feb. 2012.

[167] A. E. Cervera-Padrell, T. Skovby, S. Kiil, R. Gani, and K. V. Gernaey, "Active pharmaceutical ingredient (API) production involving continuous processes – A process system engineering (PSE)-assisted design framework," *Eur. J. Pharm. Biopharm.*, vol. 82, no. 2, pp. 437–456, Oct. 2012.

[168] R. J. P. Eder, E. K. Schmitt, J. Grill, S. Radl, H. Gruber-Woelfler, and J. G. Khinast, "Seed loading effects on the mean crystal size of acetylsalicylic acid in a continuous-flow crystallization device," *Cryst. Res. Technol.*, vol. 46, no. 3, pp. 227–237, 2011.

[169] A. J. Alvarez and A. S. Myerson, "Continuous Plug Flow Crystallization of Pharmaceutical Compounds," *Cryst. Growth Des.*, vol. 10, no. 5, pp. 2219–2228, Mar. 2010.

[170] K. L. Choong and R. Smith, "Optimization of semi-batch reactive crystallization processes," *Chem. Eng. Sci.*, vol. 59, no. 7, pp. 1529–1540, Apr. 2004.

[171] Z. K. Nagy, M. Fujiwara, and R. D. Braatz, "Modelling and control of combined cooling and antisolvent crystallization processes," *J. Process Control*, vol. 18, no. 9, pp. 856–864, 2008.

[172] PubChem, "Flufenamic Acid - PubChem." [Online]. Available: http://pubchem.ncbi.nlm.nih.gov/summary/summary.cgi?cid=3371. [Accessed: 29-Dec-2012].

[173] R. Gunawan, I. Fusman, and R. D. Braatz, "High resolution algorithms for multidimensional population balance equations," *AIChE J.*, vol. 50, no. 11, pp. 2738–2749, 2004.

[174] S. Qamar, M. P. Elsner, I. A. Angelov, G. Warnecke, and A. Seidel-Morgenstern, "A comparative study of high resolution schemes for solving population balances in crystallization," *Comput. Chem. Eng.*, vol. 30, no. 6–7, pp. 1119–1131, May 2006.

[175] A. N. Saleemi, G. Steele, N. I. Pedge, A. Freeman, and Z. K. Nagy, "Enhancing crystalline properties of a cardiovascular active pharmaceutical ingredient using a process analytical technology based crystallization feedback control strategy," *Int. J. Pharm.*, vol. 430, no. 1–2, pp. 56–64, Jul. 2012.

[176] K. Deb, A. Pratap, S. Agarwal, and T. Meyarivan, "A fast and elitist multiobjective genetic algorithm: NSGA-II," *Evol. Comput. IEEE Trans. On*, vol. 6, no. 2, pp. 182–197, Apr. 2002.

[177] Z. K. Nagy and E. Aamir, "Systematic design of supersaturation controlled crystallization processes for shaping the crystal size distribution using an analytical estimator," *Chem. Eng. Sci.*, vol. 84, no. 0, pp. 656–670, Dec. 2012.

[178] R. McGraw, "Description of Aerosol Dynamics by the Quadrature Method of Moments," *Aerosol Sci. Technol.*, vol. 27, no. 2, pp. 255–265, Jan. 1997.

[179] D. L. Marchisio, J. T. Pikturna, R. O. Fox, R. D. Vigil, and A. A. Barresi, "Quadrature method of moments for population-balance equations," *AIChE J.*, vol. 49, no. 5, pp. 1266–1276, 2003.

[180] V. Kariwala, Y. Cao, and Z. K. Nagy, "Automatic differentiation-based quadrature method of moments for solving population balance equations," *AIChE J.*, vol. 58, no. 3, pp. 842–854, 2012.

[181] A. E. Flood, "Thoughts on Recovering Particle Size Distributions from the Moment Form of the Population Balance," *Dev. Chem. Eng. Miner. Process.*, vol. 10, no. 5–6, pp. 501–519, 2002.

[182] B. Wan and T. A. Ring, "Verification of SMOM and QMOM population balance modeling in CFD code using analytical solutions for batch particulate processes," *China Particuology*, vol. 4, no. 5, pp. 243–249, Oct. 2006.
[183] Y. I. Lim, J.-M. Le Lann, X. M. Meyer, X. Joulia, G. Lee, and E. S. Yoon, "On the solution of population balance equations (PBE) with accurate front tracking methods in practical crystallization processes," *Chem. Eng. Sci.*, vol. 57, no. 17, pp. 3715–3732, Sep. 2002.
[184] A. E. Bouaswaig and S. Engell, "WENO scheme with static grid adaptation for tracking steep moving fronts," *Chem. Eng. Sci.*, vol. 64, no. 14, pp. 3214–3226, Jul. 2009.
[185] A. W. Mahoney and D. Ramkrishna, "Efficient solution of population balance equations with discontinuities by finite elements," *Chem. Eng. Sci.*, vol. 57, no. 7, pp. 1107–1119, Apr. 2002.
[186] V. John, T. Mitkova, M. Roland, K. Sundmacher, L. Tobiska, and A. Voigt, "Simulations of population balance systems with one internal coordinate using finite element methods," *3rd Int. Conf. Popul. Balance Model.*, vol. 64, no. 4, pp. 733–741, Feb. 2009.
[187] F. Févotte and G. Févotte, "A method of characteristics for solving population balance equations (PBE) describing the adsorption of impurities during crystallization processes," *Chem. Eng. Sci.*, vol. 65, no. 10, pp. 3191–3198, May 2010.
[188] A. Majumder, V. Kariwala, S. Ansumali, and A. Rajendran, "Entropic lattice Boltzmann method for crystallization processes," *Chem. Eng. Sci.*, vol. 65, no. 13, pp. 3928–3936, Jul. 2010.
[189] A. Majumder, V. Kariwala, S. Ansumali, and A. Rajendran, "Lattice Boltzmann method for population balance equations with simultaneous growth, nucleation, aggregation and breakage," *Chem. Eng. Sci.*, vol. 69, no. 1, pp. 316–328, Feb. 2012.
[190] M. Smith and T. Matsoukas, "Constant-number Monte Carlo simulation of population balances," *Chem. Eng. Sci.*, vol. 53, no. 9, pp. 1777–1786, May 1998.
[191] S. Khalili, Y. Lin, A. Armaou, and T. Matsoukas, "Constant number Monte Carlo simulation of population balances with multiple growth mechanisms," *AIChE J.*, vol. 56, no. 12, pp. 3137–3145, 2010.
[192] R. Haghpanah, A. Majumder, R. Nilam, A. Rajendran, S. Farooq, I. A. Karimi, and M. Amanullah, "Multiobjective Optimization of a Four-Step Adsorption Process for Postcombustion CO2 Capture Via Finite Volume Simulation," *Ind. Eng. Chem. Res.*, vol. 52, no. 11, pp. 4249–4265, Jan. 2013.
[193] I. Grossmann, "Enterprise-wide optimization: A new frontier in process systems engineering," *AIChE J.*, vol. 51, no. 7, pp. 1846–1857, 2005.
[194] I. E. Grossmann and A. W. Westerberg, "Research challenges in process systems engineering," *AIChE J.*, vol. 46, no. 9, pp. 1700–1703, 2000.
[195] M. R. Abu Bakar, Z. K. Nagy, A. N. Saleemi, and C. D. Rielly, "The impact of direct nucleation control on crystal size distribution in pharmaceutical crystallization processes," *Cryst. Growth Des.*, vol. 9, no. 3, pp. 1378–1384, 2009.

[196] Y.-H. Luo, G.-G. Wu, and B.-W. Sun, “Antisolvent Crystallization of Biapenem: Estimation of Growth and Nucleation Kinetics,” *J. Chem. Eng. Data*, vol. 58, no. 3, pp. 588–597, Feb. 2013.
[197] A. Tarafder, *DataToGraph*. .
[198] W. H. Press, S. A. Teukolsky, W. Vetterling, and B. P. Flannery, *Numerical recipes in C - The art of scientific computing*, 2nd ed. New York: Cambridge University Press, 1992.
[199] K. J. Beers, *Numerical methods for chemical engineering: applications in Matlab*. Cambridge University Press, 2006.

VITA

VITA

Bradley James Ridder was born September 24, 1985 in Spring Hill, Florida, USA. Bradley decided to major in chemical engineering at the end of high school, and enrolled at the University of South Florida in Tampa, Florida. He graduated with honors and distinction in May of 2010. That same year, Bradley enrolled in the doctoral program at Purdue University's School of Chemical Engineering. Since the summer of 2012, Bradley has worked on the simulation and optimization of crystallization processes for the production of pharmaceuticals. Bradley's interests in chemical engineering are more along the process systems side of things, such as optimization, control theory, optimal control, and also transport phenomena.